Synthesis and Applications of Indenopyrazine based polymers for use in Organic Electronics

George Barnes

Submitted in partial fulfilment of the requirements for the degree of

Doctor of Philosophy in Physics

Imperial College London

August 2014

To Judy and Henry

Declaration

The work performed in this thesis was carried out in the Chemistry Department, Imperial College London, between October 2010 and September 2013 under the supervision of Prof. Martin Heeney and is the work of the author unless otherwise stated.

George Barnes August 2014

Contributions

The work presented in this thesis was carried out in collaboration with a wide variety of people due to the interdisciplinary nature of the research and would not have been possible without their input.

The organic solar cells were fabricated at Imperial College London by Dr. Raja Shahid Ashraf.

The organic transistors were fabricated by Yang Han at Imperial College London.

Single crystal structure measurements and analysis was carried out by Dr Andrew White at Imperial College London.

PESA measurements were carried out in CSIRO (Melbourne, Australia) by Dr Scott Watkins.

Co-monomers in Chapter 3 were synthesised by Abby Casey, Imperial College London.

ASE and Time of Flight measurements were carried out by Mohammad Chaudary, Imperial College London.

Acknowledgements

I would first like to thank Prof. Martin Heeney for all the time and effort that he put in reading this thesis. I am also grateful for the constant encouragement throughout the years and the helpful advice in bringing this work to completion.

I would like to thank all the people in the Harwood laboratory with a special mention going to Prof. Iain McCulloch, Dr Hugo Bronstein, Dr Jonathan Marshall, Dr Bob Schroeder, Dr. David James, Dr. Zhuping Fei, Dr. Yang Han, Daniel Beatrup and Iain Meager. All of whom played their own roles in offering advice on all my lab based troubles. It would be unfair not to mention Jess, Josh, Abby, Rolf, Big Chris, Pang, Adam, Iain, Tom and Dickson as outstanding members of the Heeney group.

I would like to give special mention to my parents and brother who have been there for me since I first started my time at Imperial College London. Without them I would not have been able to get to where I am today.

It would not feel right if I was not to mention Andrew McGlashan, Ioan Owen, Dr. James Fletcher, Dr. Frederico Sanches, Dr. Flannan O'Mahony and Marc Dalla-Riva for being great friends and always letting me get the first round in outside of the lab.

Finally I would like to thank my girlfriend Chiara Lattuada. We met at a time when the pressure of finishing this work was really starting to build up and though she may not realise, she has been there for me when work was getting too much and I felt I could escape with her for a few hours.

Abstract

The first part of this thesis is devoted to the synthesis, purification and application of a series of indenopyrazine based polymers for their use in optoelectronic devices. The work focuses on the effect of alternating chain length on the degree of polymerisation, optical and charge carrier properties

The next section studies the copolymerisation of indenopyrazine with dithiophene benzothiadiazole acceptor units and the effect substituents have on the planarity of the polymer backbone and the delocalisation of molecular orbitals and solar cell performance.

The final part of this thesis investigates indenopyrazine based polymers as charge carrier materials in p-type transistors and probes the effect p-dopants have on the energy levels, charge carrier mobility and optical properties. The second part is the synthesis of the novel alkylidene-indenopyrazine monomer and probes the introduction of enforced planarity and finally the synthesis towards the novel the semiconductor indenopyrazinedithiophene.

Contents

Abbreviations

AM1.5	Air Mass 1.5 spectrum
ASE	Amplified spontaneous emission
a.u	arbitrary units
BHJ	Bulk heterojunction
BT	Benzothiadiazole
CB	Chlorobenzene
COD	Cyclooctadiene
CV	Cyclic voltammetry
D-A	Donor-Acceptor
DCM	Dichloromethane
DFT	Density functional theory
DMF	*N, N*-Dimethylformamide
DMSO	Dimethyl sulfoxide
DSC	Differential scanning calorimetry
DPP	Diketopyrrolopyrrole
V_D	Drain voltage
E_g	Band gap
EI	Electron ionisation
EQE	External quantum efficiency
eV	Electron-volt
FF	Fill factor
V_G	Gate voltage
GPC	Gel permeation chromatography
HOMO	highest occupied molecular orbital
ICT	Internal charge transfer
IP	Indenopyrazine

IR	Intrared
ISC	Intersystem crossing
ITO	Indium tin oxide
J_{sc}	Short circuit current
LUMO	Lowest unoccupied molecular orbital
MS	Mass spectrometry
NMR	Nuclear magnetic resonance
M_n	Number average molecular weight
V_{oc}	Open circuit voltage
OFET	Organic field-effect transistor
OLED	Organic light emitting diode
OPV	Organic photovoltaic
OSC	Organic semiconductor
P3HT	Poly(3-hexylthiophene)
PCBM	Phenyl-C_{60}-butyric acid methyl ester
PCE	Power conversion efficiency
PEDOT	Poly(ethylenedioxythiophene)
PESA	Photo electron spectroscopy in air
PDI	Polydispersity index
PPV	Poly(*p*-phenylene vinylene)
PSS	Polystyrene sulfonate
T	Thiophene
THF	Tetrahydrofuran
TOF	Time of Flight
TT	Thieno[3,2-b]thiophene
UV	Ultraviolet

Chapter 1 - Introduction

General Introduction and Band Theory

Organic semiconductors are materials that are based primarily on the element carbon. Due to the electronic configuration, when chains of carbon are bound in alternating single and double bonds they are said to be conjugated and it is possible to transfer charge. It is the sp^2 hybridisation present in carbon that leaves a single unpaired electron in the p_z orbital that gives carbon its semiconducting properties (Figure 1).[1]

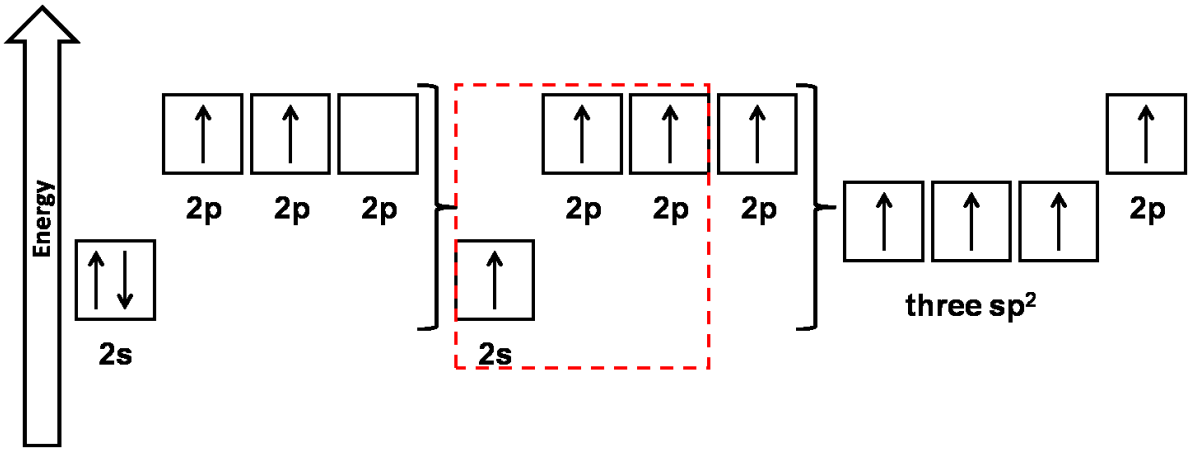

Figure 1. Hybridisation of atomic orbitals in carbon

In a multi-centered carbon chain the p_z orbital residing on each atomic centre can either be in phase or out of phase with respect to its neighbouring p_z orbital and they delocalise to form molecular orbitals. Ethene (Figure 2) consists of two configurations of the p_z orbitals, the lower energy in-phase configuration and the higher energy out of phase molecular orbital. Based on molecular orbital theory, the lowest energy orbitals fill first to produce one bonding and one anti bonding orbital. As the number of carbons in the backbone is extended, the possible configurations of the p_z orbitals increase. For butadiene (Figure 2) there are 4 possible configurations and the four available p_z electrons fill the lowest energy molecular orbitals. The orbital configuration increases in complexity as more carbon and heteroatoms are introduced into the system, building up complex molecular orbitals which form part of the

fundamentals of charge carrying materials in organic electronic applications such as lasers,[2] OLEDs,[3,4] transistors[5] and solar cells.[6]

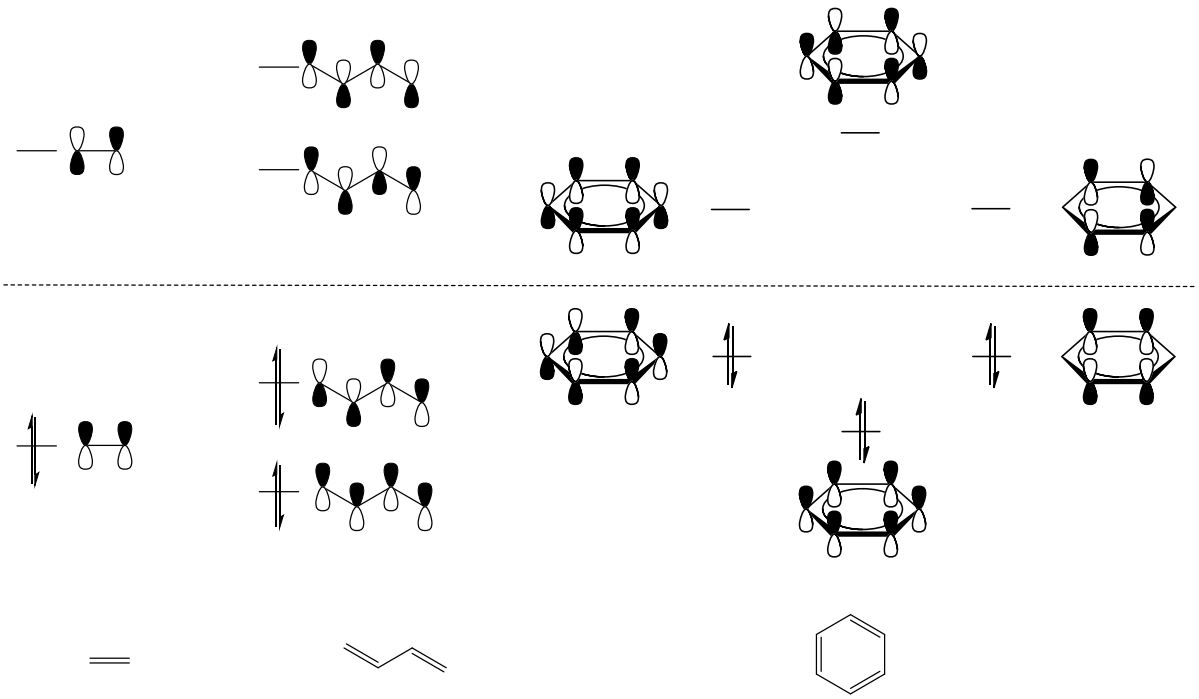

Figure 2. p_z Orbital configurations for ethene (left), butadiene (middle) and benzene

Benzene which consists of 6 sp^2 carbon atoms bound in a ring structure has 6 unpaired p_z electrons, filling the molecular orbitals as shown in Figure 2. The highest occupied molecular orbital (HOMO) and the lowest unoccupied molecular orbital (LUMO) and the associated energy gap between the filled bonding and unfilled anti-bonding orbitals is the origin of what is commonly referred to as the band gap. Only the 3 lowest energy molecular orbitals are filled with electron pairs and the 3 higher energy molecular orbitals are left unoccupied.[7]

As the conjugation length of the molecule increases more delocalised electrons are in the system; this results in the HOMO energy level increasing and the LUMO decreasing.[8] However, eventually the change in the energy levels saturates and the addition of further monomer units do not influence the band gap. The value that this saturation occurs is

commonly known as the effective conjugation length where additional repeat units do not greatly affect the optoelectronic properties, although physical properties such as solution viscosity have expected to show strong dependent on molecular weight.

For the majority of semiconductor active layers, the material will not be in its ground state. The semiconductor will need to support and sustain excitations, and in charge carrying applications these excitations must be mobile. When an electron is removed from the HOMO or added to the LUMO a radical ion is created. These radical ions are termed hole or electron polarons and they are the charge carrying species within organic semiconductors. Following the addition or removal of an electron in the semiconductor, there is a redistribution of charge to minimise the energy. The redistribution of charge results in a change of bond angles, bond length and nuclear position (Figure 3) and is known as the reorganisation energy.

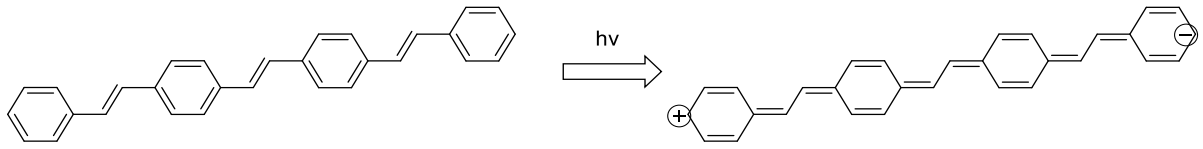

Figure 3. Benzoidal and quinoidal structures in poly(p-phenylene vinylene) (PPV).

These reorganisations occur in order to reduce the overall energy of the system. The new energy levels for the hole and electron polarons appear within the HOMO-LUMO band gap. The combined entity of lattice distortion and charge move through the material together. When a hole and electron polaron meet, a strong coulombic binding results in a release of energy, the exciton binding energy (E_b) (Figure 4) and an exciton is formed.

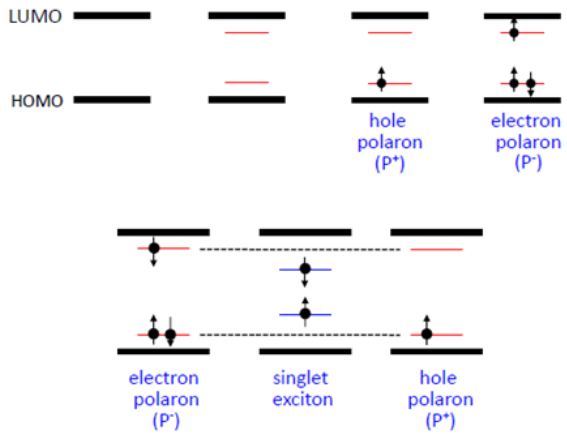

Figure 4. (Top line) Energy level diagram for hole and electron polaron is compared to the neutral molecule. (Bottom line) Formation of a singlet exciton from a hole and electron polaron.

An exciton is a coulombically bound state of an electron and a hole. Under the band-picture for inorganic semiconductors, it consists of an electron in the conduction band and a hole in the valence band. For organic semiconductors an exciton consists of an electron in the LUMO bound to a hole in the HOMO. The electron-hole pair resides very closely together on the molecular chain, but its wavefunction extends over a few repeat units.[10] If $E_b > kT$ then the exciton will be stable to dissociation. If $E_b < kT$ then the electron and hole will easily dissociate into free charge carriers. Apart from the combination of electron and hole polarons by electrical excitation, excitons can be also generated by optical excitation (Figure 5).

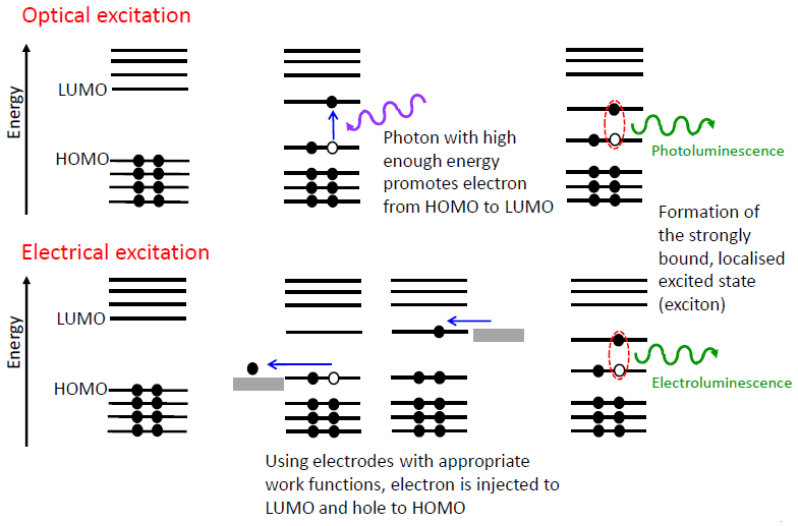

Figure 5. Optical and electrical formation of excitons.

In semiconductors, due to the effect of disorder in the chains there is an energy range of excitons that are generated and the energy states can be described as having a Gaussian distribution. Due to the excitons being mobile they diffuse to a region on the chain that will have a smaller energy gap (Figure 6).

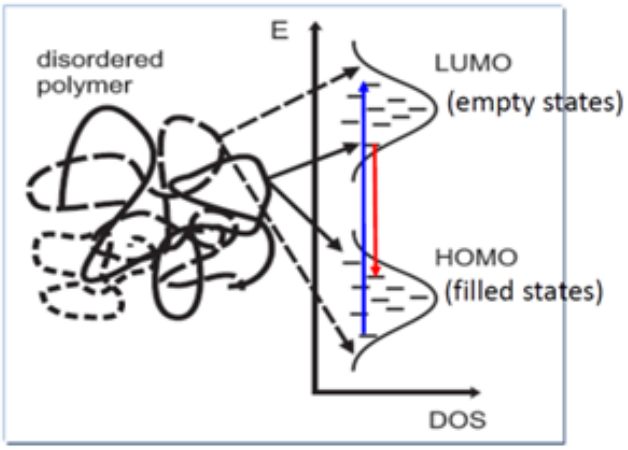

Figure 6. Gaussian distribution of HOMO LUMO energy levels.

Charge Transport

Charge transport is important for the design of almost all polymer active layers in organic electronics. There are two main methods of charge transport, intrachain transport along the chain and interchain or intrachain hoping transport.[11] On top of these 3 methods the transport of charges is different for holes and electrons.[10] The simultaneous transport of holes and electrons, ambipolar transport, is not easily achieved and presently most reported materials are hole transporting. Electron transport or n-channel devices are constantly improving in efficiency. A suggested reason for the disparity lies with electron trapping sites.[12] For example oxygen, with its strong electronegativity attracts electrons and is almost ever present in the form of water. There are methods of eliminating water from devices such as vacuum treatment but for large scale, low cost production not rigorously understood this can be expensive.[13] One design principle for overcoming electron trap sites is the lowering of the

polymer LUMO energy level. Semiconductors that have an electron affinity greater than 4 eV are generally regarded as air-stable, as the resulting radical anion is generally sufficiently stable not to interact with hydroxyl groups. Polymers that contain nitrogen in a conjugated fused ring system have been shown to have potential as good electron transporting materials, for example, poly(phenylquinoxaline) which was one of the first reported (Figure 7).[14]

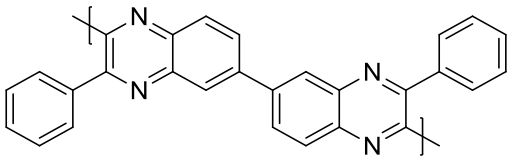

Figure 7. Poly(phenylquinoxaline)

These polymers have a high electron affinity which is beneficial for efficient electron injection and for raising the barrier to oxidation. A second suggestion for the difference in mobilities of holes and electrons is associated with the orbitals in which they reside and transport between.[15] Hole transport is associated with the HOMO and electron transport is associated with the LUMO. In many cases, LUMO orbitals are known to be more localised than HOMO orbitals as has been shown by DFT methods.[16] It can be more difficult to ensure good overlap of localised LUMOs on adjacent polymer backbones versus more delocalised systems, which can reduce the rate of charge hopping. The wavefunction of the electron or hole polaron is affected by an applied electric field and the polaron travels along the chain under the influence of the electric field. For intrachain transport, the mobility is heavily dependent on the orientation of the polymer. If the polymer is crystalline and not aligned with the electric field then for the polaron to contribute to intrachain transport it has to first hop onto a neighbouring chain.[11] This is different for the case of amorphous polymers as there will be little order within the polymeric system. The transport is also affected by lattice vibrations which scatter polarons and reduce charge carrier mobility.

Hopping is much more prevalent when considering transport mechanisms due to the disordered nature of the materials that are involved. Hopping (quantum tunnelling) is the process by which polarons transfer from one chain to the adjacent chain (interchain), or in highly disordered, amorphous systems that contain polymers kinks, the charge can transfer to another part of the same chain without travelling along it. For non-conjugated polymers such as poly(vinyl carbazole) (Figure 8) it will be exclusively a hopping transport mechanism that contributes to the charge carrier mobility.[17]

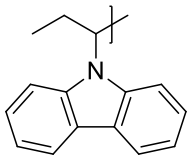

Figure 8. Poly(vinyl carbazole)

Hopping transport gives rise to lower mobilities than intrachain transport.[11] One factor that reduces hopping transport is the need to overcome the activation energy. If the charge does have enough energy to hop then there is also the factor of distance it has to travel to the adjacent polymer chain and the energy levels of the hopping sites involved.[18]

Conjugated Systems Design

Organic semiconductors in transistors have the general requirements of being solution processable, stable at ambient conditions and possessing high charge carrier mobility. Fluorene and poly(aryl amine) co-polymers were some of the first semiconductors to demonstrate their ease of processability and ambient stability but they lacked the structural order to obtain high charge carrier mobilities.[19] PTAA has been shown to have a mobility of 4×10^{-3} cm^2 V^{-1} s^{-1} despite lacking a crystalline nature and an ionisation potential of 5.2 eV.[20] To improve mobility, most approaches have concentrated upon an improvement in chain rigidity by the inclusion of fused aromatic co-monomers.[21] Control of the macroscopic properties is also important, and has been nicely demonstrated in the liquid crystalline co-

polymer of fluorene and bithiophene (F8T2).[11] Here annealing in the liquid crystalline phase was shown to improve mobility up to 0.01 - 0.02 $cm^2 V^{-1} s^{-1}$.[11] These results were particularly interesting because the alternative polymeric system at the time (P3HT) had its high mobilities attributed to the high degree of $\pi - \pi$ stacking present. The F82T system however had alkyl chains that were perpendicular to the polymer backbone, thus hindering close $\pi - \pi$ stacking and the high mobility was attributed to high intrachain mobilities.[11] More recently two trends can be observed in efforts to improve charge carrier mobility, firstly by extending the backbone conjugation through the use of extended fused aromatic units; these units often contain solubilising sidechains on bridging atoms. In addition dipole – dipole interactions between conjugated polymers chains have been suggested to promote close contacts and enhance mobility, as exemplified by one of the present leading co-monomers diketopyrrolopyrrole.[22-23]

Organic semiconductors used in OPVs can be split into two categories. The first are small molecules which are mainly processed using thermal evaporation in a high vacuum environment. The second category is solution processable organic polymers. With their associated weak van der Waals interactions it enables them to be deposited via large area, low-cost solution techniques.[24] Some of the earliest materials used for polymer solar cells were discovered by Wudl *et al*.. Wudl was one of the first to work on MEH-PPV and also invented one of the most important fullerene derivates, PCBM.[25-26] It was Yu *et al.* that first blended them together to produced a polymer solar cell with a significant PCE.[27] Further improvements were limited by the narrow absorption ranges and low hole mobilities for this class of polymer. Soluble thiophenes such as P3HT became very popular due to their higher hole mobility and broader spectral coverage producing cells with a PCE of 4-5 %.[28–30] Fast forward 10 years and some of the current state of the art polymers are produced by Yu *et al*. and based on the now popular benzodithiophene unit.[31–33] It was the industry demands of

low-cost, high through-put production that ushered in the current wave of polymer-based organic semiconductors. Two of the three methods of polymerisation described below, allow for the creation of alternating copolymers. The combination of molecular orbitals from two types of monomers into an alternating A-B type structure results in the formation of new polymer molecular orbitals and energy levels.

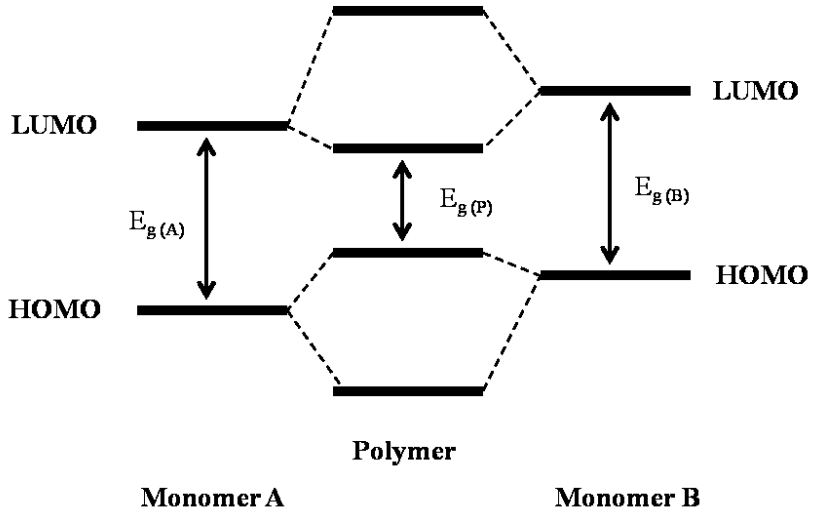

Figure 9. Schematic energy levels of monomer (M_a) and monomer (M_b) and the resulting low band gap of the polymer (P)

Combining both electron poor and electron rich monomers create what is often called a push-pull copolymer. These push-pull alternating copolymers have been favoured for use as the active layer in solar cells because their band gap can be readily tuned by choice of appropriate donor and acceptor monomers. F8BT is an example which involves the co-polymerisation of 9,9-dioctylfluorene and benzo[2,1,3]thiadiazole. The fluorene unit can be considered to act as the donor due to its relatively high electron density, distributed evenly across the monomer unit. As a result, the homopolymer, poly(9,9-dioctylfluorene) possesses a large band gap and emits light towards the blue end of the spectrum. In contrast, benzothiadiazole is strongly electron accepting. Copolymerisation with 9,9-dioctylfluorene results in hybridisation of the molecular orbitals as shown in Figure 9, and a significant reduction in the band gap. As a result F8BT emits in the green region of the spectrum.

The use of electron withdrawing and donating substituents and heterocycles are the chemist's primary way of controlling the band gap and the localisation of electron density in the backbone. The localisation of electron density and presence of electron withdrawing substituents also has an effect on the charge transport. The greater the number of electron withdrawing groups present, the lower the HOMO will be and the more difficult it will be to oxidise the polymer i.e. inject a hole. However, increasing the numbering of electron withdrawing substituents will result in a lowering of the LUMO level, facilitating the injection of electrons. This will typically improve electron mobility by reducing the number of trap sites that are present whilst simultaneously reducing the barrier to injection of electrons.

Polymerisation Techniques

There are a range of different polymerisation techniques that can be employed for the synthesis of conjugated polymers. It is important to choose the appropriate polymerisation technique to achieve high yields and high molecular weight polymers. A brief overview of the three main polymerisation techniques used in this work will now be covered.

Yamamoto polymerisation

Yamamoto polymerisation is a nickel (0) catalysed carbon – carbon coupling reaction of aromatic bis(triflates) or more commonly dihaloaromatic species.[34] It is commonly used to produce either homopolymers or random co-polymers from mixtures of two or more dihalogenated monomers.

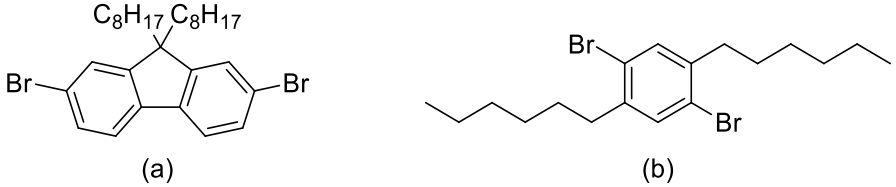

Figure 10. Fluorenes (a) and phenylenes (b).

Typically a nickel precatalyst is used such as Nickel(0) bis(cyclooctadiene) [$Ni(COD)_2$] in the presence of 2,2'-bipyridine, which is the effective ligand. The nickel is in the Ni(0) oxidation state and has two vacant electron sites that makes the metal ideal for oxidative addition reactions. The reactions mechanism begins with the oxidative addition of the halogenated species.

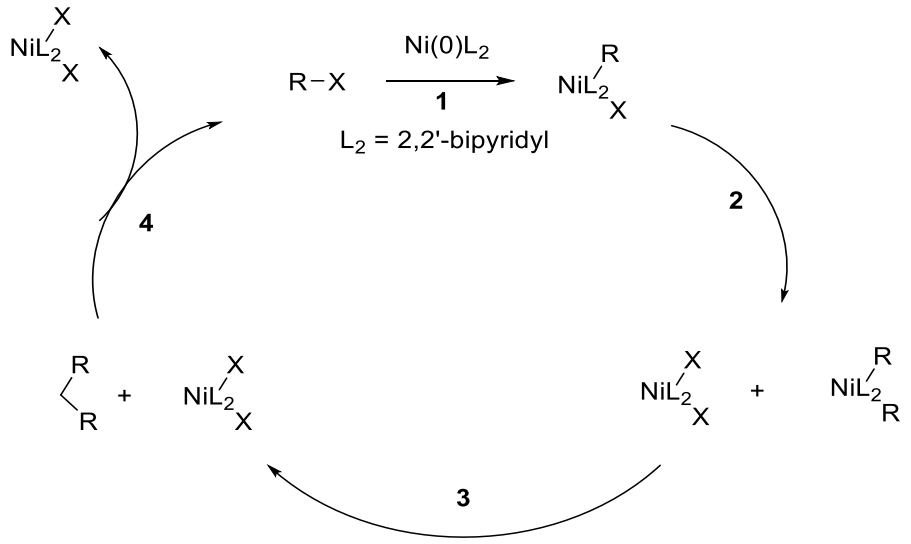

Scheme 1. Yamamoto reaction cycle

The oxidative addition of an aryl halide to a Ni(0) complex forms a stable 18 electron square planar Ni(II) complex. The next step in the mechanism is a metathesis step of two of the Ni(II) complexes to exchange ligands. There is no change in the net oxidation state. The 16 electron diaryl Ni(II) complexes are well suited for reductive elimination to complete the catalytic cycle by forming the aryl-aryl bond. The reaction does consume half the nickel in the form $Ni(II)X_2$ and for this reason Nickel (0) is typically added in stoichiometric quantities, a major drawback for large scale polymerisation. Modifications have been developed in which a reductant such a metallic zinc is added to reduce the $Ni(II)X_2$ back to Ni(0) *in situ*. Another drawback of the reaction is the necessity to perform the reaction in a high boiling aprotic solvent like DMF. Such solvents are usually poor solvents for aromatic polymers.[34]

Suzuki polymerisation

The Suzuki cross-coupling of an aryl halide with an organoboron reagent has been extensively used for the preparation of many conjugated polymers. It is particularly useful for the synthesis of polyfluorene or polyphenyl based materials, but has been less utilised in the preparation of electron rich polymers based on thiophene.[24] One of the issues is that the use of electron rich thienyl boronic acids or esters can lead to deboronation of the monomers or growing polymer chain during the polymerisation, limiting molecular weight. Therefore, the organoboron-containing monomer should preferentially be on a non-thiophene if possible. A second complication with the Suzuki polymerisation is the requirement for a base to activate the boronic ester/acid for cross-coupling. Many of the commonly used bases are aqueous thus this can lead to two-phase reaction media, and require the addition phase transfer catalysts to facilitate mixing. The solubility of the growing polymer can be a problem in such two phase mixtures. An early reported issue with Suzuki polymerisations was the end-capping of the growing polymer chain via the transfer of aryl groups from the phosphine ligands that are used in the polymerisation process. This can be suppressed by the use of more bulky ligands like tri(o-tolyl)phosphine or by the use of ligand-free catalysts.[35]

The mechanism is a three step process. The first step is the oxidative addition of palladium (0) into a carbon-halogen bond. Prior to the transmetallation addition, a base displaces the halogen on the palladium (II) species to create a more controlled reaction route for the boronic ester.

$$L_2PdR'X + NaOH \rightarrow L_2PdR'OH + NaX$$

The organoboron can then react after being activated by a Lewis base as it increases the rate of reaction due to its relatively low electropositivity. Finally reductive elimination occurs and the new C-C bond is formed.

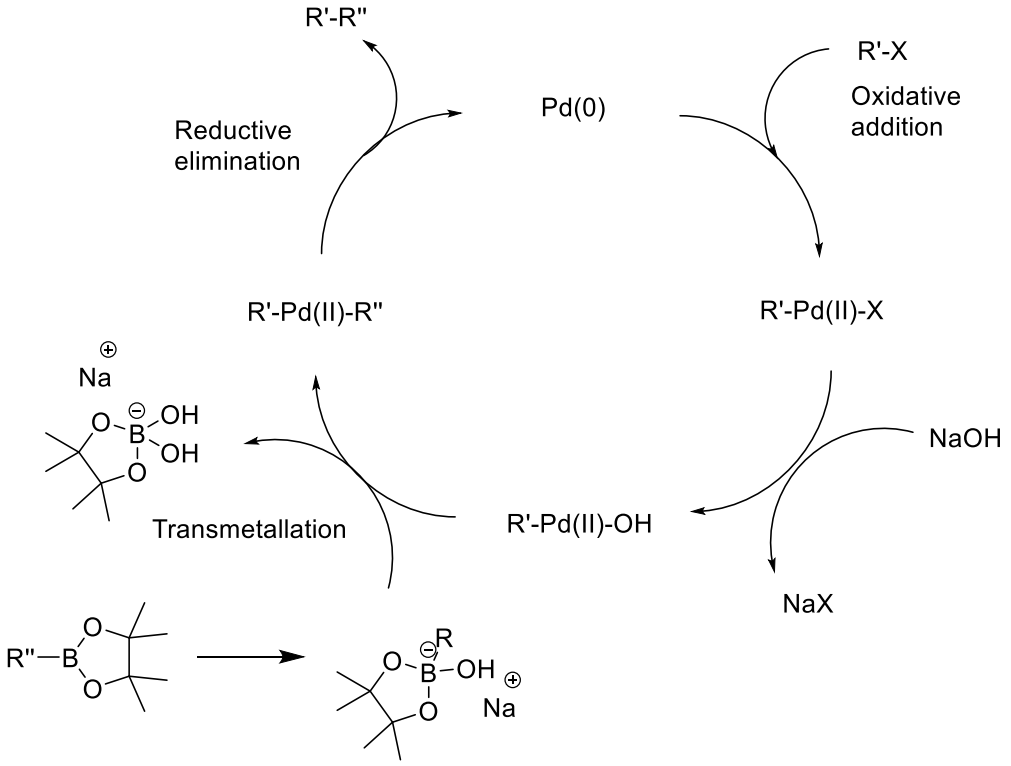

Scheme 2. Suzuki polymerisation catalytic cycle

One of the main advantages of using Suzuki coupling is the use of boronic ester monomers that are air stable and can be purified via flash chromatography. Also for large scale synthesis, the boronic esters are largely low in toxicity.

Stille polymerisation

Stille coupling is a simplified version of Suzuki coupling. The cross-coupling involves three steps as shown in Scheme 3. The first is the oxidative addition of the aryl halide, followed by the transmetallation and finally the reductive elimination. The primary drawback of large-scale Stille reactions are the large amounts of organostannanes as they are highly toxic. Despite the toxicity of tin they are still widely used as they react with a wide variety of functional groups.

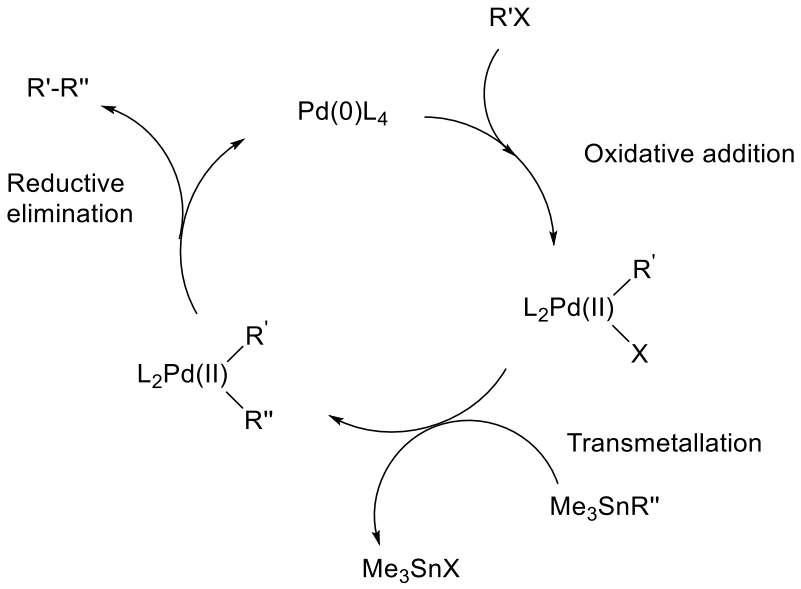

Scheme 3. Stille polymerisation catalytic cycle

There are two different type of polymer chain growth. All of the above mentioned polymerization techniques are a step growth mechanism. Step growth mechanisms involve monomers reacting with one another or any size oligomers or polymer and a high percentage conversion is needed in order to obtain high molecular weight polymers. Additionally with the step growth mechanism there is a rapid loss of monomer. Chain growth is the other mechanism and involves monomers reacting with an active centre of the growing chain. With step growth mechanism control of the molecular weights can be achieved by using an imbalance of monomer to selectively obtain low molecular weights.[36]

Carothers Equation

The above-mentioned condensation reactions take place as a one pot synthesis consisting of monomers, catalyst, solvent and ligands. The key components from a mathematical consideration however, are the monomers and the growing polymer chain. To judge how successful a polymerisation reaction is a number of different properties are assessed. Firstly the effectiveness of a polymerisation reaction can be judged on the extent of the reaction, ρ,

yield. This is the ratio of the number of monomers that have reacted and the number of monomers present at the start of the reaction and given by the equation

Equation 1

$$\rho(t) = \frac{n_0 - n(t)}{n_0}$$

Where n(t) is the number of monomers that are yet to react and n_0 is the number of monomers present at time t = 0. The degree of polymerisation is important as it relates to the polymer molecular weight by the total possible length of polymer divided by the number of unreacted monomers.

Equation 2

$$X_n(t) = \frac{n_0}{n\,(t)}$$

For the degree of polymerisation to be very high the number of monomers left in the reaction mixture has to be low. Combing the two equations give

Equation 3

$$X_n(t) = \frac{1}{1 - \rho(t)}$$

This is the Carothers equations and the important factor is that polymers do not form except at very high conversions in step polymerisations. This equation however only gives an average of the polymer chains lengths. For example if half the monomers have reacted, X = 2, but that does not means that the reaction mixture now consists of a mixture of dimers and monomers. It is only an average; specifically, it is the number average degree of polymerisation.

Equation 4

$$M_n = \frac{\sum_{i-1}^{\infty} n_i M_i}{\sum_{i=1}^{\infty} n_i}$$

Where M_n is the molar mass of the chain with a polymerisation index of n_i. The final parameter that is vital to assessing a polymer is weight average molecular weight as it gives an understanding of the dispersity of a polymer sample i.e. a distribution of the molar masses of the polymer chains. The weight average molecular weight is given by

Equation 5

$$M_w = \sum_{i=1}^{\infty} \omega_i M_i$$

Where ω is given by Equation 6.

Equation 6

$$\omega_i = \frac{n_i M_i}{\sum_{i-1}^{\infty} n_i M_i}$$

Combining the Equation 5 and Equation 6 gives Equation 7

Equation 7

$$M_\omega = \frac{\sum_{i=1}^{\infty} n_i \, M_i^2}{\sum_{i=1}^{\infty} n_i \, M_i}$$

The dispersity index of a polymer sample is therefore define as M_n / M_ω.

References

1. Heeger, A. J. Synthesis of Electrically Conducting Polymers. *Journal of the Chemical Society, Chemical Communications.* **16**, 578–580 (1977).

2. Samuel, I. D. W. & Turnbull, G. Organic semiconductor lasers. *Chemical reviews* **107**, 1272–95 (2007).

3. Tang, C. W. & VanSlyke, S. Organic electroluminescent diodes. *Applied Physics Letters* **51**, 913 (1987).

4. J. H. Burroughes *et al.* Light-emitting diodes based on conjugated polymers. *Nature* **347**, 539–541 (1990).

5. Tsumura, A. Koezuka, H. & Ando, T. Macromolecular Electronic device: Field-effect transistor with a polythiophene thin film. *Applied Physics Letters* **49**, 1210 (1986).

6. Tang, C. W. Two-layer organic photovoltaic cell. *Applied Physics Letters* **48**, 183 (1986).

7. Clayden, J. *et al.* Organic Chemistry. *Oxford University Press* **8,** 105-106 (2001).

8. Geoghegan, M. *et al.*, Polymer Electronics. *Oxford University Press* **1, 25-26** (2012).

9. Zheng, Q., Jung, B. J., Sun, J. & Katz, H. E. Ladder-type oligo-p-phenylene-containing copolymers with high open-circuit voltages and ambient photovoltaic activity. *Journal of the American Chemical Society* **132**, 5394–404 (2010).

10. Heeger, A. J. Semiconducting polymers: the Third Generation. *Chemical Society reviews* **39**, 2354–71 (2010).

11. Sirringhaus, H. *et al.* Mobility enhancement in conjugated polymer field-effect transistors through chain alignment in a liquid-crystalline phase. *Applied Physics Letters* **77**, 406 (2000).

12. Zhao, Y., Guo, Y. & Liu, Y. 25th Anniversary Article: Recent Advances in n-Type and Ambipolar Organic Field-Effect Transistors. *Advanced Materials* **25**, 5372-5391 (2013)

13. Bao, B. Z. Materials and Fabrication Needs for Low-Cost Organic Transistor Circuits. *Advance Materials* **12**, 227–230 (2000).

14. O'Brien, D., Bleyer, a., Bradley, D. D. . & Meng, S. Electroluminescence applications of a poly(phenyl quinoxaline). *Synthetic Metals* **76**, 105–108 (1996).

15. Lu, J.-Q. *et al.* Electronic transport mechanism of a molecular electronic device: structural effects and terminal atoms. *Physics Letters A* **323**, 154–158 (2004).

16. Kim, J.-S., Ho, P. K. H., Murphy, C. E. & Friend, R. H. Phase Separation in Polyfluorene-Based Conjugated Polymer Blends: Lateral and Vertical Analysis of Blend Spin-Cast Thin Films. *Macromolecules* **37**, 2861–2871 (2004).

17. Gill, W. D. Drift mobilities in amorphous charge-transfer complexes of trinitrofluorenone and poly-n-vinylcarbazole. *Journal of Applied Physics* **43**, 5033 (1972).

18. Forrest, S. R. The path of ubiqutous and low-cost organic electronic appliances on plastic. *Nature* **428** 911–918 (2004).

19. Mathijssen, S. G. J. *et al.* Dynamics of Threshold Voltage Shifts in Organic and Amorphous Silicon Field-Effect Transistors. *Advanced Materials* **19**, 2785–2789 (2007).

20. Zhang, W. *et al.* Systematic improvement in charge carrier mobility of air stable triarylamine copolymers. *Journal of the American Chemical Society* **131**, 10814–5 (2009).

21. Wu, W., Liu, Y. & Zhu, D. Pi-conjugated molecules with fused rings for organic field-effect transistors: design, synthesis and applications. *Chemical Society reviews* **39**, 1489–502 (2010).

22. Turbiez, M., Leeuw, D. M. De & Janssen, A. J. Poly (diketopyrrolopyrrole-terthiophene) for Ambipolar Logic and Photovoltaics. *Journal of the American Chemical Society* **131,** 16616–16617 (2009)

23. Holliday, S., Donaghey, J. E. & Mcculloch, I. Advances in Charge Carrier Mobilities of Semiconducting Polymers Used in Organic Transistors. *Chemistry of Materials* **26**, 647-663 (2013).

24. Thompson, B. C. & Fréchet, J. M. J. Polymer-fullerene composite solar cells. *Angewandte Chemie (International ed. in English)* **47**, 58–77 (2008).

25. Wudl, F. & Srdanov, G. Conducting polymer formed of poly(2-methoxy-5-(2′-ethylhexyloxy)-p-phenylene vinylene). *US Patent* **5,189,136**, (1993).

26. Knight, B. W. & Wudl, F. Preparation and Characterization of Fulleroid and Methanofullerene Derivatives. *Journal of Orgnic Chemistry* **60**, 532–538 (1995).

27. Yu, G., Gao, J., Hummelen, J. C., Wudl, F. & Heeger, A. J. Polymer photovoltaic cells — enhanced efficiencies via a network of internal donor–acceptor heterojunctions. *Science* **270**, 1789–1791 (1995).

28. Bao, Z., Dodabalapur, A. & Lovinger, A. J. Soluble and processable regioregular poly(3-hexylthiophene) for thin film field-effect transistor applications with high mobility. *Applied Physics Letters* **69**, 4108 (1996).

29. Ma, W., Yang, C., Gong, X., Lee, K. & Heeger, a. J. Thermally Stable, Efficient Polymer Solar Cells with Nanoscale Control of the Interpenetrating Network Morphology. *Advanced Functional Materials* **15**, 1617–1622 (2005).

30. Li, G. *et al.* High-efficiency solution processable polymer photovoltaic cells by self-organization of polymer blends. *Nature Materials* **4**, 864–868 (2005).

31. Liang, Y. *et al.* Highly efficient solar cell polymers developed via fine-tuning of structural and electronic properties. *Journal of the American Chemical Society* **131**, 7792–9 (2009).

32. Chen, H. *et al.* Polymer solar cells with enhanced open-circuit voltage and efficiency. *Nature Photonics* **3**, 649–653 (2009).

33. Liang, Y. *et al.* Development of new semiconducting polymers for high performance solar cells. *Journal of the American Chemical Society* **131**, 56–7 (2009).

34. Yamamoto, T. p-Conjugated Polymers with Electronic and Optical Functionalities : Preparation by Organometallic Polycondensation , Properties , and Applications. *Macromolecules rapid communications* **23**, 583–606 (2002).

35. Sakamoto, J., Rehahn, M., Wegner, G. & Schlüter, a D. Suzuki Polycondensation: Polyarylenes à la Carte. *Macromolecular rapid communications* **30**, 653–87 (2009).

36. Marsh, H. S. *et al.* Control of polythiophene film microstructure and charge carrier dynamics through crystallization temperature. *Journal of Polymer Science Part B: Polymer Physics* **52**, 700–707 (2014).

Chapter 2 - Synthesis and Device characteristics of Semiconducting polymers based on Indenopyrazine and Fluorene

Introduction

There are many reasons why organic semiconductors and their photophysical properties are relevant to optically pumped lasers. Firstly, organic semiconductors can have high molar absorption coefficients which result in light being absorbed very readily. For example, a thin film of 100 nm thickness of a typical conjugated polymer such as P3HT would absorb 90 % of the light incident upon it at the maximum absorption wavelength. This gives rise to light being absorbed over a very short path length which is a necessary requirement for achieving optical gain and stimulated emission. Both of these attributes have been discussed in Tessler's work on lasing using conjugated polymer films of poly(*p*-phenylenevinylene).[1] A third reason why organic semiconductors are well suited for use as laser materials is because their fluorescence spectra are broad and readily tuned, via a variety of synthetic modifications. Finally, a broad fluorescence spectrum allows for short pulse generation and broad-band optical amplification.

For lasers and organic light emitting diodes, materials that emit light efficiently are highly desired. The photoluminescence quantum efficiency (PLQE) describes quantitatively the efficiency of light emission. The PLQE is defined as the ratio of number of photons emitted from a sample over the number of photons that are absorbed (Equation 8).

Equation 8.

$$PLQE = \frac{Number\ of\ photons\ emitted}{Number\ of\ photons\ absorbed}$$

The measurement of photoluminescence efficiencies in thin film is different to that in solution. Thin films are difficult to quantify due to a series of optical problems that can influence the measurements, many of which can be overcome by methods suggested by de Mello *et al* using an integrating sphere.[2] Considerable work has focussed upon controlling PLQE, which at a fundamental level is related to the control and understanding of

intermolecular interactions. In the solid state or in concentrated solutions, organic semiconducting polymer chains can interact with adjacent polymer chains leading to the formation of aggregates, dimers or excimers which can quench light emission.[3] Organic semiconductors are used almost exclusively in the solid state in practical applications. Therefore a common approach to avoid quenching of emission in the solid state involves increasing the spacing between the light emitting units to prevent solid state quenching. With conjugated polymers this is commonly achieved by using long bulky side chains, which offer the dual properties of conferring solubility whilst keeping the polymers chains apart.

Optical gain is the most important requirement for the realisation of an organic semiconducting laser.[4] Optical gain describes the amplification of an optical signal directly without the need for conversion to an electrical signal as an intermediate. Using a simplified two level electronic system, when a photon is incident on an organic semiconductor, provided the photon is of sufficient energy, it causes an electron to be promoted from the lower $\mathbf{S_0}$ to the excited $\mathbf{S_1}$ energy level. This is the process commonly known as absorption. When a photon is incident on a material that is already in an excited state, it can stimulate the electron in the excited state, without being absorbed, to fall from the higher $\mathbf{S_1}$ energy level to the ground $\mathbf{S_0}$ energy level and cause the emission of a second photon (Figure 11).

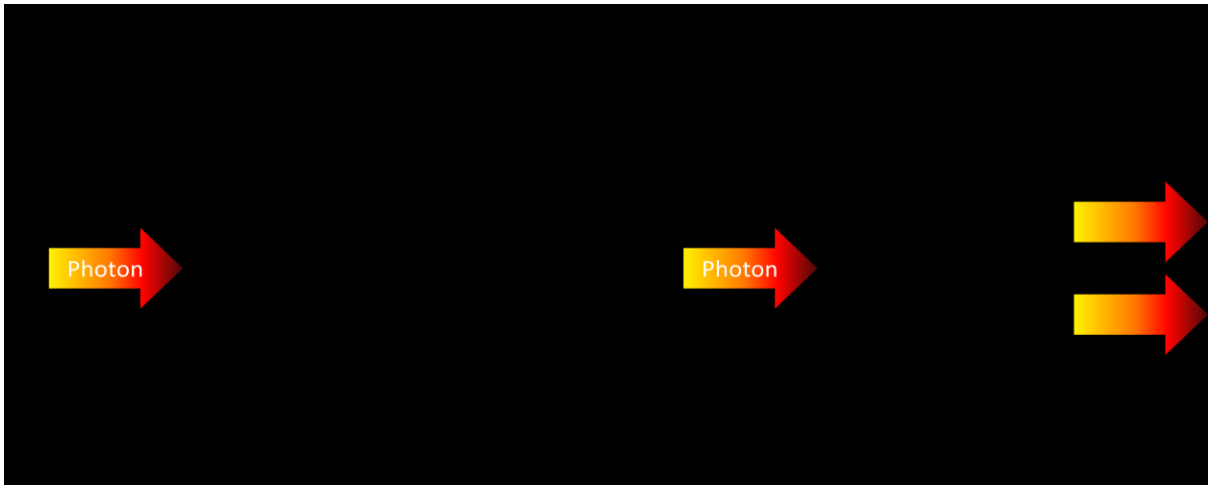

Figure 11. Optical absorption (left). Stimulated emission (right)

In optically pumped lasers this process is referred to as stimulated emission. It was Einstein who first proposed this idea based on thermodynamic considerations. The key fact is that the photon that is emitted on stimulated relaxation from the excited $\mathbf{S_1}$ to the lower energy $\mathbf{S_0}$ level has the same frequency, phase and direction as that of the incident photon. Therefore, the emission of this additional photon means that there has been amplification of the incident photon. For the case of organic semiconductors, as light travels further through the medium, there is stimulated emission of an exponentially increasing number of photons and so for small signals, the intensity, *I(z)*, increases exponentially with distance and can be expressed by Equation 9,[5] where *g* is the wavelength dependent gain coefficient of the medium and z is the distance the light travels through the medium.

Equation 9.

$$I(z) = I(z = 0)\exp(gz)$$

For a particular transition the cross-section for absorption and stimulated emission are equal. In order to obtain more stimulated emission than absorption at a particular wavelength, a greater number of species need to be present in the excited state than in the ground state i.e. population inversion. It is the product of the population inversion density, *N*, and stimulated emission cross-section, σ that gives the gain coefficient as described by Equation 10.

Equation 10.

$$g = \sigma N$$

In the simple $\mathbf{S_0}$ and $\mathbf{S_1}$ energy level diagram of Figure 11, population inversion cannot be practically achieved. However due to each energy level in organic semiconductors possessing additional sub vibrational energy levels, this population inversion can be achieved as depicted in Figure 12 due to the relative rates of the transitions that are involved.

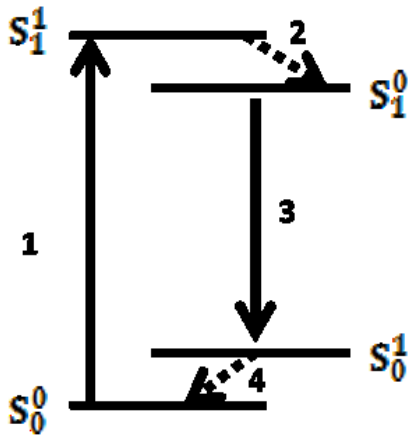

Figure 12. Four level energy diagram absorption transition (1) emission transitions (3) and two thermal relaxation transitions 2 and 4.

A four-level system is analogous to the vibronic levels within the $\mathbf{S_0}$ - $\mathbf{S_1}$ model. When a photon possessing an energy that is greater than the energy required for the promotion from the ground state to the lowest excited state, the electron can go into the higher energy first vibronic level $\mathbf{S_1^1}$ of the $\mathbf{S_1}$. This is represented by the transition **1** and is equivalent to absorption. From this excited vibronic state of the $\mathbf{S_1}$ level the electron rapidly relaxes down to the $\mathbf{S_1^0}$ level through a process of vibrational cooling depicted by transition **2**. From this lowest energy singlet state, emission and lasing are able to take place (transition **3**) resulting in relaxation to the vibrational excited ground state of $\mathbf{S_0^1}$ and emission of light. The electron can also decay through a series of non-radiative pathways, which is a loss mechanism. Finally there is the rapid transition from the excited vibronic ground state $\mathbf{S_0^1}$ to the $\mathbf{S_0^0}$ with the

excess energy being dissipated as vibronic and thermal relaxation. It is the rapid transition of **2** and **4** that allow for the creation of a population inversion between the $\mathbf{S_0^1}$ and the $\mathbf{S_1^0}$ for a very low rate of excitation. In this scenario it can be said the threshold for lasing is low. Relaxation can also take place from the $\mathbf{S_1^0}$ to the ground state of the $\mathbf{S_0}$ causing emission of a photon of a higher energy than transition **3**.

The vibrational relaxation of the excited state to $\mathbf{S_0^1}$ gives rise to a photon emission that is of a lower energy than that of the photon absorbed, and contributes to the overall Stokes shift of a particular polymer. Another factor that gives rise to a shift to a longer wavelength of emission, is the distribution of effective conjugation chain lengths within a polymeric system. Promotion to the singlet state on one polymer chain does not necessarily result in emission from the excited state of that particular chain. The excited state can transfer to a neighbouring polymer chain which has a lower excited state energy level. This is more prevalent in the solid state where closer packing is generally observed and interchain transfer is more probable.

The larger the shift in emission wavelength the better suited the material is for use in lasing because it reduces the self-absorption at the lasing wavelength. Attempts have been made to increase the separation between absorption and emission by blending two different materials with varying band gaps.[6,7] Another related way of separating the emission from absorption is to use copolymers consisting of a donor (wider band gap) and an acceptor (narrower band gap) moiety (Figure 13). [8,9] Here absorption would occur from the delocalised HOMO and then the exciton would transfer to the localised acceptor and emit.

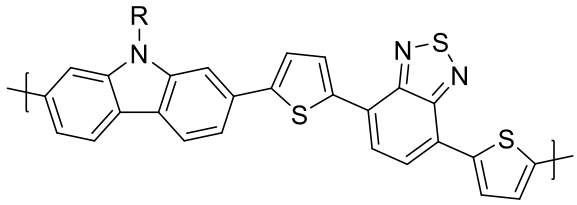

Figure 13. PCDTBT

There are a number of different approaches to improving optical gain. One is to dilute the material in a polymer matrix in order to enhance the luminescence efficiency by preventing quenching.[10] For conventional polymers like poly(3-hexylthiophene), dilution of the polymer in a matrix in order to enhance their luminescence dramatically reduces their charge carrier mobility, and a low charge carrier mobility limits the thickness of films that can be used.[11,12] An alternative approach to polymer dilution recognizes that effective charge carrier transport can result from a mixture of high interchain mobility and the existence of a set of preferential interchain hopping sites that connect otherwise relatively isolated neighbouring chains.[13]

There are two main approaches to studying gain in organic semiconducting materials. The first is transient absorption spectroscopy. This involves a sample being excited by a short pulse pump to generate excited species. This is followed by a time delayed probe pulse in order to measure the change in the transmission due to the presence of the generated excited species. The alternative approach is amplified spontaneous emission which involves producing a slab waveguide of the organic semiconductor. The edge of the sample is excited with a pulse laser beam and studying the light that is emitted from the semiconductor the amount of stimulated emission that is emitted can be calculated.

There are a range of different materials that are interesting in terms of their luminescent properties and can be considered attractive in terms of their feasibility to be used in lasers. This can be classified into four groups and are depicted in Figure 14. The first group of note are small molecules such as anthracene (Figure 14, **a**) and tris (8-hydroxyquinoline)

aluminium (Figure 14, **b**) which have previously been used as active layers in green OLEDs.[14] Originally the work focused on single crystals, however handling and growing these proved to be problematic. It was the discovery of electroluminescence in evaporated thin films of small molecules that attracted a great deal of attention.[15] The second group are conjugated dendrimers (Figure 14, **e**).[16] This consist of a core chromophore which defines the optical properties such as the wavelength of the light emitted. The core is surrounded by dendrons and at the end of these dendrons are the surface groups that offer solubility. The third type are spiro—compounds (Figure 14, **f**).[17] These consist of a pair of conjugated oligomers coupled to each other via a spiro linkage. Such an orthogonal arrangement can suppress molecular stacking in the solid state.

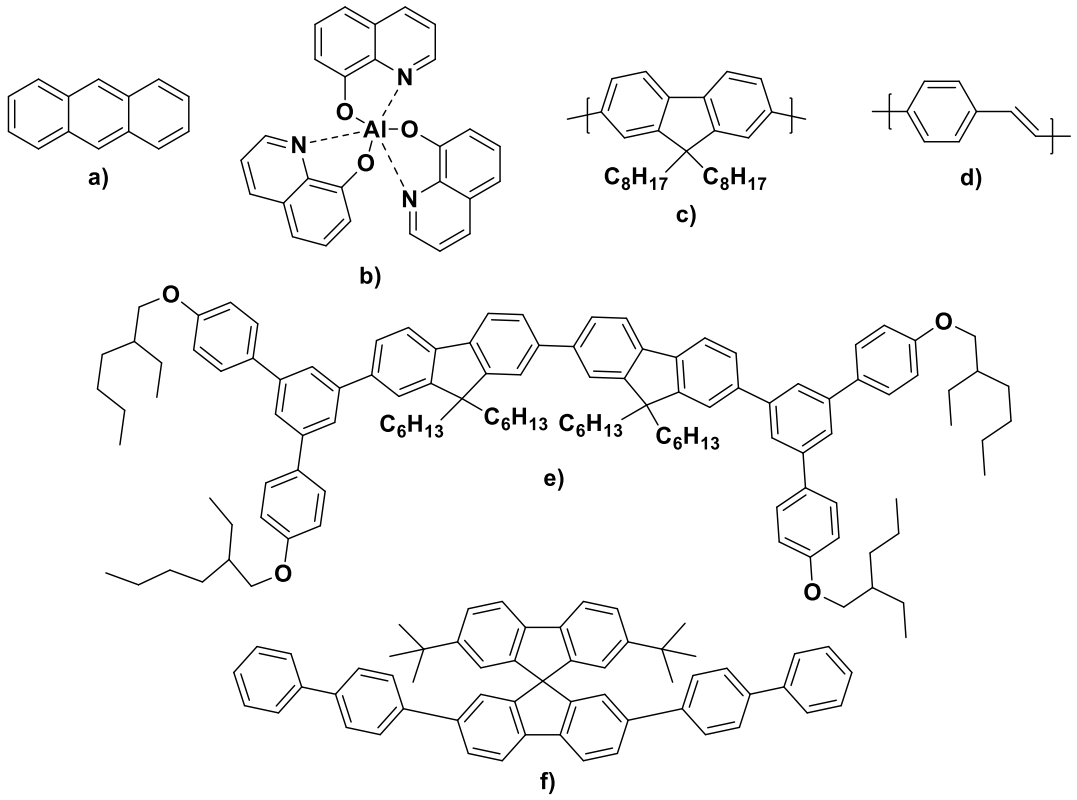

Figure 14. Classes of current popular materials: (a) Anthracene; (b), Tris-(8-hydroxyquinoline)aluminium; (c) poly(9,9--di-*n*-octylfluorenyl-2,7-diyl); (d) poly(*p*-phenylene vinylene); (e) bis(fluorene) cored first generation dendrimer and (f) spiro linked oligomer.

The fourth and final group are conjugated polymers. They are more linear than the branched dendrimer molecules and their synthesis is typically easier than the spiro molecules. Two

polymers that have been studied extensively are poly(dialkylfluorenes) (Figure 14 **c**) and poly(phenylene vinylene) (Figure 14 **d**).

Polyfluorene has attracted considerable attention due to its high photoluminescence and liquid crystalline behaviour.[18] Considerable work has combined polyfluorenes with other monomers such as the work by Theander *et al* who investigated the combination of polyfluorene with 2-methoxy-5-(2'ethyl-hexyloxy)-*p*-phenylenevinylene (MEH-PV).[19] The combination of a small amount of narrow band gap and wide band gap polymers allowed for the majority of the absorption to occur on the high energy polyfluorene and then transfer via Förster transfer to the low energy section.[20]

Typically there is a trade off with designing organic semiconductors for lasing between achieving a high charge carrier mobility and efficient light emission. High carrier mobility is broadly achieved by having rigid and planar chains that promote π-stacking. A high degree of crystallinity helps to remove defects and aids the stacking of chains assisting inter-chain charge transport. For efficient optoelectronic behaviour chromophores need to avoid interference with their environment and with each other via interchain effects. Amorphous materials have the advantage of not having grain boundaries, avoiding light scattering. However amorphous materials tend to have lower charge carrier mobilities. Bradley *et al* demonstrated an interesting approach to overcome this dilemma, demonstrating simultaneous optimisation of charge carrier mobility and optical gain in semiconducting polymer films of poly(dialkylfluorenes) with the introduction of a limited number of hopping sites between relatively isolated polyfluorene chains (Figure 15). This approach led to polymer films with mobilities in the order of 10^{-2} cm^2 $V^{-1}s^{-1}$ and excellent light-emission characteristics.[13] In their study they used a series of polymers consisting of the 9,9-di-*n*-octylfluorene copolymerised with 9,9-di-1-methyl-4-butyl-fluorene. They produced a range of polymers that had alternating short and long chains (Figure 15). The presence of the short-chain containing

fluorene monomers was suggested to allow close intermolecular contacts at limited points along the polymer backbone, where two short chain monomers on adjacent polymer chains were in close contact. These sites facilitated charge transport at a limited number of sites, such that overall luminescence efficiency was not substantially influenced. Such an approach appears attractive for the development of electrically pumped organic lasers. It is important to be able to inject sufficient charge into the structure to reach the electron density lasing threshold, and therefore high mobility materials with high luminescence efficiency are required.

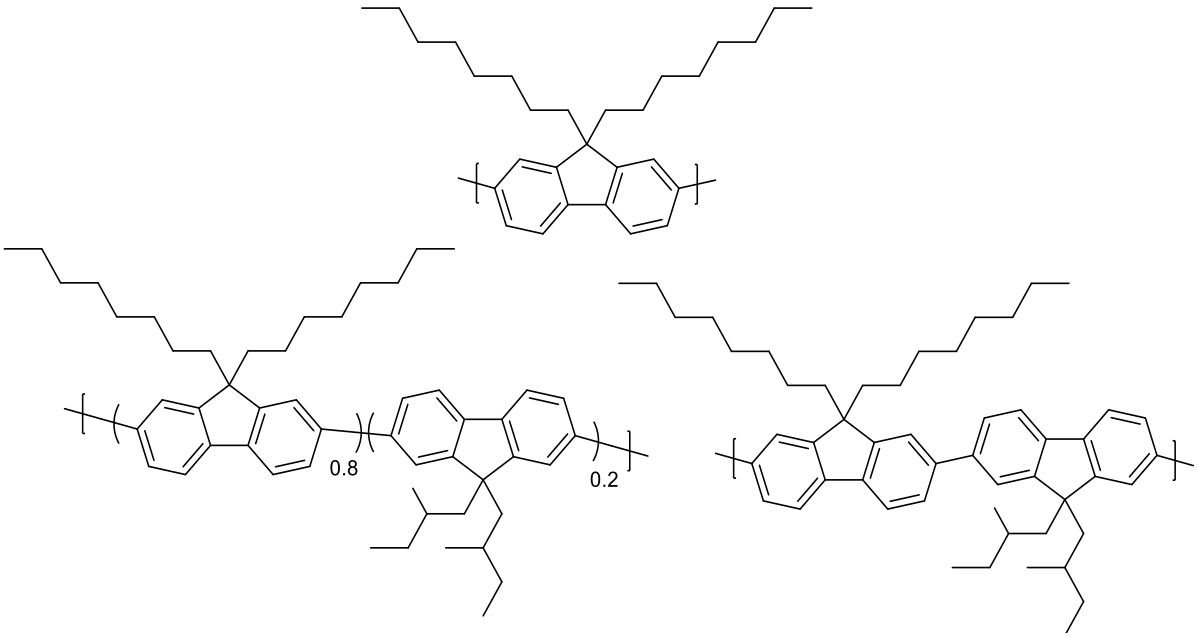

Figure 15. Series of Polyfluorene containing polymers reported by Bradley *et al.*[13]

Aims

Building on the work reported on the alternating fluorene systems, the aim of this study was to synthesise a series of novel polymers with improved charge carrier mobility whilst still retaining their strong photoluminescence characteristics. In particular we also desired to improve the electron transport of the target polymers. Our approach was to extend the conjugation length of the polymer by the incorporation of rigid, extended aromatics instead of fluorene. Here the expectation was that the reduced conformational disorder might improve charge transport. A second design criterion was to incorporate electron deficient groups in order to modify the LUMO of the polymer and facilitate electron injection and perhaps improve electron transport. Therefore we believed indenopyrazine (Figure 16) was an interesting co-monomer target. Previous computational studies by Jung *et al*[21] had investigated the difference between indenofluorene and indenopyrazine. DFT simulations of the two small molecules found that there was a predicted reduction in the band gap on replacing the central benzo unit with pyrazine.[21] This reduction in the band gap occurs because the LUMO is stabilised by a greater amount with respect to the HOMO on changing from the benzo to pyrazine unit. The nitrogen atoms plays a key role in the stabilisation of the LUMO. Figure 16 shows the calculated energy orbitals for the HOMO and LUMO of indenofluorene and indenopyrazine. It can be seen that the size of the lobes on the nitrogen atom on indenopyrazine are much larger in the LUMO than the HOMO. Based on quantitative atomic contributions, the contribution of the nitrogen to the HOMO is 2.17% whereas for the LUMO the nitrogen contributes 35.26%. Therefore the nitrogen is introducing more stabilisation of the LUMO than the HOMO resulting in a smaller HOMO-LUMO band gap for indenopyrazine than indenofluorene.

Table 1. Percentage contribution of the nitrogen atom to the HOMO and LUMO of the indenopyrazine ring[21]

	HOMO contribution (%)	LUMO contribution (%)
Indenopyrazine	2.17	35.26

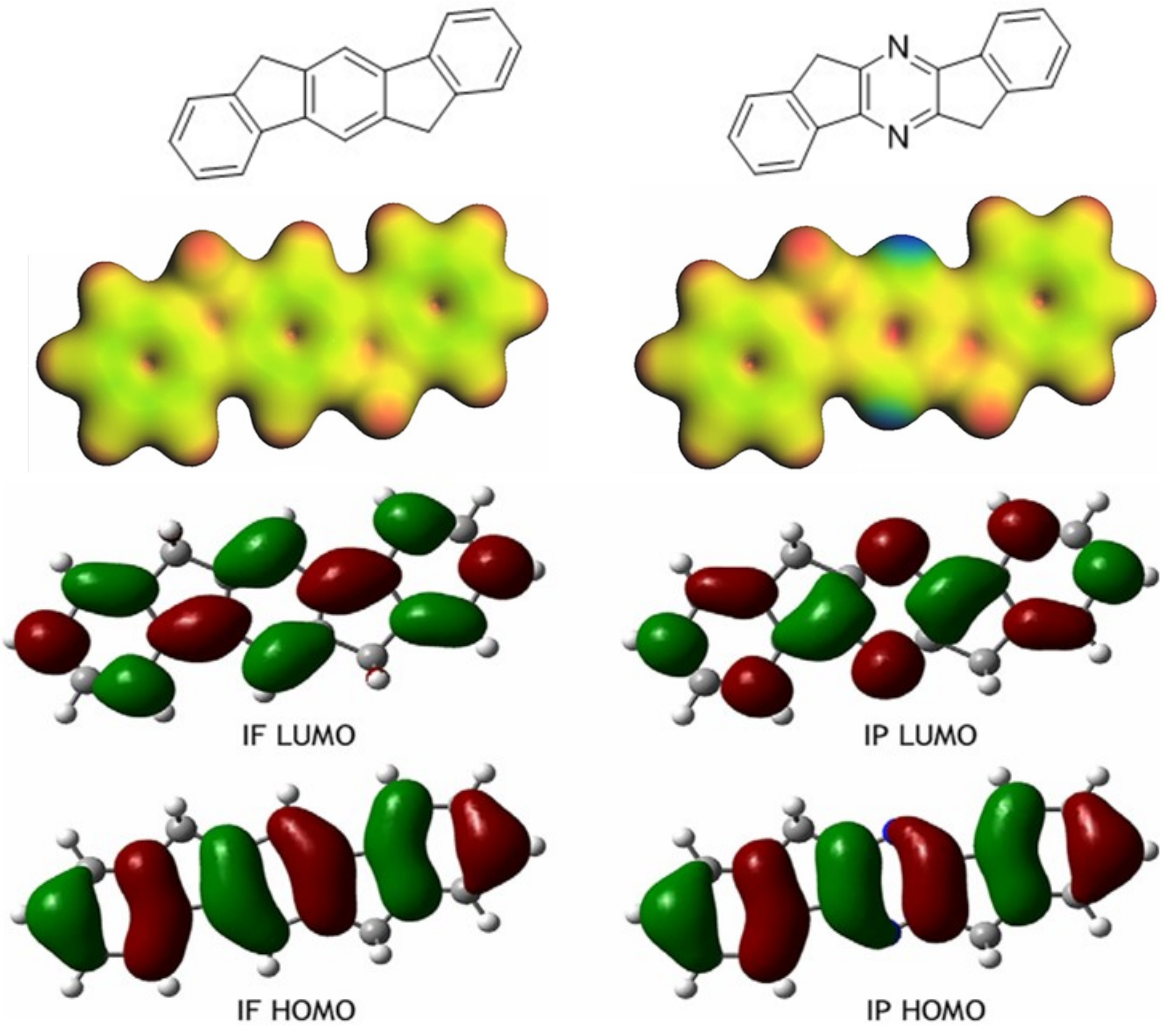

Figure 16. The potential energy surface, HOMO and LUMO levels of indenofluorene (IF) on the left and indenopyrazine (IP) on the right. Modified from reference.[21]

Similar to the work of Bradley et al, we planned to maximise mobility whilst trying to maintain adequate levels of PLQE by the copolymerisation of both a short alkyl chain (C_3H_7) and a long alkyl chain (C_8H_{17}) fluorene, with a branched short chain ($C_1C_4H_{11}$) and long chain (C_8H_{17}) indenopyrazine to produce a full complement of short and long chain alternating copolymers. For the indenopyrazine, a short branched alkyl chain was used in order to be able to draw comparisons with the short branched chain of the fluorene stated

studies.[13] A series of the homo indenopyrazine polymers with branched-C_1C_4, branched-C_2C_6 and straight-C_8 alkyl chains were also synthesised and their physical properties recorded (Figure 17).

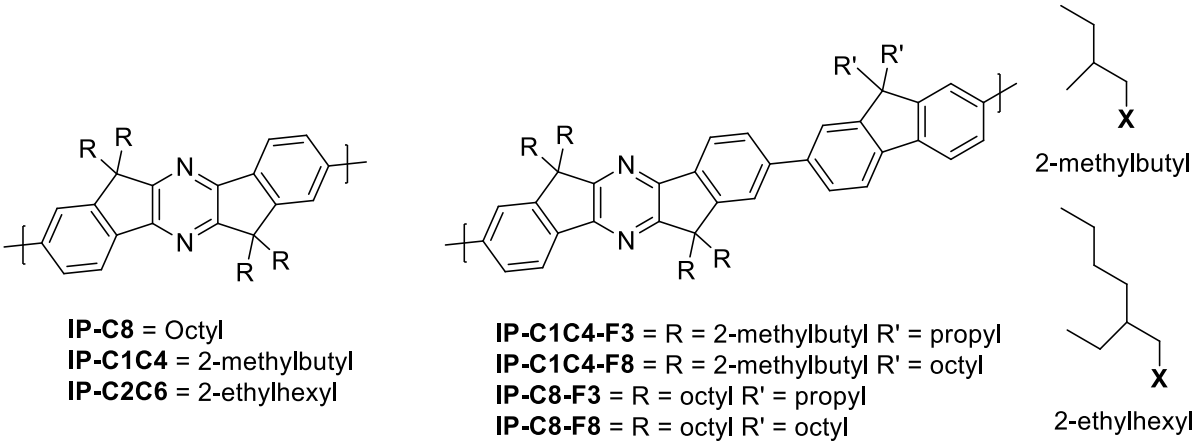

Figure 17. Target polymers of indenopyrazine and copolymers of indenopyrazine with fluorene.

Octyl and 1-methylbutyl alkyl chains were chosen for use in the indenopyrazine-fluorene series as it was predicted that the combination of short and long alkyl chains would promote packing between polymer chains whilst not compromising on solubility (Figure 18). Furthermore they were the same two alkyl chains used in the previous study, allowing for a comparison of results. The 2-ethylhexyl side chain was also chosen for use in later work when the indenopyrazine monomer was to be copolymerised with an electron-withdrawing accepting unit, whereby the resultant polymers were to be tested for use as active layers in solar cells. Ethylhexyl side chains have been shown to be some of the most successful in solar cell performance.[22]

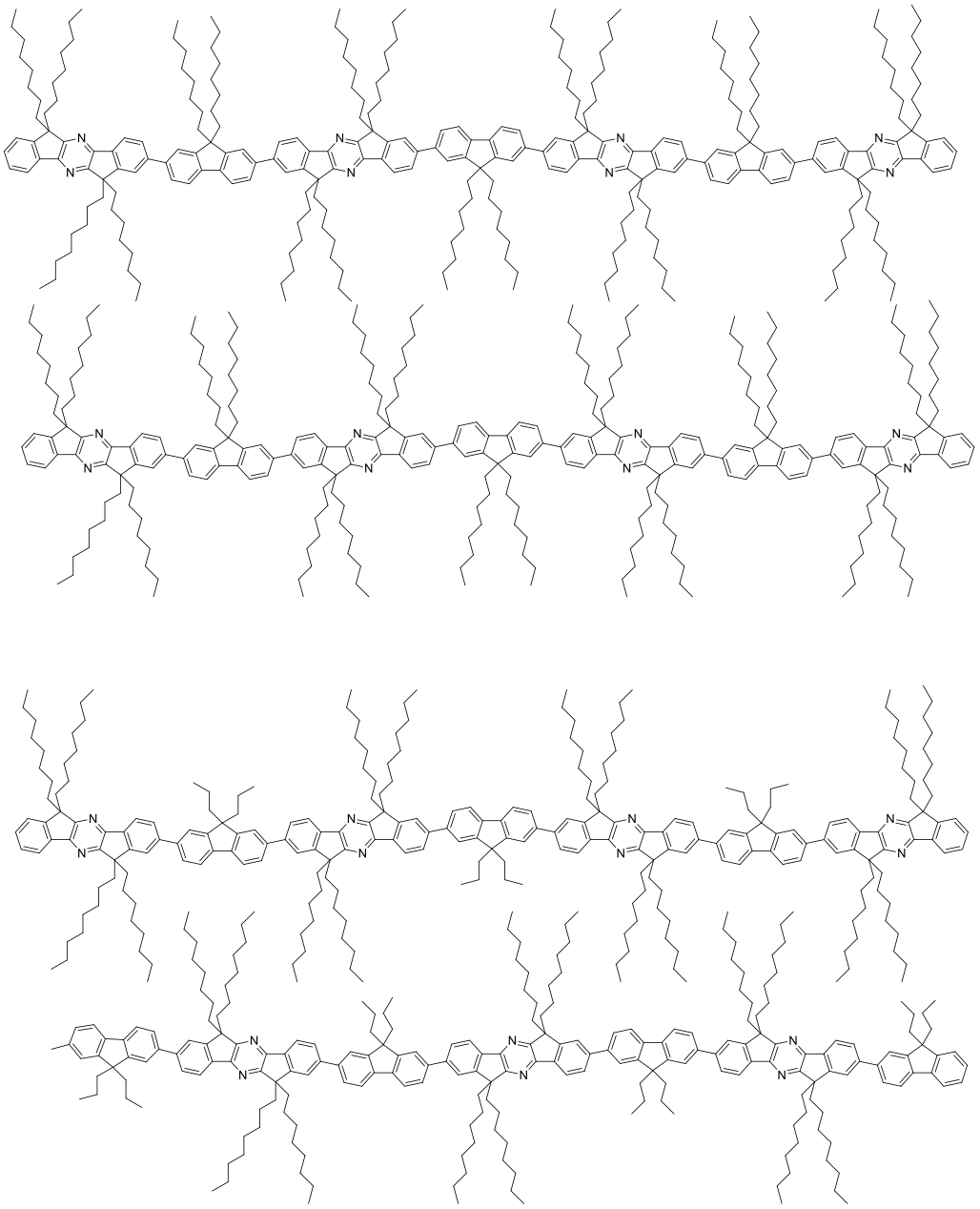

Figure 18. Difference in packing due to side chain length

Synthesis and Characterisation of Indenopyrazine monomers and homo-polymers

The synthesis of the target materials is shown in Scheme 4. The synthesis of monomer **1** was performed via a modified literature procedure.[23,24] The first modification was made to the initial step. In the original procedure, dry hydrochloric acid was bubbled through a benzene solution of the 5-bromoindanone in the presence of iso-pentylnitrite at 40°C. We found that stirring a toluene solution of 5-bromoindanone, iso-pentylnitrite and concentrated hydrochloric acid solution at 40°C gave a slightly improved yield (from 77 % to 80 %), but, more importantly, it allowed the reaction to be performed on a much larger scale without any special precautions. Formation of the dihydrodiindenopyrazine by the reduction of 5-bromo-2,3-dihydro-2-(hydroxyimino)inden-1-one in the presence of ammonia proceeded smoothly over 3 days to give a reasonable yield of product (61%). Due to poor solubility, this was washed and used without further purification.

For the alkylation of the dihydrodiindenopyrazine, the original literature procedure which utilised DMSO as the reaction solvent was also modified to facilitate purification. Dihydrodiindenopyrazine and the respective alkyl bromide and a phase transfer agent (tetrabutylammonium bromide) were dissolved in carefully degassed toluene and degassed sodium hydroxide solution was added. The resultant two-phase mixture was refluxed under argon in the absence of light for 3 days to afford the tetralkylated indenopyrazines **1**-**3**. We found stringent exclusion of oxygen was necessary to prevent undesired oxidation of the bridged benzylic positions. Following purification by column chromatography yields of the straight chain octyl derivative **1** were good (80%), with a slightly lower yield for the branched 2-ethylhexyl derivative **3** (62%), probably due to the fact that **1** was a crystalline solid, whereas **3** was a colourless oil. For the short chain derivative **2**, a much lower yield of 30% was obtained, possibly due to an increased tendency for 1-bromo-2-methylbutane to

undergo undesired elimination reactions to 2-methyl-but-1-ene in the presence of base. It was believed that 1-bromo-2-methylbutane may have a higher tendency to undergo elimination than 1-bromo-2-ethylhexane due to the reduced steric crowding around the hydrogen β to the Br for the former over the latter.

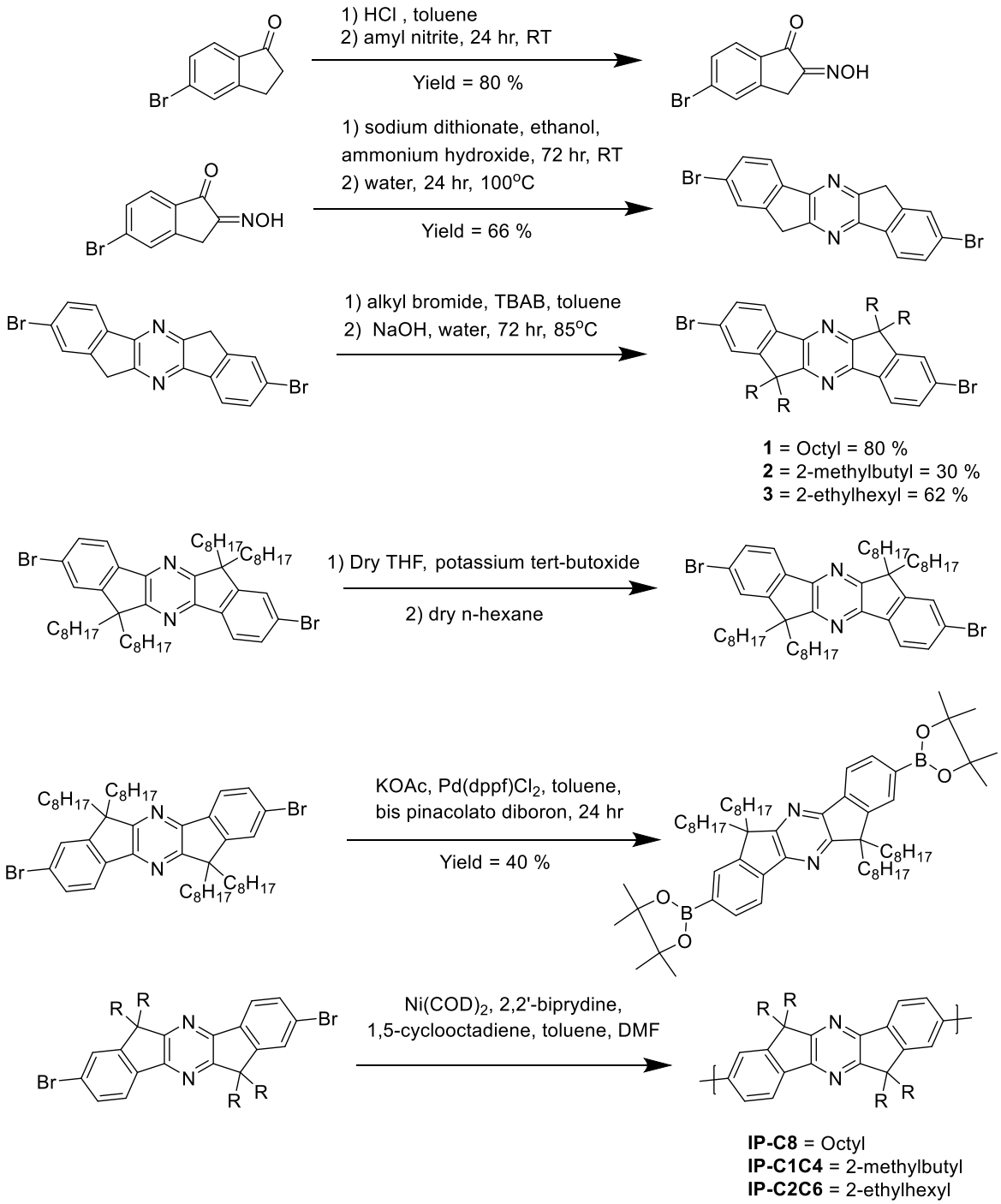

Scheme 4. Synthesis of Indenopyrazine monomer 1, 2, 3 and the corresponding homo polymers IP-C8, IP-C1C4 and IP-C2C6.

For monomers **1-3** an extra purification step was performed, based on previous work by Meijer et al.[25]

Prior to their study, the emission from polyfluorenes, was described as exhibiting a narrow emission band accompanied by a broad red-shifted emission contribution,[26] with the broad red shifted emission being attributed to the bulk properties of polyfluorene. Many attempts were made such as block copolymerisation,[27] dendronisation[28] and end-capping[29] to alter these bulk properties and a conclusion was drawn that intermolecular interactions dominate the bulk material properties. However, List *et al*. demonstrated that many of the emissive characteristics can be reproduced by incorporating a keto defect into the polymer backbone.[30]

Meijer worked on a series of oligo- and polyfluorenes and studied their photoluminescence properties. They proposed an extra purification step to remove any partially alkylated fluorene present, since they have an acidic hydrogen present that leads to defects in the final polymer. Stirring the monomer materials in the presence of a base in anhydrous hexane would react with any partially alkylated fluorene due to the acidity of the bridgehead protons and therefore become insoluble salts. The resulting salt could be simply removed by filtration through a short silica column. They concluded that the origin of the broad red-shifted emission band was due to on-chain defects and that the removal of the occurrence of this rapid on-chain diffusion is a route to improving performance.[31]

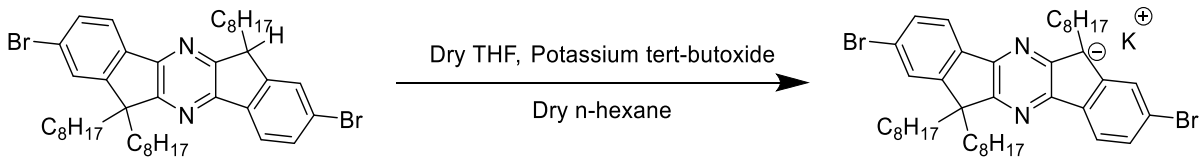

Scheme 5. Purification of octyl indenopyrazine monomer

Following the procedure previously performed by Meijer *et al,* **1-3** were dissolved in dry THF and stirred with potassium tert-butoxide to react with any trace amounts of mono, di or

tri-alkylated products that had an acidic hydrogen present to form the potassium salt. Subsequent removal of THF under high vacuum, and dissolution of the product in dry hexane allowed the insoluble potassium salt to be removed via vacuum filtration. In all cases about 85 % of the purified material was recovered, with the main loss being due to transfer issues. However, in all cases ^{1}H NMR showed there was no difference in the spectra before and after this step.

For 2,8-dibromo-6,6,12,12-tetra-2-methylbutyl-6-12-dihydro-diindeno[1,2-b,1',2'-e]pyrazine it was possible to grow and isolate a crystal from a dilute solution of the monomer in hexane (approx. 1 mg/10 mL), for which a crystal structure was isolated (Figure 19). It clearly demonstrates the planar backbone of the five fused rings and perpendicular orientation of the branched alkyl chains with respect to that backbone.

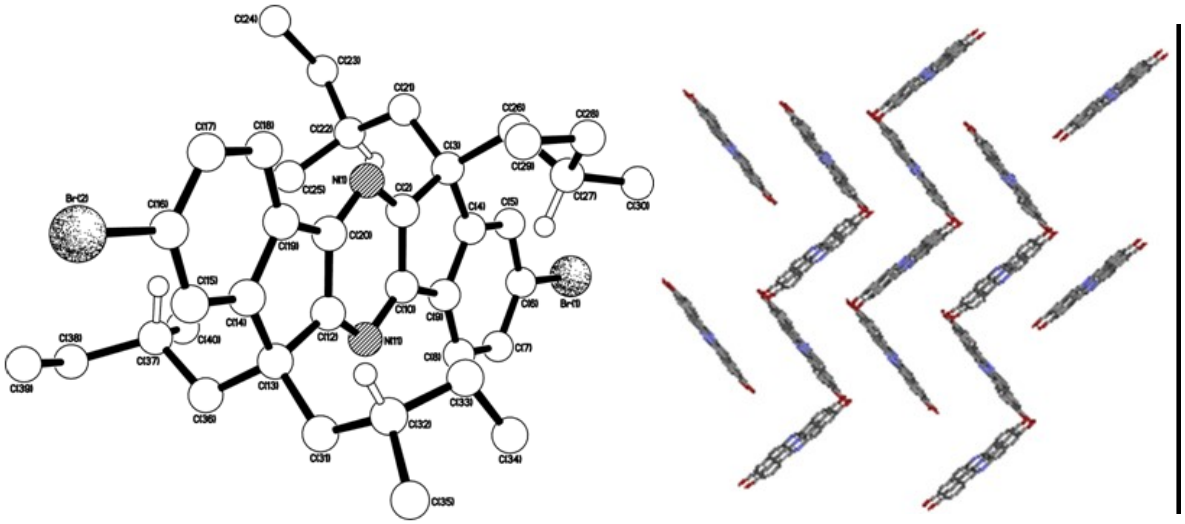

Figure 19. Left: Crystal structure of 2,8-dibromo-6,6,12,12-tetramethylbutyl-6-12-dihydro-diindeno[1,2-b,1',2'-e]pyrazine showing the orientation of the alkyl chains in relation to the monomer backbone. All the hydrogens have been removed except for the tertiary hydrogen present on each of the 4 alkyl side chains. Right: Packing of individual indenopyrazine molecules (side chains removed for clarity). *Crystal data for* 1: $C_{38}H_{50}Br_2N_2$, M = 694.62, orthorhombic, $P2_12_12_1$ (no. 19), a = 8.6592(2), b = 19.8570(5), c = 20.3443(6) Å, V = 3498.12(16) Å^3, Z = 4, D_c = 1.319 g cm^{-3}, μ(Mo-Kα) = 2.345 mm^{-1}, T = 173 K, pale yellow tablets, Oxford Diffraction Xcalibur 3 diffractometer; 11825 independent measured reflections (R_{int} = 0.0397), F^2 refinement.[43] R_1(obs) = 0.0556, wR_2(all) = 0.1350, 7662 independent observed absorption-corrected reflections [$|F_o| > 4\sigma(|F_o|)$, $2\theta_{max}$ = 65°], 413 parameters. The absolute structure of 1 was determined by a combination of R-factor tests [R_1^+ = 0.0556, R_1^- = 0.0697] and by use of the Flack parameter [x^+ = 0.000(11)].

The three homo polymerisations were carried out under Yamamoto polymerisation conditions in sealed microwave vials and the results are recorded in Table 2. A thoroughly degassed solution of indenopyrazine monomer in a DMF/toluene was added to 2.2 equivalents of $Ni(COD)_2$, 2,2'bipyridine, and 1,5-cyclooctadiene in DMF/toluene and the reaction was heated to 80 °C for 72 hr. A mixed solvent system of toluene and DMF was utilised, since the Ni catalyst requires a polar, aprotic solvent like DMF to be present. However the polymer is poorly soluble in DMF, so a co-solvent of toluene was added to help the growing polymer remain in solution. The Yamamoto polymerisation has previously been shown to be quite sensitive to the ratio of the solvent, so we utilised a 1:1 ratio as a compromise between reactivity of the catalyst and solubility of the polymer. After an initial 1 hour of heating, a colour change from dark green to a much lighter luminescent green/blue was observed. The polymerisations were carried out for 3 days to ensure a high molecular weight was achieved because of the step growth method of polymerisation. The resulting polymers were precipitated into methanol and low molecular weight impurities and catalyst residues removed by extraction (Soxhlet) with methanol and acetone. The polymer was then extracted into hexane followed by chloroform, concentrated, re-dissolved in chlorobenzene and precipitated into cold methanol. This yielded the resulting polymers as bright yellow fibres.

Table 2. Yield, molecular number (Mn), molecular weight (Mw), polydispersity index (PDI) and the degree of polymerisation (DP) for the three homo polymers

Polymer	Yield (%)	M_n/kg/mol	M_w/kg/mol	PDI	D.P[1]
IP-C8	42	37	82	2.2	52
IP-C1C4	12	8	14	1.8	14
IP-C2C6	40	42	52	1.2	59

[1] Degree of polymerisation is based on Mn divided by molecular weight of repeat unit

The yields were calculated based on the fraction of the soxhlet extraction where the majority of the polymer resided. For **IP-C8** and **IP-C2C6** this was the hexane fraction. Chloroform extraction of these two polymers was performed but only trace amounts of polymer were

recovered containing similar molecular weights to the previous hexane fractions. The high solubility in hexane is probably due to the high alkyl chain density on the polymer backbone. For **IP-C1C4** the majority of the polymer was soluble in the acetone fraction. This difference in solubility can be attributed to the difference in length of polymer and alkyl chains. **IP-C1C4**, having the shortest of alkyl chains, was likely to have been the first to precipitate out of solution during the polymerisation due to poor solubility in the reaction solvent. This low molecular weight then resulted in solubility in acetone. The repeat units in **IP-C2C6** and **IP-C8** both possess longer alkyl chains than that of the repeat unit in **IP-C1C4**.

The degree of polymerisation was calculated to take into account the different length and weight of the alkyl chains. This was done by dividing the molecular number of each polymer by the molecular weight of the repeating unit. The straight chain **IP-C8** had the largest degree of polymerisation with an average of 52 repeat units. The branched polymers of **IP-C1C4** had a lower degree of polymerisation 14 repeat units. The larger degree of polymerisation of **IP-C8 and IP-C2C6** can be attributed to the solubility of the polymers in solution during polymerisation. **IP-C2C6** had a bimodal distribution of molecular weights which can be attributed to the increased solubility due to side-chain effects.

Optical Properties and Energy Levels

The wavelengths of the absorption and emission maxima are an important property of semiconducting polymers with regards to achieving amplified spontaneous emission. The UV-Vis absorption of **IP-C8, IP-C2C6** and **IP-C1C4**, in both solution and spun-cast thin film were recorded and are displayed in Figure 20 and summarised in Table 3. The UV-Vis graph of **IP-C8** has an absorbance maximum in chloroform of 450 nm and in the solid state had a very similar absorption at 451 nm. The small change in the position of the absorbance maximum suggests little order in the solid state. There is also a slight shoulder around 420

nm for both the solution and thin film spectra, and the intensity of this peak increases slightly upon film formation.

The solution UV-Vis spectrum of **IP-C2C6** is similar to that of **IP-C8** having an absorption maximum at 452 nm. This value is very similar to the reported emission of **IP-C2C6** on glass 449 nm[32], and a slightly more pronounced lower wavelength shoulder. This is to be expected because electronically the alkyl chains only contribute a very small amount to the overall energy levels of the final polymer. Upon film formation, there is again very little change to the absorption spectra, with the absorption maximum occurring at 449 nm, a slight hypsochromic shift compared to solution, and the shoulder peak becoming more pronounced upon film formation for this polymer.

The solution and thin film UV-Vis spectrum of **IP-C1C4** were recorded but the film quality was very poor due to the low molecular weight nature of the polymer. This gave rise to the large comparative absorbance of the glass, probably due to scattering. The absorption maximum for **IP-C1C4** is 440 nm which is blue-shifted by 10 nm compared to both **IP-C8** and **IP-C2C6** and can be attributed to the low molecular weight of the polymer. The solid state spectrum appears considerably different to the other polymers, with an appreciable broadening of the absorption and the appearance of a new longer wavelength shoulder. This could perhaps be indicative of some intramolecular ordering in the thin film. In addition, the indenopyrazine polymer show a high molar extinction coefficient of 59 000 M^{-1} cm^{-1} and 57 100 M^{-1} cm^{-1} at 450 nm (Table 3).

Variable temperature solution UV-Vis spectroscopy was also performed in order to investigate the formation of any solution aggregates. In all cases, the increased temperature simply resulted in a reduction in absorption intensity, related to the thermal expansion of the solvent, rather than any change of shape, suggesting that the polymers do not form aggregates

in solution which is in agreement with **IP-C2C6** having a bimodal distribution of molecular weights rather than forming aggregates. As expected, **IP-C8**, **IP-C1C4** and **IP-C2C6** all exhibit a large optical band gap of 2.60, 2.81 and 2.58 eV respectively based upon the onset of absorption in thin film.

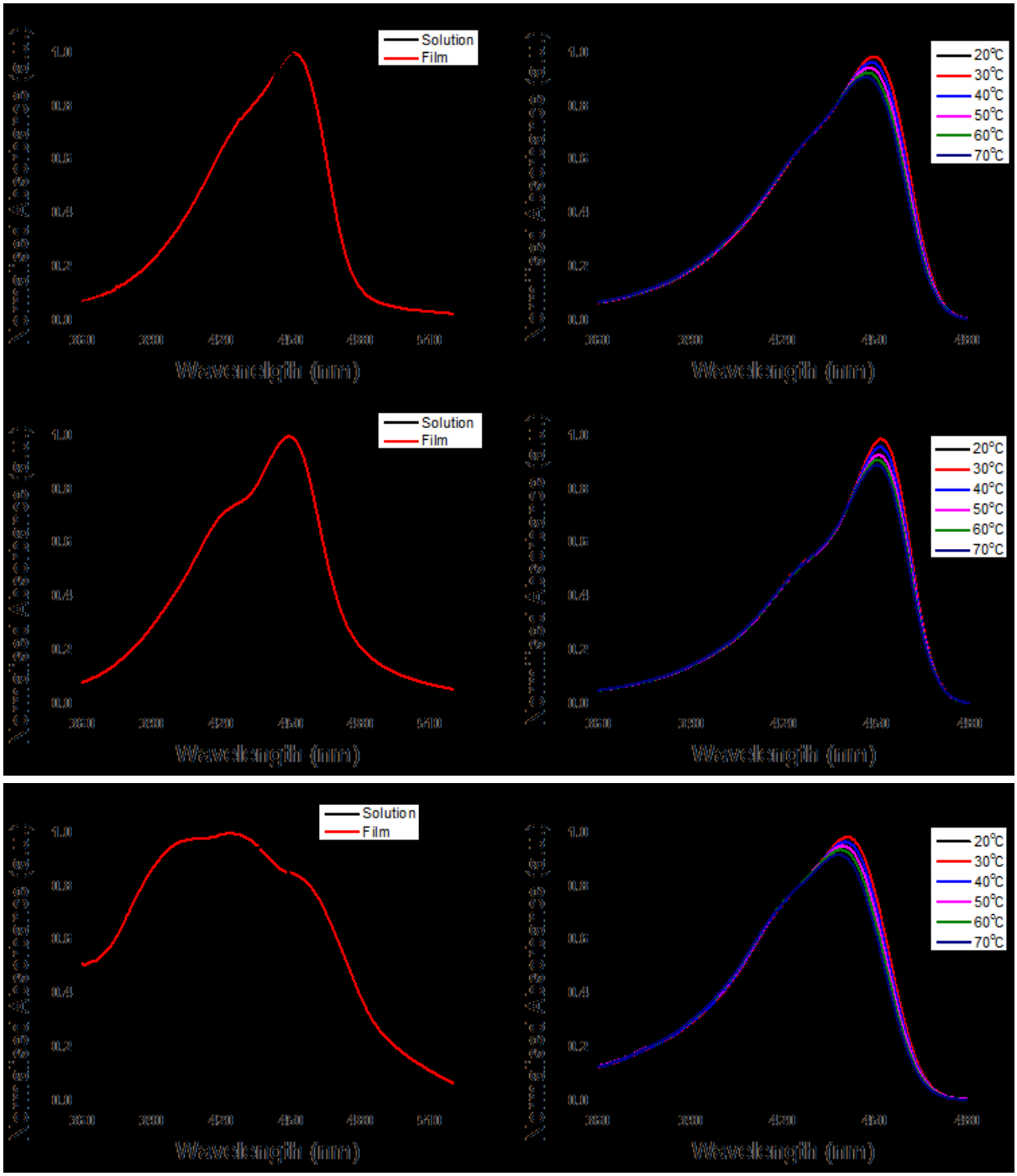

Figure 20. UV-Vis absorption spectrum of IP-C8, IP-C2C6 and IP-C1C4 (bottom left) in chloroform and thin film.

Table 3. Optical and energy level data for IP-C8, IP-C1C4 and IP-C2C6.

Polymer	λ_{max}(nm) (M^{-1} cm^{-1}) Solution	Film	λ_{onset}(nm) Film	I.P.(eV)[1]	LUMO (eV)[2]	E_g^{opt} (eV)
IP-C8	450 (59 500)	451	476	- 6.0	- 3.4	2.6
IP-C1C4	441	425	501	N/A	N/A	2.8
IP-C2C6	452 (57 100)	449	479	- 6.0	- 3.4	2.6

[1]Ionisation potential recorded via PESa
[2] LUMO calculated based on onset of absorption

The spectra were recorded in chlorobenzene and thin films spun from a 5 mg/mL solution of polymer in chlorobenzene. The ionisation potential was measured via photoelectron spectroscopy in air (error ±0.05 eV). The LUMO was estimated by subtraction of the optical band gap from the measured HOMO level. The optical band gap was estimated from the onset of absorption in the thin film. **IP-C8** and **IP-C2C6** had very similar low lying HOMO energy levels of -5.97 eV and -6.02 eV respectively, which are identical within the error of the measurements (± 0.05 eV). The low lying HOMO levels can be attributed to the electronic structure of the indenopyrazine repeat unit which is comprised of fully aromatic benzene and pyrazine units. We were not able to perform measurements on the C1C4 polymer due to the difficulties in forming homogenous films.

The photoluminescence spectra of **IP-C8** and **IP-C2C6** were recorded in chloroform solution of varying concentrations as well as thin films (Figure 11). We were not able to record a consistent PL spectrum of **IP-C1C4** due to poor film quality, which produced inconsistent results.

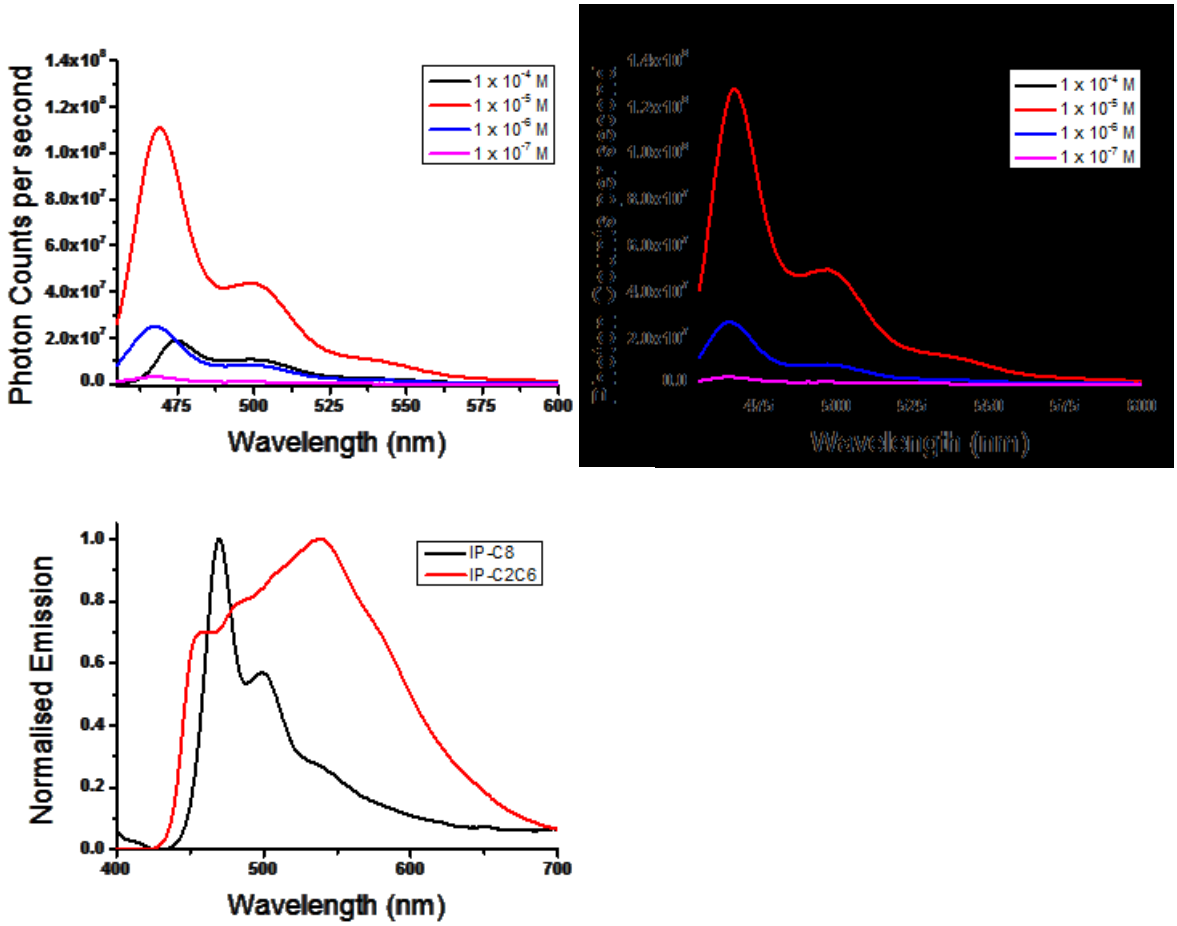

Figure 21. Solution photoluminescence spectroscopy of both IP-C8 (top left) and IP-C2C6 (top right). The lower graph shows both IP-C8 and IP-C2C6 in thin film.

The concentration dependent photoluminescence spectroscopy for both the **IP-C8** and **IP-C2C6** showed similar results; concentrations ranging from 10^{-4}-10^{-7} M were made up in chloroform. For dilute solutions, as the concentration increased from 10^{-7} to 10^{-6} M and finally 10^{-5} M, the emission intensity also increased with clear vibronic structure and well resolved peak maxima at 469 nm, 499 nm and 541 nm respectively. Increasing the concentration further did not correspond to an increase in emission intensity, but rather a decrease. For solutions of concentration of 10^{-4} M the emission intensity decreases with the primary $\mathbf{S_1^0}$ to $\mathbf{S_0^0}$ transition shifting to a longer wavelength of 475 nm. This reduction in emission intensity can be attributed to the increase in chromophore density and the resulting quenching of emission.

In the solid state **IP-C8** displayed clear vibronic structure with peaks at 470 nm, 498 nm and 538 nm, the Stokes shift in emission was 19 nm. These three emission peaks can be attributed to emission from the excited level of $\mathbf{S_1^0}$, to the $\mathbf{S_0^2}$, $\mathbf{S_0^1}$ and $\mathbf{S_0^0}$ vibronic levels. The $\mathbf{S_1^0 \rightarrow S_0^0}$ has the greatest intensity of emission followed by $\mathbf{S_1^0 \rightarrow S_0^1}$ and then a weak broad emission for the $\mathbf{S_1^0 \rightarrow S_0^2}$**. IPC2C6** exhibits a vastly different emission in the solid state compared to that of **IP-C8. IP-C2C6** had the first emission peak maxima at 458 nm which corresponds to a 9 nm Stokes shift and exhibited 3 further broad emission speaks at 488 nm, 507 nm and 538 nm. Unlike **IP-C8** which has decreasing emission intensity as wavelength increases, the emission intensity increases. This is uncharacteristic of polymers and points to the suggestion that **IP-C2C6** is aggregating in the solid state and emission from the ecxiplex occurs. Neither polymer observed emission at 700 nm, characteristic of a keto defect.[33]

Table 4. Wavelength at with the 1st, 2nd and 3rd peak maxima occur for IP-C8 and IP-C2C6 in thin film spun from chlorobenzene.

Polymer	Emission Onset (nm)	1st peak Emission Max (nm)	2nd peak Emission Max (nm)	3nd peak Emission Max (nm)	4th peak Emission Max (nm)	Stokes Shift (nm)
IP-C8	442	470	498	538	N/A	19
IP-C2C6	432	458	488	507	538	9

Differential Scanning Calorimetry

The varying of the structure of alkyl chains alters how polymers align in the solid state. **IP-C8** and **IP-C2C6** were subjected to differential scanning calorimetry between -40 and 300°C in order to assess if they possessed any crystalline features.

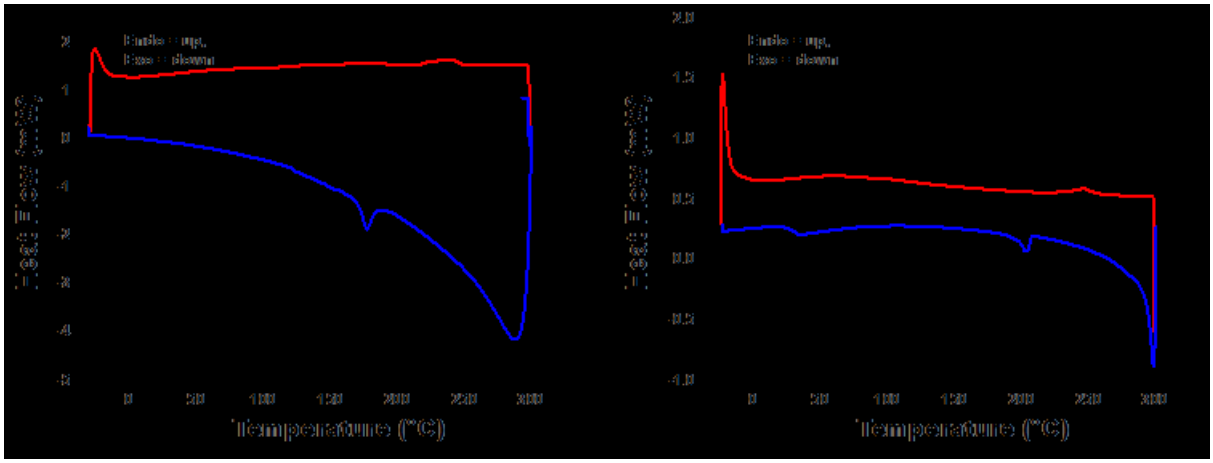

Figure 22. Second full cycle of the DSC of IP-C8 (left) IP-C2C6 (right). The scans were run between the temperatures of -40°C and 300°C. The peak at 50°C was a known defect in the machine.

Table 5. Melting and crystallisation data of IP-C8 and IP-C2C6

Polymer	IP-C8	IP-C2C6
Melt Onset Temperature (°C)	217	219
Melt Peak Temperature (°C)	238	224
Crystallisation Onset Temperature (°C)	183	205
Crystallisation Peak Temperature (°C)	177	201
Supercooling (°C)	33	14
Enthalpy of melting (J/g)	3	2
Enthalpy of Crystallisation (J/g)	2	2

Both polymers exhibited a degree of crystallinity. **IP-C8** had a melting onset at 217 °C and a crystallisation onset at 183 °C, with a small enthalpy of fusion for both transitions. **IP-C2C6** showed a similar melting onset at a temperature of 219 °C with a crystallisation onset at 205 °C. The difference between melting and crystallisation onset is referred to as supercooling. The small supercooling value for **IP-C2C6** suggests it could be liquid crystalline in nature. Similar liquid crystal phase transitions have been observed in many polyfluorene derivatives.

Conclusion

From the studies of the homopolymers it can be concluded that the inclusion of n-octyl side chains affords highly soluble polymers with good molecular weight and little tendency to aggregate, either in solution or in the solid state. The incorporation of branched alkyl side chains has a significant effect on the properties of the polymer, with C1C4 branched chains being insufficient to afford soluble polymers of high molecular weight.

Synthesis and Characterisation of Indenopyrazine - Fluorene Copolymers

Aims

Based on the previous work by Bradley *et al* a series of 4 co-polymers comprised of indenopyrazine and fluorene were designed and synthesised to combine alternating short and long alkyl chains and observe the effect on the polymerisation, absorption, emission, crystallinity, bulk mobility and amplified spontaneous emission.

The four monomers investigated were: a short branched 1-methyl butyl indenopyrazine; a longer straight octly chain indenopyrazine; a short propyl fluorene and longer octyl fluorene unit (Scheme 6). This combination produced a series of fours copolymers: the short chain indenopyrazine – short chain fluorene, **IP-C1C4-F3**; the short chain indenopyrazine – long chain fluorene, **IP-C1C4-F8**; the long chain indenopyrazine – short chain fluorene, **IP-C8-F3** and the long chain indenopyrazine – long chain fluorene, **IP-C8-F8**. A short branched indenopyrazine unit was used rather than an indenopyrazine containing a straight short chain to offer the balance of short chain length whilst not compromising the solubility of the resultant polymers. The design principle of alternating short and long alkyl chains was to observe how the physical properties were affected by the proposed increase in interdigitation in the solid state. This desired increase in interdigitation was proposed to increase effective hoping between chains when compared to both **IP-C1C4-F3** and **IP-C8-F8.** Having a greater number of efficient hopping sites should, therefore, improve the charge carrier mobility of the polymers. It was hoped that maintaining a distance between adjacent backbones would not result in a compromise in photoluminescence quenching which affects the ability of a polymer thin film to achieve optical gain and amplified spontaneous emission.

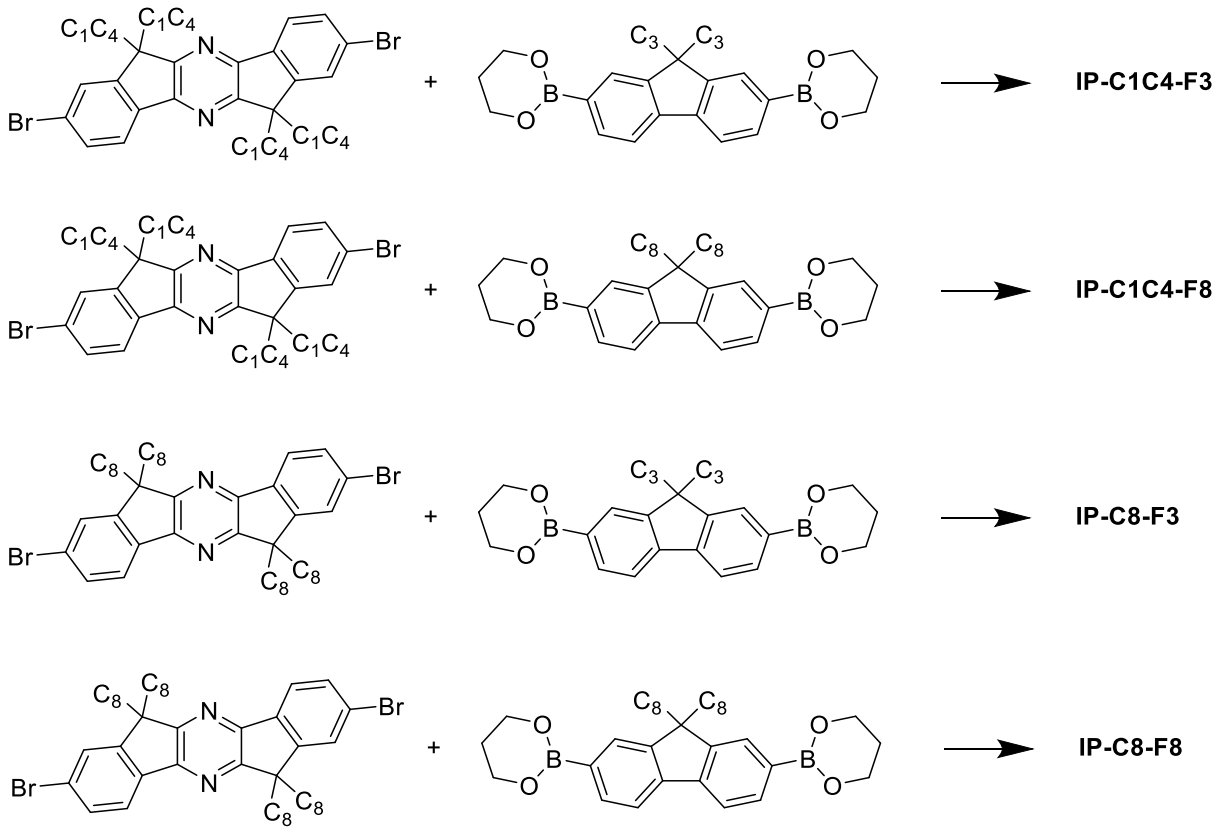

Scheme 6. Two indenopyrazine units combined with the two fluorene units to give the series of 4 polymers. C_8 = C_8H_{17}, C_3 = C_3H_7. C_1C_4 = $CH_3C_4H_8$.

Synthesis

The four polymers were all synthesised via standard Suzuki coupling. Equimolar amounts of the two monomers, indenopyrazine and fluorene were weighed into a microwave vial equipped with a small stirrer bar. Under a heavy flow of argon, degassed toluene was added along with 2 drops of Aliquot 336, tetrakis(triphenylphosphine)palladium(0) (1.3 % eqv) and 1 M $K_2CO_{3(aq)}$. The reaction was heated to 120°C for 3 days. The resulting reactions were precipitated into cold methanol and long weight oligomers and catalyst residues were extracted using methanol and acetone. The polymers were extracted into hexane and after removal of the solvent, dissolved in chloroform. Palladium residues were removed by washing with sodium diethyldithiocarbonate[34] After extraction and washing, the final polymers were obtained by precipitation into methanol as bright green/yellow fibres.

Table 6. Physical properties of the IP-F series. All the results were obtained based on the soxhlet fraction which contained the majority of the polymer. In all four cases this was the hexane fraction.

Polymer	Yield %	M_n/kg/mol	M_w/kg/mol	PDI	DP[1]
IP-C1C4-F3	43	12	19	1.6	14
IP-C1C4-F8	50	37	82	2.2	38
IP-C8-F3	44	12	22	1.8	12
IP-C8-F8	56	22	48	2.2	20

[1] Degree of polymerisation based on Mn

The results of the polymerisations indicate that the inclusion of the short chain fluorene moiety had the greatest influence on the overall molecular weight, by both number and weight average. This can be attributed to the degree of solubility that is lost on shortening the alkyl chains on the fluorene and the resultant polymers precipitating out of solution preventing any further growth in chain length. Comparing the two **F3** containing polymers there is little difference in the M_n between **IP-C1C4-F3** and **IP-C8-F3**. From the earlier results on the homo indenopyrazine polymers it was expected that the increased solubility that the **IP-C8** co-monomer offered compared to **IP-C1C4** would be sufficient to promote polymer solubility. The fact that it wasn't, suggests that the **F3** unit dictated polymer solubility. The two polymers **IP-C1C4-F3** and **IP-C8-F3** both had molecular numbers of half of that of their **F8** containing counterparts. Nevertheless the **F3** containing polymers consisted of an average of over 10 repeat units. Although GPC is known to overestimate molecular weight, the fact that the repeat unit contains two aromatic monomers containing five individual phenyl rings suggests that these weights are still sufficient to reach the effective conjugation length.[35,36,37] Therefore we expect that for the majority of physical analyses the molecular weight differences would not have a significant affect. The two **F8** containing polymers had a slightly larger PDI. This again can be attributed to the difference in solubility between the **F8** and **F3** moieties and the latter's tendency to precipitate out of solution during polymerisation, limiting the polydispersity. The yields of all the polymers

were high despite the problems encountered with the poor solubility of the of the homopolymer **IP-C1C4**.

Optical Properties and Energy Levels

The UV-Vis and photoluminescence spectra of the **IP-F** series were recorded to observe the effect varying the alkyl chains would have on the position of the absorption maximum in both solution and thin film. All spectra were recorded in dilute solution with their concentration adjusted to give an absorption value between 0.2 - 0.6. The UV-Vis spectroscopy results are presented in Figure 23 and summarised in Table 7.

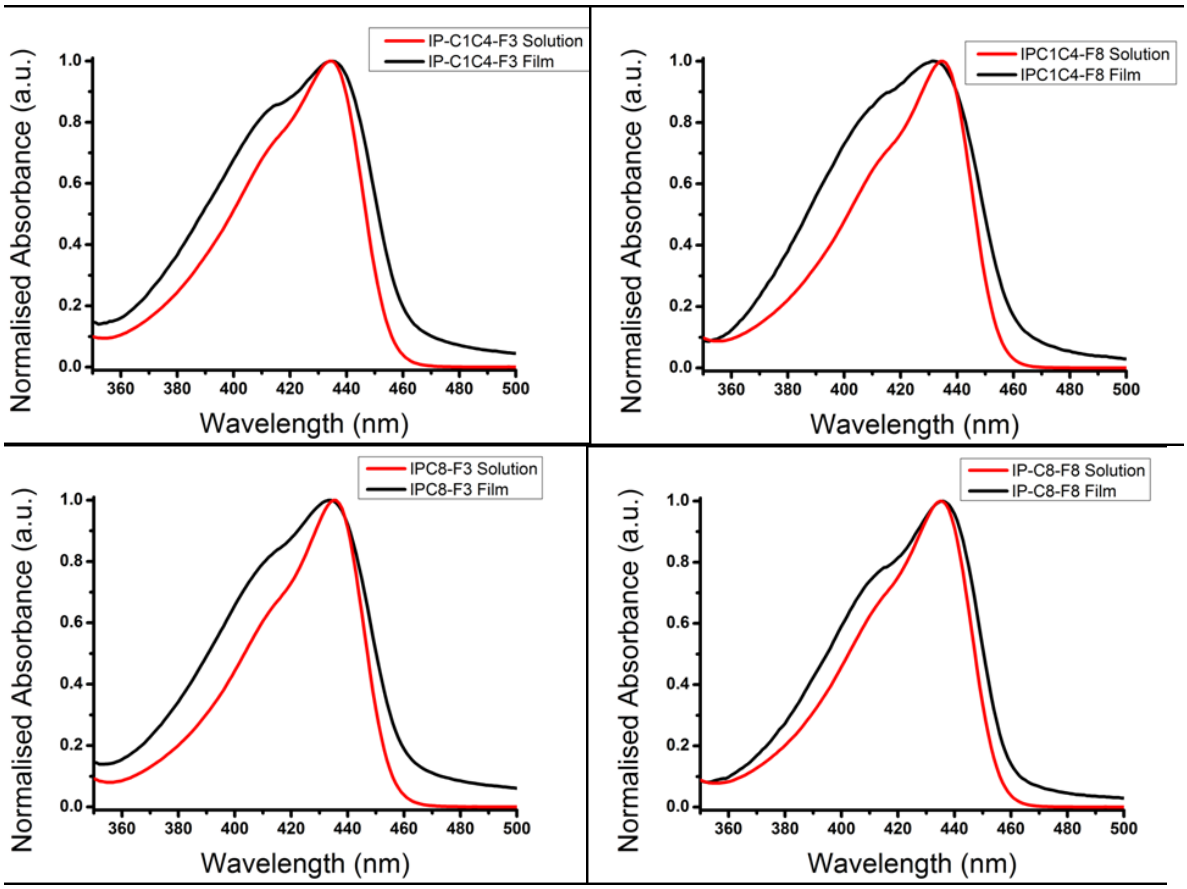

Figure 23. Solution and thin film UV-Vis absorption spectrum for the series of polymers IP-C1C4-F3, IP-C1C4-F8, IP-C8-F3 and IP-C8-F8.

The UV-Vis spectroscopy data shows that all four co-polymers exhibit a similar λ_{max} in the solid state at 435 nm. **IPC1C4-F3** and **IPC8-F8**, the polymers containing short – short or long – long alkyl chains exhibit a small bathochromic shift of approximately 1 nm when

going from solution to film. **IP-C1C4-F8** and **IP-C8-F3**, the two polymers containing a mixture of the short and long alkyl chains, undergo a slight hypsochromic shift of 1-3 nm on going from solution to film. They all exhibit a very similar λ_{onset} at 456 nm. This onset corresponds to an optical band gap of 2.72 eV.

Table 7. Optoelectronic results for IP-F series.

	λ_{max}(nm)		λ_{onset}(nm)			
Polymer	**Solution**	**Film**	**Film**	**IP (eV)[1]**	**LUMO (eV)**	**E_g^{opt} (eV) [2]**
IPC1C4-F3	435	434	454	5.86	- 3.14	2.73
IPC1C4-F8	432	435	453	5.87	- 3.14	2.72
IPC8-F3	435	434	454	5.89	- 3.17	2.73
IPC8-F8	435	436	454	5.87	- 3.13	2.73

[1] IP was estimated via PESa

[2] the optical band gap was estimated by the onset of absorption.

The introduction of fluorene into the polymer backbone raises both the HOMO and LUMO energy levels closer to vacuum with respect to that of the homo indenopyrazine polymers. The HOMO energy level rose by approximately 0.15 eV and the LUMO by 0.2 eV. This is because fluorene is slightly more electron rich than indenopyrazine. The increase in the band gap also results in the absorption maxima blue-shifting to a shorter wavelength by approximately 20 nm.

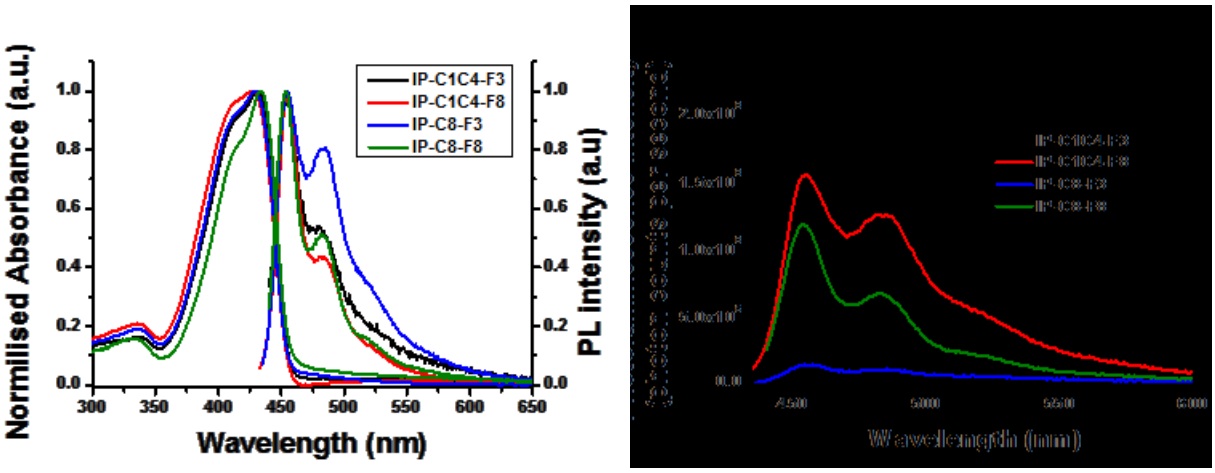

Figure 24. Thin film UV Vis-PL spectra on glass (left). Excitation intensity (right).

The emission spectra in the solid state for **IP-C1C4-F3 IP-C1C4-F8**, **IP-C8-F3** and **IP-C8-F8** shown in Figure 24 were measured via an integrating sphere. The absorption spectra are also included to show the corresponding Stokes shift. As can be seen from Figure 24 all four polymers exhibit clear and well resolved vibronic structure with peaks at 470 nm, 490 nm and 525 nm in the emission spectra. The right hand graph is a plot of the emission peak intensity against wavelength, corrected for film thickness. It can be seen clearly that **IP-C1C4-F3, IP-C1C4-F8** and **IP-C8-F8** have similar emission intensities. **IP-C8-F3** has a much lower intensity.

Table 8. Photoluminescence spectroscopy results of the series of IP-F polymers

Polymer	Emission Onset (nm)	1st peak Max (nm)	2nd peak Max (nm)	3nd peak Max (nm)	Stokes Shift (nm)
IP-C1C4-F3	431	455	479	N/A	24
IPC1C4-F8	427	455	484	N/A	29
IPC8-F3	439	455	485	520	14
IPC8-F8	434	455	483	521	21

IP-C1C4-F3, **IP-C1C4-F8** and **IPC8-F8** all exhibit a larger Stokes shift than the corresponding HOMO polymer **IP-C8**, which can be related to the reduction in rigidity of the backbone of all three polymer versus IP-C8**. IPC8-F3** has, however, a smaller Stokes shift although we note that the weak and rather broad emission affords a larger error in determining the maxima. **IP-C1C4-F3**, **IP-C1C4-F8** and **IPC8-F8** all have similar transitions which can be attributed to the $\mathbf{S_1^0 \rightarrow S_0^0}$ at 455 nm, $\mathbf{S_1^0 \rightarrow S_0^1}$ at 480 nm and a broad emission for the $\mathbf{S_1^0 \rightarrow S_0^2}$ at 520 nm.

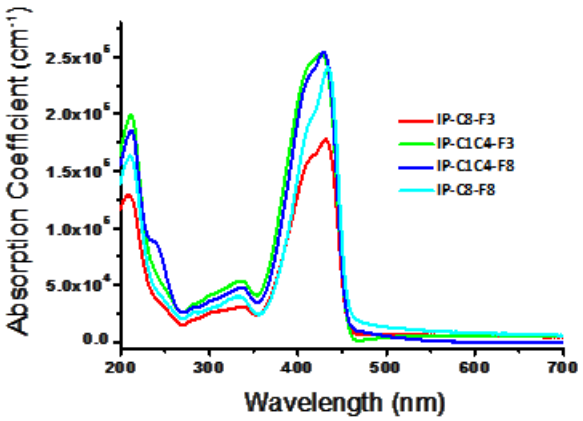

Figure 25. Non normalised absorption coefficients

A correlation that appears to be present in the polymer series is the relationship between alkyl chain density and photon counts per second. The right hand graph in Figure 24 shows the polymer exhibiting the greatest number of photons counts per second as **IP-C1C4-F3** which has the lowest density of carbons on the alkyl chains per repeat unit in the series. As the number of carbons on the alkyl chains increase per repeat unit, the intensity or number of photon counts per second decreases. An anomaly arises with **IP-C8-F3** which has a far reduced intensity than the other three polymers. This can be attributed to the fact that IP-C8-F3 shows far lower absorption intensity (Figure 25) possibly due to film roughness.

Differential Scanning Calorimetry

The four polymers were studied using differential scanning calorimetry (DSC) to observe if the alternating long and short alkyl chains had an effect on the thermal behaviour of the polymers. The samples were prepared by dissolving a known amount of polymer in chlorobenzene and drop casting it into a DSC pan. The pan was then stored under argon overnight in order to remove the solvent. Due to the nature of the polymer this method of sample preparation was preferred because it produced samples which had uniform contact with the base of the DSC pan.

The DSCs of the four samples show that **IP-C1C4-F3** and **IP-C8-F8** are featureless between the ranges of -50°C – 300°C. **IP-C8-F3** and **IP-C1C4-F8**, however, show semi-crystalline characteristics. On heating, the melt onset of **IP-C8-F3** occurs at 259.0°C and **IP-C1C4-F8** at 260.7°C. The second feature being a crystallisation on cooling and having an onset at 226.8°C and 216.7°C respectively. These features appear only on the polymers that contain alternating short and long alkyl chains and not on the polymers which contain either all short or all long chains. This date supports the theory that the combinations of alternating long and short chains allows the polymers to interdigitate, resulting in a more ordered structured. The enthalpies of melting were similar (2.1 J/g and 1.9°C **IP-C8-F3** and **IP-C1C4-F8** respectively), and that of crystallisation was 4.2 J/g and 3.8 J/g.

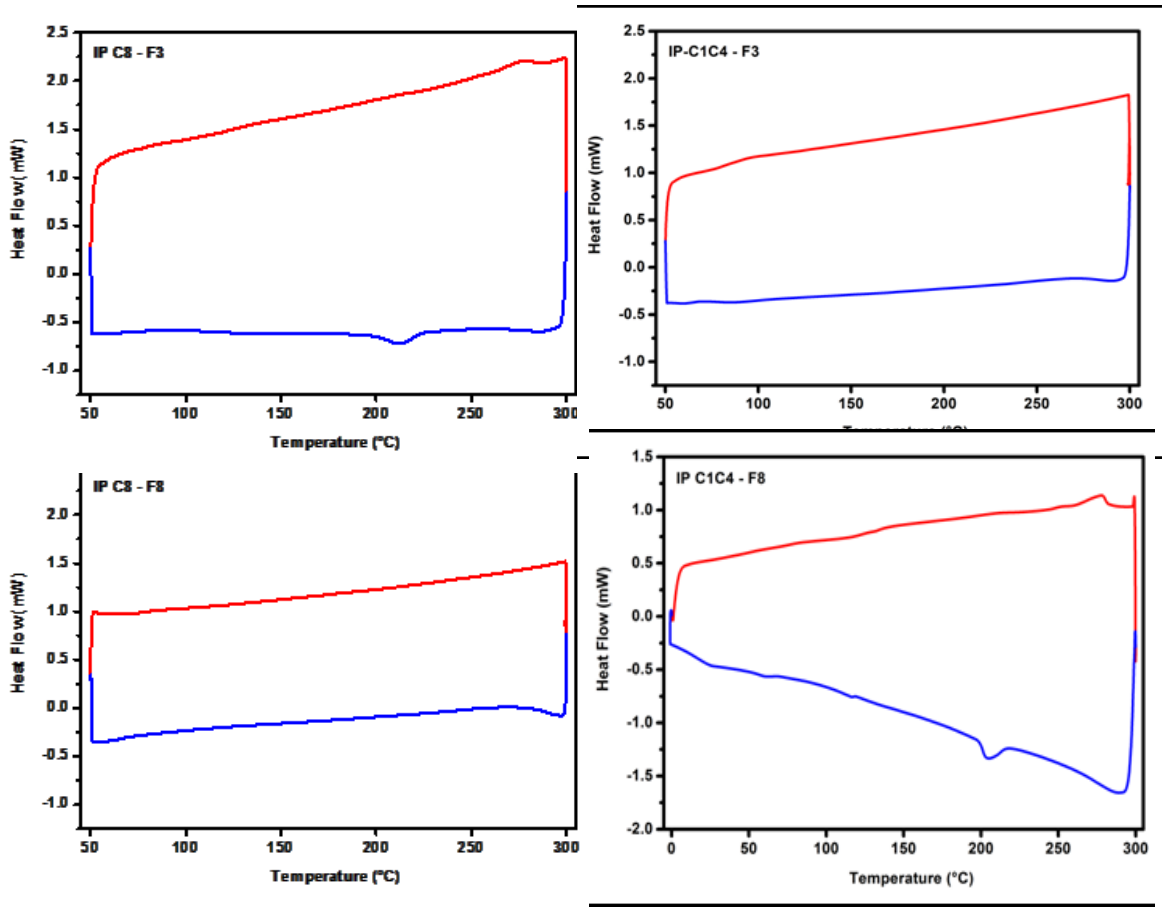

Figure 26. DSC of the series of the IP-F co-polymers. All 4 graphs are of the 1st cycle. Endo up/Exo down

Table 9. Comparison of thermal behaviour of IP-C8-F3 and IP-C1C4-F8 (first cycle)

Polymer	IP-C8-F3	IP-C1C4-F8
Melt Onset Temperature (°C)	259.0	260.8
Melt Peak Temperature (°C)	277.5	277.8
Enthalpy of Melting (J/g)	2.1	1.9
Crystallisation Onset Temperature (°C)	226.8	216.7
Crystallisation Peak Temperature (°C)	213.6	204.2
Enthalpy of Crystallisation (J/g)	4.2	3.8
Difference in Onset Temperatures (°C)	32.2	44.1

In the second and third cycles of the DSC, the previously mentioned features in **IP-C8-F3** and **IP-C1C4-F8** were no longer present. There was no change in the thermal behaviour of **IP-C1C4-F3** and **IP-C8-F8.** The change in behaviour on the second and third cycle might suggest that the initial endotherms were related to a thin film phase formed from solution that is not reformed upon thermal cycling.

Amplified Spontaneous Emission

Organic semiconductors are believed to be suitable for use in lasers because they absorb light strongly and do so over a short distance. As stimulated emission is closely related to absorption this results in strong gain possibilities. One of the requirements of a laser material is that it emits light efficiently. The photoluminescence quantum efficiency (PLQE) is defined as the ratio of the number of photons emitted over the number of incident photons absorbed. The four copolymers were optically characterised in the form of thin films spin-coated on glass. Figure 27 shows the combined absorption, photoluminescence and amplified spontaneous emission (ASE) spectra. The thin film samples were prepared via spin coating on glass from toluene.

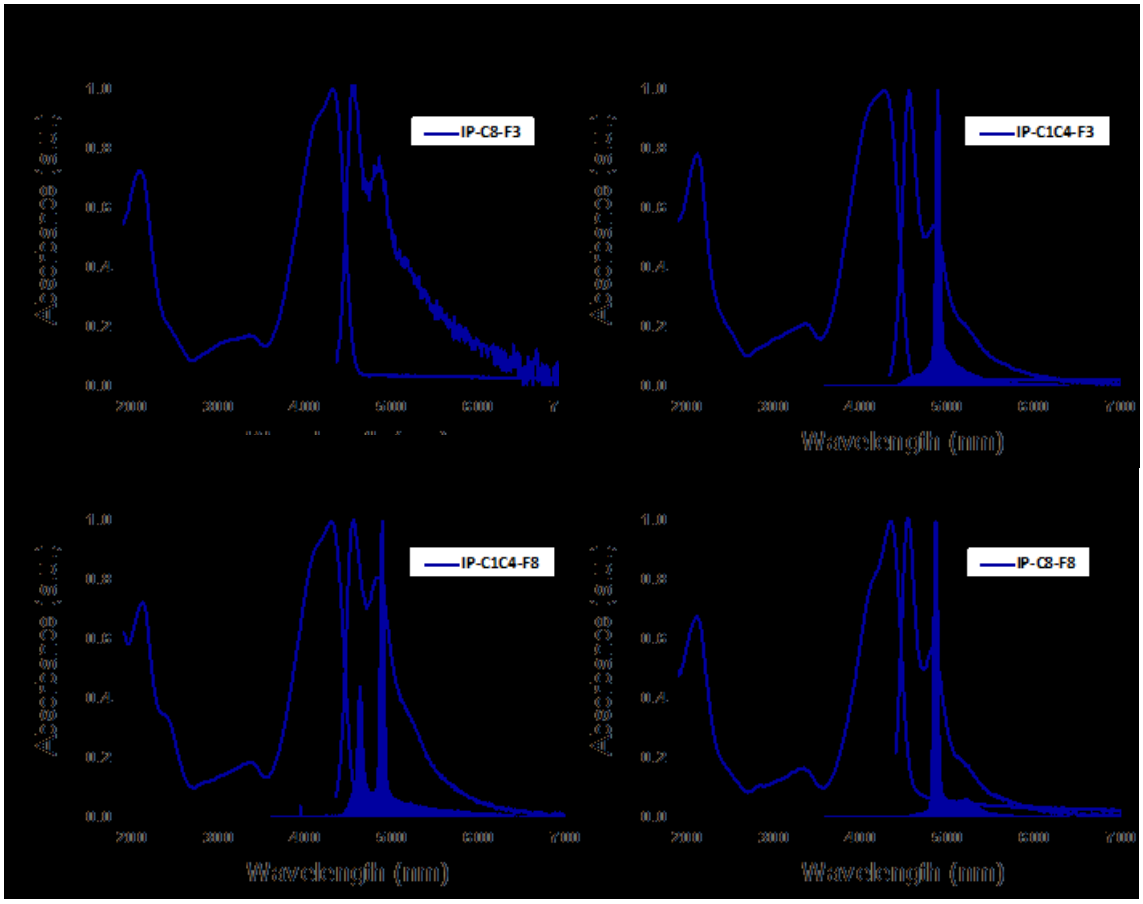

Figure 27. Amplified spontaneous emission of IP-C1C4-F3, IP-C1C4-F8 and IP-C8-F8. The films were spun at 20 mg/mL

The ASE spectra were measured by spinning thin films of the respective polymers from a toluene solution of 20 mg / mL onto a quartz substrate. The film thicknesses were 117.5 nm, 107 nm, 183nm and 70 nm. Each film was optically excited by a laser light source at 355 nm and the emission intensity recorded. The photoluminescence quantum efficiency was recorded for all four of the polymers and the results are tabulated in Table 10. **IP-C8-F8** has the highest recorded PLQE of the samples tested, with an efficiency of 25.7 %. Factors that limit the PLQE in the solid state include the formation of dimers, aggregates and excimers, all of which can quench emission. With **IP-C8-F8** consisting of long alkyl chains throughout the backbone, **IP-C8-F8** will potentially exhibit the largest spacing between polymer chains and therefore be the least likely to form dimers or excimers, and is the least likely to undergo

emission quenching. The next highest PLQE is from the combination of the two short chains, **IP-C1C4-F3** with a PLQE of 15.2 %. This is interesting because it would be expected that having a combination of the two shortest chains would lead to the closest packing in the solid state and therefore potentially the largest amount of emission quenching. We believe therefore that the branched side chain may help suppress solid state packing. **IP-C1C4-F8** and **IPC8-F3** have lower PLQE values of 13.6 % and 11.6 % respectively. This is in agreement with earlier results from the differential scanning calorimetry where peaks representing melting and crystallisation were observed suggesting that having the combination of alternating long and short alkyl chains do allow the polymer chains to interdigitate and order somewhat in the solid state. Even though this causes a reduction in the PLQE, for optimum lasing conditions the system requires a balance of PLQE and charge carrier mobility. So while the interdigitation is the likely cause in the reduction of the PLQE, it is predicted that this interdigitation leads to closer chain packing.

Table 10. The maximum absorption coefficient, the PLQE, the wavelength at which ASE occurs and the full width half maximum of the narrowed emission.

Polymer	IPC1C4-F3	IPC1C4-F8	IPC8-F3	IPC8-F8
Maximum absorption coefficient, (10^5 cm^{-1})	2.5	2.5	1.7	2.3
Photoluminescence quantum efficiency, (%)	15.2	13.6	11.4	25.7
ASE wavelength λ_{ASE} (nm)	489	488	-	485
FWHM narrowed emission (nm)	5	5	-	5

In three of the four polymers, gain was observed via amplified spontaneous emission. **IPC8-F3** was not able to undergo amplified spontaneous emission and this can be attributed the low absorption coefficient of the polymer. The ASE was measured by spinning thin films of **IP-C8-F3**, **IP-C1C4-F3**, **IPC1C4-F8** and **IPC8-F8** from a toluene solution of 20 mg / mL onto a quartz substrate. Each film was optically excited by a laser light source (355 nm) and the emission intensity recorded. Above the pumping intensity required to induce gain a

spectral change was observed in the emission of **IP-C1C4-F3**, **IP-C1C4-F8** and **IP-C8-F8**. Light at the peak of the gain spectrum was amplified more than other light, giving a spectrally narrowed emission.

Compared to the previously published data on the alternating polyfluorene series the observed maximum absorption coefficients for **IP-C1C4-F3** and **IP-C1C4-F8** were greater at 2.5 x 10^5 (cm^{-1}) than for PFO (2.1 x 10^5 (cm^{-1})) which was comparable to **IP-C8-F8**.[13] **IP-C1C4-F3** and **IP-C1C4-F8** however, had a lower maximum absorption coefficient than the 50/50 F8-F5 alternating polyfluorene. The lower absorption coefficient can be attributed to chain density with **PFO** and **IP-C8-F8** > **IP-C1C4-F3** and **IP-C1C4-F8** > **50/50 F8-F5.** The highest PLQE measured was for **IP-C8F8** which gave a quantum efficiency of 25.7 %. Disappointingly this was half the value of that recorded for pure PFO. The alternating PFO had a PLQE efficiency as high as 60%. The amplified spontaneous emission wavelength was red shifted by approximately 30 nm compared to the polyfluorene series. This is due to the red-shifted absorption of indenopyrazines compared to polyfluorenes.[13]

Current Density – Voltage

The current density – voltage characteristics of the four polymers were recorded via the steady state current – voltage (J-V) measurement and the transient space charge limited dark injection in order to obtain the bulk mobility of the charges. The main difference between the dark injection method and the space charge limited current measurement is that dark injection is a transient measurement and JV is steady state. Despite attempted electrode modification, reliable results for the steady state current – voltage and space charge limited dark injection measurements were not able to be recorded due to the depth of the HOMO resulting in poor charge injection. Times of flight measurements were also attempted but due

to the poor absorption at 355 nm wavelength, a tight packet of charges was not able to be formed thus producing unreliable data.

Conclusion

The use of alternating short and long chain copolymers produced some promising results, with ASE results showing amplification of the $\mathbf{S_1^0 \rightarrow S_0^1}$ transition and a FWHM narrowing of emission to 5 nm. However due to the low PLQE, further optimisation is required before the materials are suitable for use in an optical laser. The depth of the HOMO level being close to 5.8 eV proved to be problematic for the majority of the charge carrier measurements. However the electron affinity of the polymer was increased compared to PFO, from 2.85 eV of PFO to 3.14 eV.

Synthesis and Characterisation of Indenopyrazine-Triarylamine polymers

Triarylamine semiconducting polymers have been shown to have excellent stability in air.[38] Zhang *et al* reported on the incorporation of fluorene and indenofluorene into triarylamine copolymers (Figure 28).[39] The incorporation of these fused aromatics increased the charge carrier mobility of triarylamine polymers by an order of magnitude whilst retaining their air stability. Planar conjugated aromatic repeat units in polymer backbones have been shown to promote highly ordered microstructures and extensive π stacking conformations.[40]

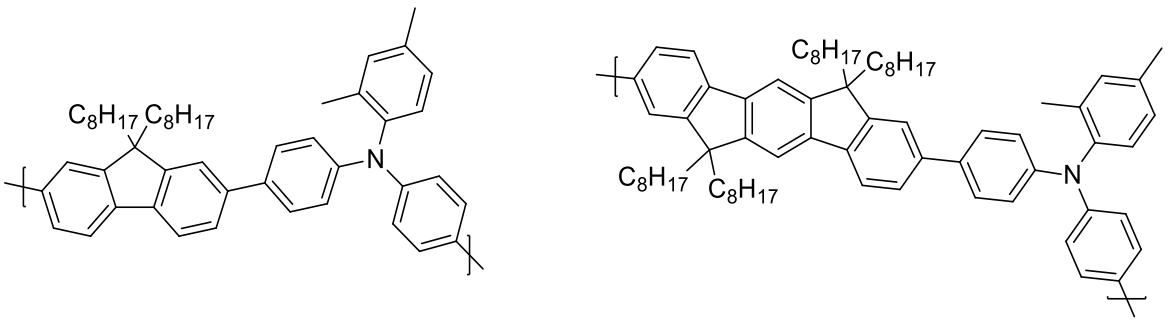

Figure 28. Structures of fluorene and indenofluorene copolymerised with triarylamine.

With the substitution of an indenopyrazine unit in place of an indenofluorene it was proposed that the stability offered by the pyrazine would lower the LUMO, promoting electron injection. In addition the lone pair of electrons on the central pyrazine unit might be able to interact with Lewis acids and transition metals for potential use in organic sensing devices. It was also predicted that the combination of the electron rich triarylamine and indenopyrazine would result in a higher HOMO compared to the indenopyrazine – fluorene series discussed earlier. The higher lying HOMO should reduce the barrier to injection previously seen for the indenopyrazine – fluorene series and thereby facilitate measurement of the mobility.

Synthesis

The polymer was synthesised via a Suzuki coupling of dibromoindenopyrazine and the diboronic ester of 4-bromo-N-(4-bromophenyl)-N-(2,4-dimethylphenyl)benzenamine, following the conditions previously reported for the indenofluorene-TAA polymer. Here only the octyl substituted indenopyrazine was used to ensure good solubility of the resultant polymer. The resulting polymer was precipitated into methanol and low molecular weight impurities and catalyst residues removed by extraction (Soxhlet) with methanol and acetone. The polymer was then extracted into hexane followed by chloroform. Palladium residues were removed by washing with sodium diethyldithiocarbonate[34] After extraction and washing, the final polymer was obtained by precipitation into methanol from hot chlorobenzene as bright green/yellow fibres.

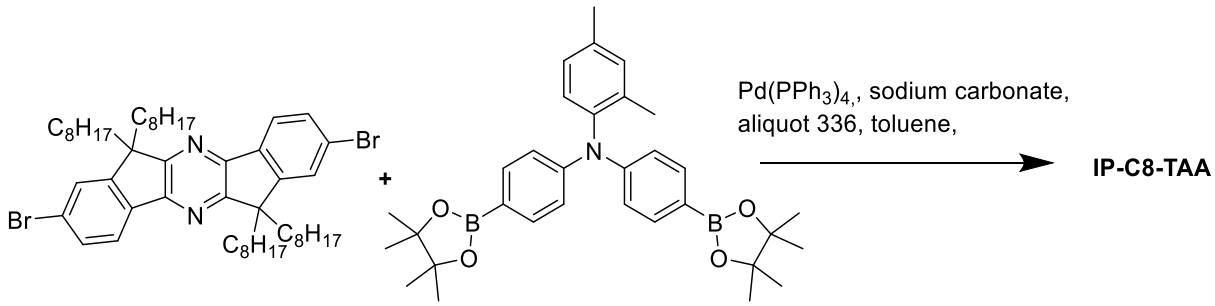

Scheme 7. Suzuki copolymerisation of indenopyrazine C8 monomer with the diboronic ester triarylamine

The physical properties of the isolated polymer **IP-C8-TAA** are displayed in Table 11. The reaction gave a polymer consisting of 18 repeat units. **IP-C8-TAA** was highly soluble in hexane and chloroform and had a yield of 48%.

Table 11. Yield, molecular number, molecular weight, PD and the degree of polymerisation for the triarylamine based polymer.

Polymer	Yield (%)	M_n/kg.mol^{-1}	M_w/kg.mol^{-1}	PDI	DP
IP-C8-TAA	48	20	38	1.9	18

As **IP-C8-TAA** was synthesised in a relatively large amount it allowed for a significant fraction to be purified by preparative gel permeation chromatography (GPC), to test if the removal of low molecular weight undefined impurities would have a beneficial impact on performance. Previous studies in the literature have suggested that minor impurities present can have a significant impact on performance for solar cell donor polymers[41]. Running a test sample of 1 mg through the GPC with the UV detector set at two different wavelengths showed a clear low molecular weight impurity that had an enhanced absorption at 300 nm compared to the bulk of the polymer.

Figure 29. UV output from the GPC. The black line corresponds to the 300 nm wavelength. The pink line corresponds to the reading at 400 nm.

In order to probe this observed peak more closely, a solution of 100 mg of **IP-C8-TAA** in chlorobenzene was prepared and filtered through a 0.4 micron PFTE filter. The solution was split into three portions. The first was not passed through the GPC machine and was simply concentrated under reduced pressure as the blank. The second fraction was passed through the GPC and the whole sample was collected for 25 minutes to observe the effects of a simple pass through the machine. The third fraction was injected and collected until 20 minutes to avoid collecting the materials responsible for the increase in UV absorption, after which time

the collection vial was changed. After concentration the molecular weight of all three fractions, as measured on an analytical GPC was identical except for a slight reduction in PDI for the final sample from 1.9 to 1.7.

Optical Properties and Energy Levels

The solution and thin film UV-Vis spectra are shown in Figure 30 .

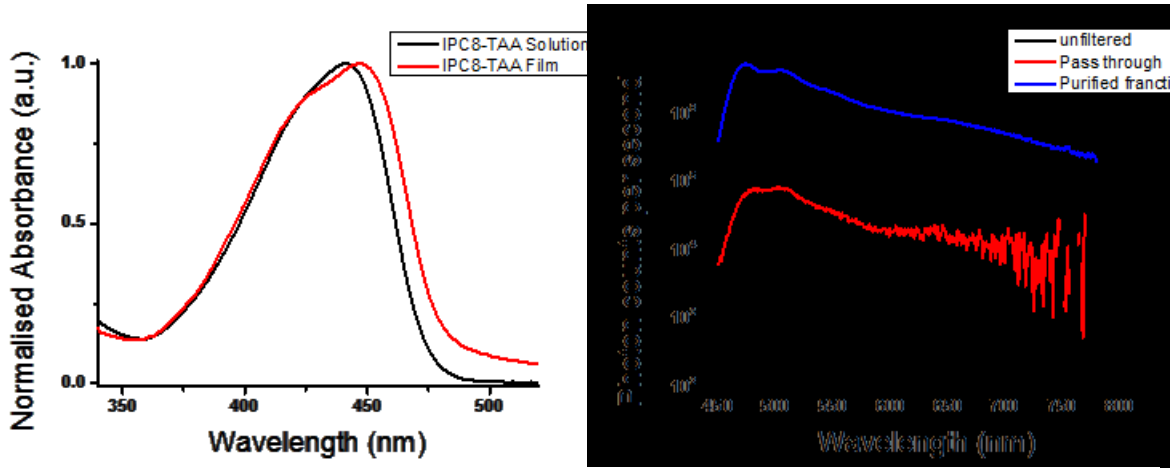

Figure 30. Solution and thin film absorption spectra of IP-C8-TAA. The solutions were made up in chloroform and the thin films were spun from chloroform on glass. The graph on the right is the photoluminescence spectroscopy for the three IPC8_TAA samples spun on quartz from 20 mg/mL chlorobenzene solution. The excitation wavelength was at 355 nm.

Table 12. Optoelectronic properties of IP-C8-TAA

Polymer	λ_{max}(nm) solution	λ_{max}(nm) Film	λ_{onset}(nm) Film	HOMO (eV)	LUMO (eV)	(E_g^{opt})
IP-C8-TAA	441	447	480	-5.49	-2.69	2.80

Figure 30 shows that **IP-C8-TAA** has a similar absorption profile to the previous **IP-F** series. **IP-C8-TAA** had an absorption maximum at 441 nm. In the solid state the absorption was bathochromically shifted to 447 nm, perhaps due to some planarization of the polymer backbone in the solid state.

In the solid state there was no noticeable difference in the absorption profile of the three fractions. A change did occur however, in the emission profile of the three fractions. The third purified sample produced an increase in emission intensity by an order of magnitude

(corrected for thickness). This can be attributed to removal of impurities that were present in the original sample. The PLQE of all the samples were also measured in an integrating sphere but all three of them had less than 5% PLQE efficiency and so we were unsuitable to record ASE spectra.

The HOMO energy levels were measured via PESA, the value of the HOMO energy level of the copolymer was 5.49 eV. This is higher than both the homo of indenopyrazine and the copolymers with fluorene, as a result of the electron rich triarylamine co-monomer. We also note that the inclusion of this co-monomer means that the backbone is no longer fully conjugated, since the sp^3 N bridge acts as a conjugation blocker.

Current – Voltage Measurements

Due to the higher energy level of the HOMO **IP-C8-TAA** it was put forward that there would now be a lower barrier to injection and that a bulk hole mobility could be recorded.

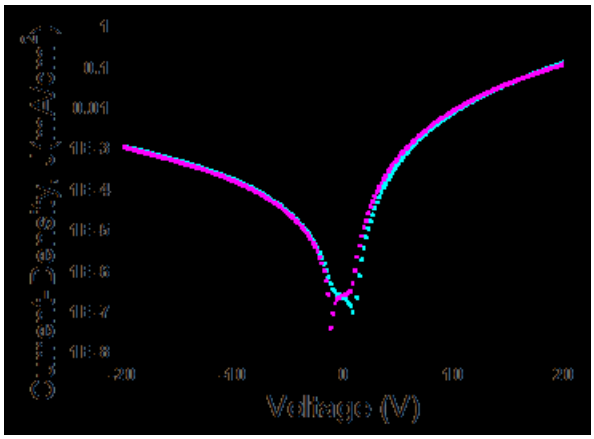

Figure 22. Current versus voltage measurement of IP-C8-TAA in a diode configuration with ITO and MoO_3 modified Au electrodes.

Diodes were fabricated using Au and ITO electrodes. Effective injection of holes was achieved. This can be ascribed to the raising of the HOMO energy level by 0.5 eV compared to that of **IP-C8** which enables an ohmic contact. The magnitude of the current density was 1 x 10^{-5} mA/cm^2. However the measurement of current density does not give enough

information to accurately estimate mobility.[42] With the prior knowledge of the HOMO level being at 5.49 eV, then it can be said that the contact of the semiconductor with the electrode is ohmic and assuming a perfect insulator with an electric field independent mobility, the Mott-Gurney equation estimates the mobility to be 1.1 x 10^{-3} cm^2/V s. This is a similar order of magnitude to the previously reported indenofluorene-triarylamine polymers which had a corresponding mobility of 3.8 x 10^{-2} cm^2/V s.[39]

Dark Injection

A second measurement of the bulk mobility of holes in **IP-C8-TAA** was carried out via space charge limited dark injection. Both the charges however, are generated electrically in contrast to time of flight measurements where the charges are generated by a laser pulse.

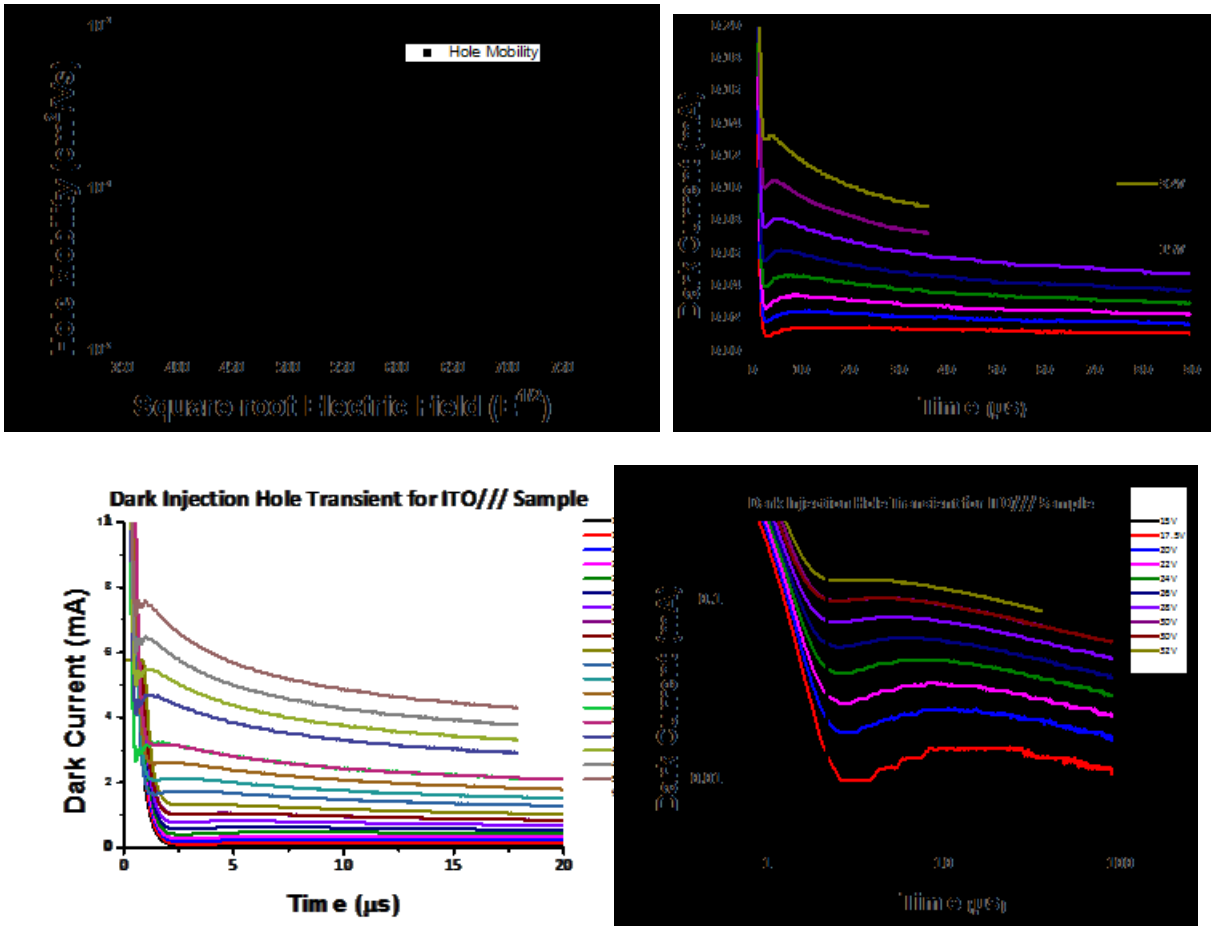

Figure 23. Space charge limited charge injection of IP-C8-TAA.

In contrast to the low HOMO polymer, charges were able to be injected efficiently through the MoO_3 modified Au electrode and the bulk mobility via dark injection was recorded to be 4 x 10^{-3} $cm^2V^{-1}s^{-1}$, which is in agreement with the previous current – voltage measurement.

Time of Flight

The third measurement of hole mobility was a time of flight measurement. The three fractions of the IPC8-TAA were all attempted to be recorded but the only sample that had a measureable time of flight was the sample that had the low molecular weight impurities.

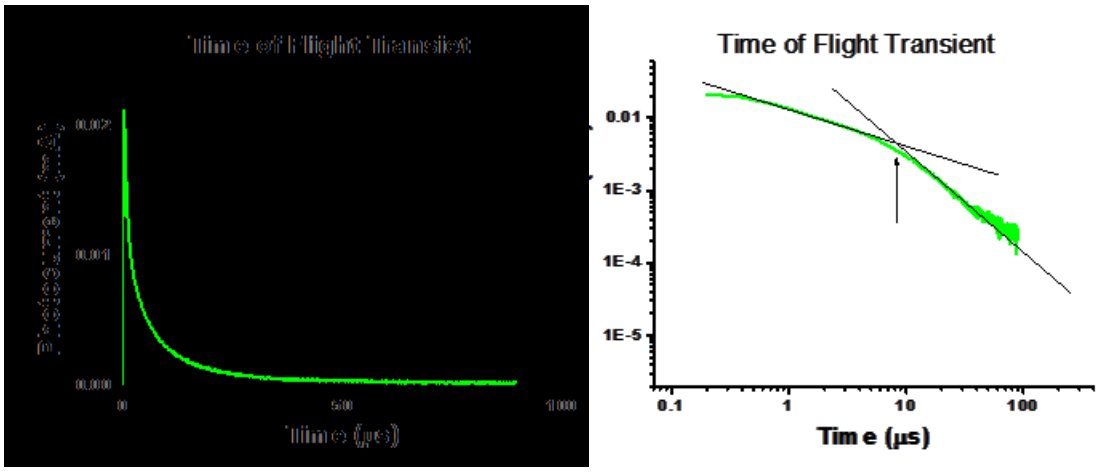

Figure 24. Time of flight transient for IP-C8-TAA. The polymer was deposited on MnO/Au electrode. It is a highly dispersive transient on a ln-ln plot at 20 V.

The time of flight mobility was calculated to be 8.53 x 10^{-4} cm^2/V.s. This is of the same order of magnitude of homo polytriarylamine polymers. In the previous work by Zhang *et al.* the incorporation of fluorene and indenofluorene increased the OFET mobility by an order of magnitude, but the bulk mobility was not measured.[39] Possible reasons why the bulk mobility did not increase could be attributed to the HOMO energy level of the polymer being lower than that of the TAA. Therefore more trap sites are present lowering the mobility of the holes.

Conclusion

In conclusion amplified spontaneous emission was observed in the series of alternating copolymers of indenopyrazine and fluorene. It was seen that the introduction of the alternating long and short alkyl chains did introduce a degree of interdigitation. This interdigitation however, compromised the resulting PLQE and in one case comprised it to such an extent that no ASE was observable. The interdigitation was supposed to give an increased mobility to compensate for the loss in PLQE but due to the resulting low lying levels of the HOMO no recordable mobility was able to be observed.

The copolymerisation of a triarylamine unit with indenopyrazine proved to raise the HOMO by a sufficient amount as to achieve hole injection and obtain a value for the hole mobility of the indenopyrazine based polymers. No ASE measurements were able to be recorded due to the less than 5% PLQE of **IP-TAA-C8**.

The series of homo indenopyrazine polymers offered more insight into the effect that the alkyl side chain had on the polymerisation and their physical properties. Both **IP-C1C4** and **IP-C2C6** were prevented from obtaining as large molecular weights as **IP-C8** due to the tendency to form aggregates. A similar scenario was also observed in the **IP-F** series with the short **F3** containing polymers being restricted due to solubility issues. Future work would be to try a combination of statistical copolymer of IP and F now a greater understanding of solubility has been realised.

In order to realise an organic laser a compromise still needs to be found of chain length, energy levels and mobility whilst maintaining acceptable levels of solubility for the ability to be solution processed.

References

1. Tessler, N., Denton, G. J. & Friend, R. H. Lasing from conjugated-polymer microcavities, *Nature.* 695 (1996).

2. de Mello, J., Wittmann, R., Friend, R., An Improvement in experimental determination of External PLQE, *Advanced materials*. 230–232 (1997).

3. Pope, M. & Swenberg, C. E., Electronic Processes in Organic Crystals and Polymers. (Oxford University Press: New York, 1999).

4. Samuel, I. D. W. & Turnbull, G. a Organic semiconductor lasers. *Chemical reviews* **107**, 1272–95 (2007).

5. Svelto, O. *Principles of Lasers*. (Plenum Press: New York, 1998).

6. Berggren, M., Dodabalapur, a. & Slusher, R. E. Stimulated emission and lasing in dye-doped organic thin films with Forster transfer. *Applied Physics Letters* **71**, 2230 (1997).

7. Gupta, R., Stevenson, M. & Heeger, a. J. Low threshold distributed feedback lasers fabricated from blends of conjugated polymers: Reduced losses through Förster transfer. *Journal of Applied Physics* **92**, 4874 (2002).

8. Brouwer, H.-J., Krasnikov, V. V., Hilberer, A., Wildeman, J. & Hadziioannou, G. Novel high efficiency copolymer laser dye in the blue wavelength region. *Applied Physics Letters* **66**, 3404 (1995).

9. Frolov, S., Vardeny, Z. & Yoshino, K. Cooperative and stimulated emission in poly(p-phenylene-vinylene) thin films and solutions. *Physical Review B* **57**, 9141–9147 (1998).

10. Virgili, T., Marinotto, D., Lanzani, G. & Bradley, D. D. C. Ultrafast resonant optical switching in isolated polyfluorenes chains. *Applied Physics Letters* **86**, 091113 (2005).

11. Babel, A. & Jenekhe, S. a. Charge Carrier Mobility in Blends of Poly(9,9-dioctylfluorene) and Poly(3-hexylthiophene). *Macromolecules* **36**, 7759–7764 (2003).

12. Tanaka, H. *et al.* Photopumped Laser Oscillation and Charge Carrier Mobility of Composite Films Based on Poly(3-hexylthiophene)s with Different Stereoregularity. *Japanese Journal of Applied Physics* **45**, L1077–L1079 (2006).

13. Yap, B. K., Xia, R., Campoy-Quiles, M., Stavrinou, P. N. & Bradley, D. D. C. Simultaneous optimization of charge-carrier mobility and optical gain in semiconducting polymer films. *Nature materials* **7**, 376–80 (2008).

14. Garbuzov, D. Z., Bulovi, V., Burrows, P. E. & Forrest, S. R. Photoluminescence efficiency and absorption of aluminum-tris-quinolate (Alq3) thin films. *Chemical Physics Latters.* **249**, 433–437 (1996).

15. Tang, C. W. & VanSlyke, S. a. Organic electroluminescent diodes. *Applied Physics Letters* **51**, 913 (1987).

16. Qu, D., Grischkowsky, D. & Zhang, W. Terahertz transmission properties of thin, subwavelength metallic hole arrays. *Optics letters* **29**, 896–8 (2004).

17. Spehr, T. *et al.* Organic solid-state ultraviolet-laser based on spiro-terphenyl. *Applied Physics Letters* **87**, 161103 (2005).

18. Schartel, B., Wachtendorf, V., Grell, M., Bradley, D. & Hennecke, M. Polarized fluorescence and orientational order parameters of a liquid-crystalline conjugated polymer. *Physical Review B* **60**, 277–283 (1999).

19. Theander, B. M., Granlund, T., Johanson, D. M., Ruseckas, A. & Sundström, V. Layer Lasing Microcavity with an Orientaed Liquid-Crystaline Polyfluorene copolymer as Active Layer. *Advanced Materials* **13**, 323–327 (2001).

20. Klarner, G., Davey, M., Chen, W., Scott, J. C. & Miller, R. Colorfast Blue-Light_Emitting Random Copolymers Derived from Di-n-hexylfluorene and Anthracene. *Advanced Materials* **10**, 993–997 (1998).

21. Lee, A. *et al.* A comparative study on the optical properties of indenofluorene and indenopyrazine. *Computational Materials Science* **49**, S251–S255 (2010).

22. Burkhart, B., Khlyabich, P. P. & Thompson, B. C. Influence of the Ethylhexyl Side-Chain Content on the Open-Circuit Voltage in rr-Poly(3-hexylthiophene- co -3-(2-ethylhexyl)thiophene) Copolymers. *Macromolecules* **45**, 3740–3748 (2012).

23. Shen, P. *et al.* Band gap and Molecular-Energy-Level Control of Conjugated-Polymer Photovoltaic Materials Based on 6,12-Dihydro-diindeno[1,2- b ;10,20- e]pyrazine. *Macromolecular Chemistry and Physics* **214**, 1147–1157 (2013).

24. Kang, J. S. *et al.* Synthesis and Luminescent Properties of Poly(alkylated indenopyrazine) and Its Copolymer Containing an Alkylated Spirofluorene Moiety. *Molecular Crystals and Liquid Crystals* **514**, 171/[501]–179/[509] (2009).

25. Craig, M. R., De Kok, M. M., Hofstraat, J. W., Schenning, A. P. H. J. & Meijer, E. W. Improving color purity and stability in a blue emitting polyfluorene by monomer purification. *Journal of Materials Chemistry* **13**, 2861 (2003).

26. Grice, a. W. *et al.* High brightness and efficiency blue light-emitting polymer diodes. *Applied Physics Letters* **73**, 629 (1998).

27. Xia, C. & Advincula, R. C. Decreased Aggregation Phenomena in Polyfluorenes by Introducing Carbazole Copolymer Units. *Macromolecules* **34**, 5854–5859 (2001).

28. Polymers, L. *et al.* Polyfluorenes with Polyphenylene Dendron Side Chains : Toward non-Aggregating, Light-Emitting Polymers. *Journal of the American Chemical Society* **123**, 946–953 (2001).

29. Neher, D. *et al.* Improving the Performance of Polyfluorene-Based Organic Light-Emitting Diodes via End-capping. *Advanced Materials* **13** 565–570 (2001).

30. List, E. J. W., Guentner, R., Scanducci de Freitas, P. & Scherf, U. The Effect of Keto Defect Sites on the Emission Properties of Polyfluorene-Type Materials. *Advanced Materials* **14**, 374 (2002).

31. Lupton, J. M., Craig, M. R. & Meijer, E. W. On-chain defect emission in electroluminescent polyfluorenes. *Applied Physics Letters* **80**, 4489 (2002).

32. Kang, J. S. *et al.* Synthesis and Luminescent Properties of Poly(alkylated indenopyrazine) and Its Copolymer Containing an Alkylated Spirofluorene Moiety. *Molecular Crystals and Liquid Crystals* **514**, 171/[501]–179/[509] (2009).

33. Kuik, M. *et al.* The Effect of Ketone Defects on the Charge Transport and Charge Recombination in Polyfluorenes. *Advanced Functional Materials* **21**, 4502–4509 (2011).

34. Schroeder, R. *et al.* Electrode specific electropolymerization of ethylenedioxythiophene: Injection enhancement in organic transistors. *Applied Physics Letters* **87**, 113501 (2005).

35. Koch, F. P. V, Smith, P. & Heeney, M. "Fibonacci's route" to regioregular oligo(3-hexylthiophene)s. *Journal of the American Chemical Society* **135**, 13695–8 (2013).

36. Izumi, T., Kobashi, S., Takimiya, K., Aso, Y. & Otsubo, T. Synthesis and spectroscopic properties of a series of beta-blocked long oligothiophenes up to the 96-mer: revaluation of effective conjugation length. *Journal of the American Chemical Society* **125**, 5286–7 (2003).

37. Zhang, R. *et al.* Nanostructure dependence of field-effect mobility in regioregular poly(3-hexylthiophene) thin film field effect transistors. *Journal of the American Chemical Society* **128**, 3480–1 (2006).

38. Mathijssen, S. G. J. *et al.* Dynamics of Threshold Voltage Shifts in Organic and Amorphous Silicon Field-Effect Transistors. *Advanced Materials* **19**, 2785–2789 (2007).

39. Zhang, W. *et al.* Systematic improvement in charge carrier mobility of air stable triarylamine copolymers. *Journal of the American Chemical Society* **131**, 10814–5 (2009).

40. DeLongchamp, D. M. *et al.* Molecular Basis of Mesophase Ordering in a Thiophene-Based Copolymer. *Macromolecules* **41**, 5709–5715 (2008).

41. Ashraf, R. S. *et al.* The influence of polymer purification on photovoltaic device performance of a series of indacenodithiophene donor polymers. *Advanced materials (Deerfield Beach, Fla.)* **25**, 2029–34 (2013).

42. Wang, Z. B., Helander, M. G., Greiner, M. T., Qiu, J. & Lu, Z. H. Carrier mobility of organic semiconductors based on current-voltage characteristics. *Journal of Applied Physics* **107**, 034506 (2010).

43. Sheldrick, G. M. A short history of SHELX. *Acta crystallographica. Section A, Foundations of crystallography* **64**, 112–22 (2008).

Chapter 3 - Synthesis and Device Characteristics of Semiconducting Donor – Acceptor Copolymers Based on Indenopyrazine

Introduction

Solar energy is one of the abundant sources of renewable energy and one of the most promising ways to tackle today's energy crisis. Current photovoltaic technology is dominated by inorganic materials with their high associated manufacturing, material and energy costs. These high costs limit the potential to be used for widescale energy generation without substantial government subsidies and also limits competition due to the high barriers to entry into the market.[1] Organic photovoltaics (OPV) are one of the leaders in low-cost photovoltaic solutions. OPV are based on organic semiconductors and one of the major differences between OPV and their silicon counterparts is the nature of the light harvesting. Organic semiconductors generate tightly bound excitons due to their low dielectric constant. The binding energy of the exciton is large and can be up to 1 eV.[2] This large binding energy prevents the exciton dissociating via an electric field into the corresponding electron and hole. This high binding energy however, is useful as previously seen for achieving high electroluminescence efficiency in OLED applications since the exciton does not dissociate in the presence of an electric field, which is a non-radiative decay pathway.

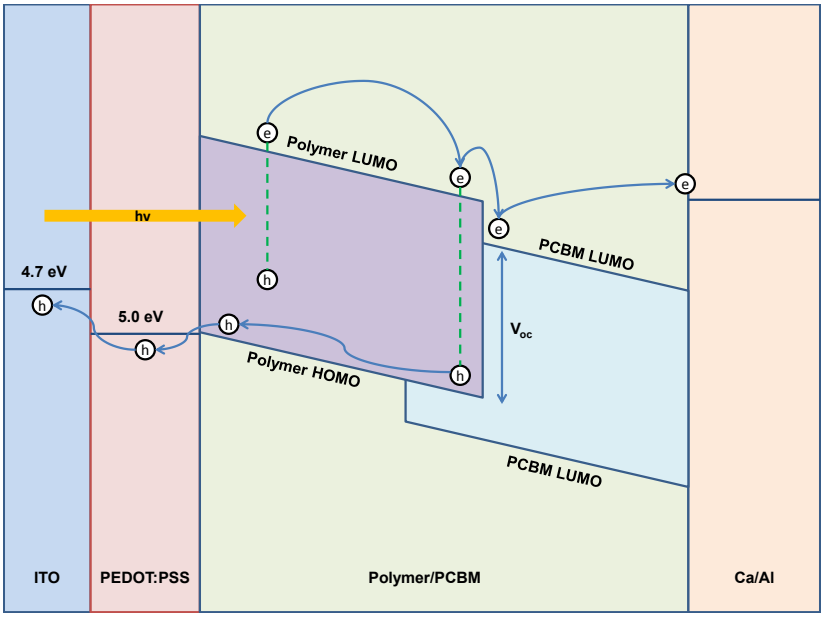

Figure 31. Energy level diagram depicting charge generation, separation and collection.

The operation of an OPV cell (Figure 31) involves the generation of free charge carries from an incident photon. As seen in the previous chapter, an incident photon of sufficient energy can cause promotion of an electron from the HOMO to the LUMO. In the previously mentioned system this generated electron – hole pair would then recombine and emit light. In order to extract energy, rather than light emission, charge separation of the associated electron-hole pair has to occur. The generated exciton migrates to the donor/acceptor interface where the difference in energy between the LUMO of the donor and the LUMO of the acceptor is the driving force for charge separation. Once the charges separate they then have to migrate towards the associated electrodes to be extracted in order to do work.

A number of features are fundamental to device physics and are often used to define the performance of a cell other than just the overall efficiency. The open circuit voltage is related to the difference in energy between the HOMO level of the donor and the LUMO level of the acceptor minus the energy associated with the exciton binding energy and this is the maximum voltage which can be extracted from a cell.[3] The short circuit current is the amount of current generated at zero voltage, and is related to the amount of photons absorbed from the solar spectrum. The external quantum efficiency is the ratio between the collected photogenerated charges and the number of incident photons, very much like the PLQE as mentioned in the previous chapter. The external quantum efficiency is made up of four efficiencies being absorption, exciton diffusion, charge separation and charge collection.

Morphology is another crucial factor in bulk heterojunction solar cells. The preferred morphology is a bicontinuous interpenetration structure of donor and acceptor domains. The domain size is also important because if the domains are too large then the generated bound excitons are unable to diffuse to an interface where charge separation can occur. The typical diffusion length of an exciton is 5-10 nm, so the ideal domain sizes would be approximately twice the exciton diffusion length.[3]

Many donor and acceptor studies have been investigated and there are numerous reviews.[3–6] In the context of this work the 4-7 bis(thiophene-2-yl)benzothia-diazole (dTBT) unit has been widely studied (Figure 32) and it was first copolymerised with both thiophene and benzothiadiazole by Sonar *et al.* via Stille and Suzuki coupling routes respectively.[7] Blends with $PC_{70}BM$ (**A)** produced the highest power conversion efficiency of 2.54%, with a polymer of number average molecular weight of 31 $kg.mol^{-1}$. Four polymers consisting of dTBT and fluorene gave a range of molecular weight polymers with **E** having the highest at 175 $kg.mol^{-1}$ and **F** the lowest at 6 kg.mol-1. The highest performing polymer for the series of four in a cell blended with $PC_{70}BM$ was **C** with an overall conversion efficiency of 3.1 %. **G** had a modest molecular number of 17 $kg.mol^{-1}$ and when blended with $PC_{61}BM$ produced a conversion efficient of 2.0 %. The final two polymers **H** and **I** had very similar molecular weights of Mn of 24 $kg.mol^{-1}$ with the indenofluorene polymer slightly outperforming the fluorene derivative by 0.2 % with a PCE of 2.6%.

Table 13. Mn/Mw, HOMO/LUMO, Voc, Jsc and PCE data. A) 1:4 $PC_{70}BM$. B) 1:4 $PC_{70}BM$. C) – F) 1:3 $PC_{70}BM$ G) $PC_{61}Bm$ 1:4. H) $PC_{71}BM$ 1:2 J) $PC_{71}BM$ 1:2.

Polymer	Mn/Mw $kg.mol^{-1}$	HOMO (eV)	LUMO (eV)	V_{oc} (V)	J_{sc} (mA/cm^2)	FF	PCE (%)
A	8.4/11.5	- 5.4	- 3.6	0.73	4.80	0.30	1.1
B	31.1/56.1	- 5.2	- 3.2	0.86	7.27	0.41	2.5
C	77.1/130.5	- 5.5	- 3.5	0.97	6.70	0.47	3.1
D	175.0/318.0	- 5.6	- 3.6	1.06	4.90	0.41	2.2
E	10.6/13.4	- 5.4	- 3.4	0.98	6.30	0.48	2.8
F	6.2/14.0	- 5.5	- 3.6	0.94	6.20	0.46	2.7
G	13.0/27.0	-5.6	- 3.7	0.97	4.86	0.43	2.1
H	23.3/40.2	- 5.4	- 3.6	0.87	6.02	0.44	2.3
I	25.5/43.2	- 5.5	- 3.7	0.90	6.12	0.48	2.6

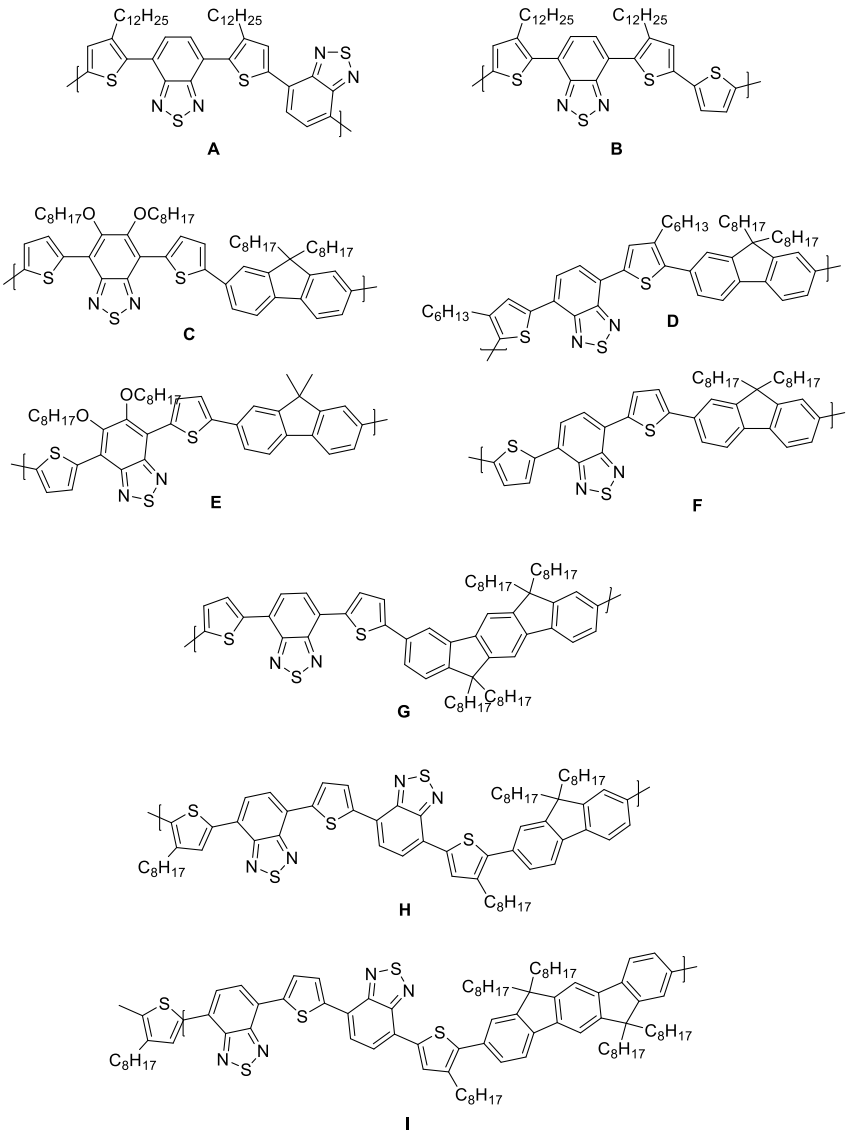

Figure 32. dTBT Copolymers. Poly[4,7-bis(3-dodecylthiophene-2-yl) benzothia-diazole-co-benzothiadiazole] (A)[7], poly[4,7-bis(3-dodecylthiophene-2-yl) benzothia-diazole-co-thiophene] (B)[7], C,[8] D,[8] E,[8] F, G[9], H[10] and I.[10]

Aims

The aim of this work was the synthesis of a range of push – pull copolymers based upon indenopyrazine as the donor, and acceptors consisting of a range of dTBT units. As discussed above indenofluorene based polymers copolymerised with dTBT produce devices with a high V_{oc} close to 1 V. With the substitution of an indenopyrazine we aim to stabilize the LUMO level in order to broaden with wavelength of light absorbed, and hopefully improve the photocurrent of the devices. A range of different dTBT units were investigated, in which the

flanking thiophenes were kept identical, but the central BT unit was modified with a variety of substituents (Figure 33).

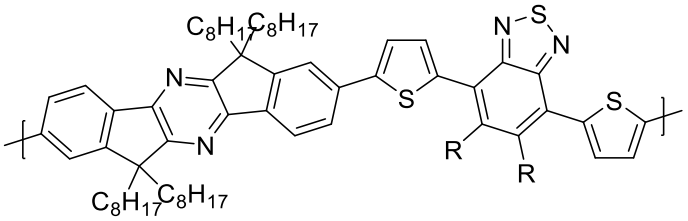

IP-dTBT; R = H,
IP-dTBT-F; R = F,
IP-dTBT-OC$_8$H$_{17}$; R = OC$_8$H$_{17}$,
IP-dTBT-SC$_{12}$H$_{25}$; R = SC$_{12}$H$_{25}$

Figure 33. Chemical structure of the proposed 4 co polymers of the IP-dTBT series.

These four substituents were chosen because they offered a comparison of varying solubility, electronegativity and atomic sizes. The unsubstituted **IP-dTBT** would have the smallest group on the BT unit consisting of a hydrogen atom. The fluorine containing **IP-dTBT-F** would be similar to **IP-dTBT** in structure as the substituents are similar in size (hydrogen has a van der Waals radius of 1.2Å whereas fluorine has a radius of 1.35Å), however, the fluorine atom is the most electronegative element (fluorine has an electronegativity rating of 4.0 on the Pauling scale compared to hydrogen at 2.2) thus influencing the polymer electronic and physical properties. The incorporation of an alkoxy chain in **IP-dTBT- OC$_8$H$_{17}$** is expected to increase solubility and also contains an oxygen substituent which acts as a an electron donor into the conjugated system.[11] The final polymer **IP-dTBT-SC$_{12}$H$_{25}$** contains a thioalkyl group which is expected to offer a similar solubility profile compared to the alkoxy side, but the increased size of the sulphur compared to the oxygen as well as its differing donating ability may result in some changes in performance. All four polymers will be compared and contrasted, and their performance in organic solar cells assessed.

Synthesis

The synthesis of monomer 2,8-bis-(4,4,5,5-tetramethyl-1,3,2-dioxaborolan-2-yl)-6,6,12,12-tetraoctyl-6,12-dihydrodiindeno[1,2-b:1',2'-e]pyrazine was performed as explained in chapter 2. The four co monomers were synthesised according to literature procedures.[12–14]

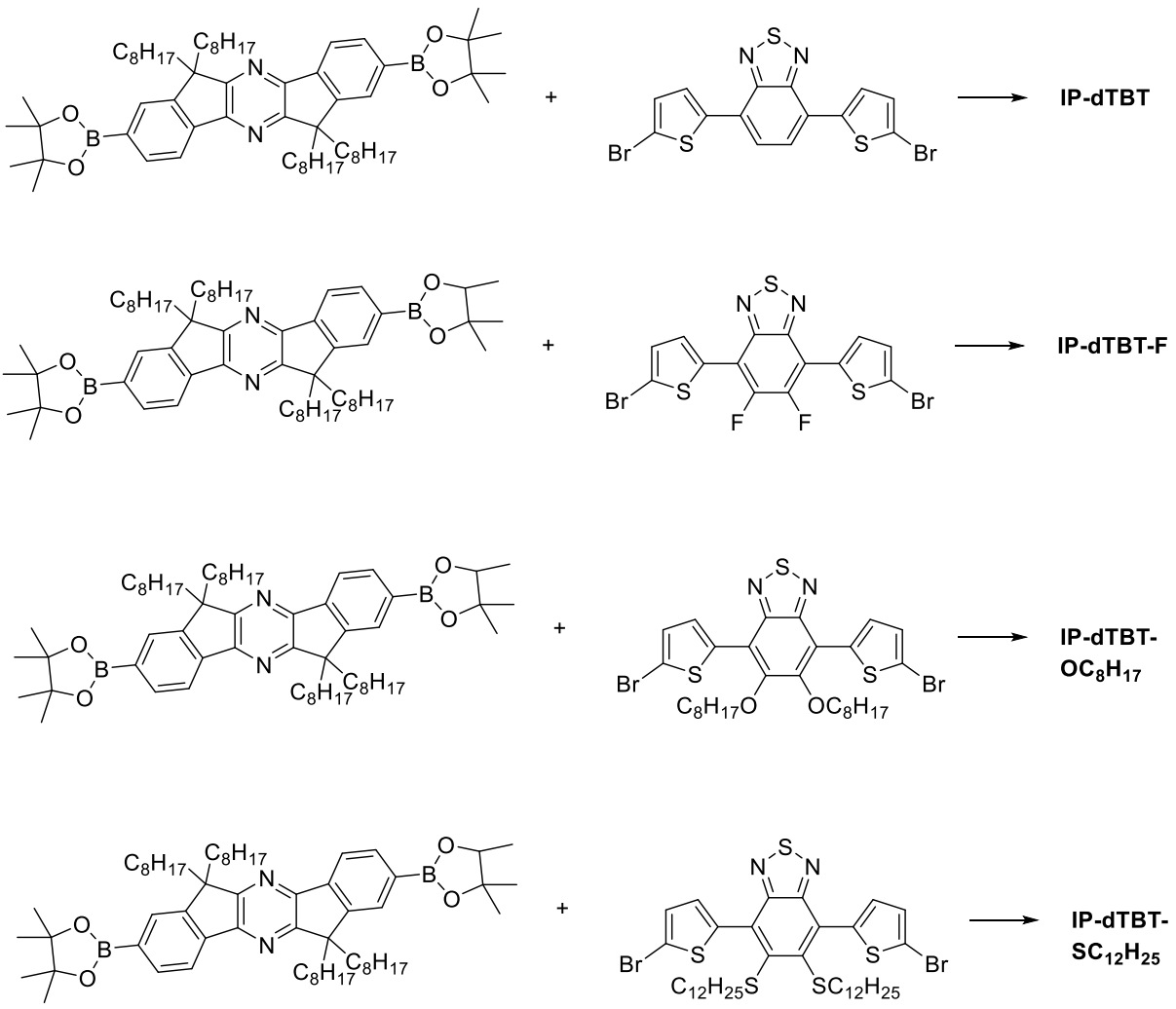

Scheme 8. Synthesis of the four polymers in the IP-dTBT series.

All four polymers were synthesised via palladium catalysed Suzuki coupling. The monomers were heated in toluene in the presence of the phase transfer agent aliquot 336™, $Pd(PPh_3)_4$ and aqueous K_2CO_3 as the base. The polymerisation proceeded slowly and was heated at 105 °C for 3 days. The polymers were purified by soxhlet extraction with methanol, acetone and hexane to remove low molecular oligomers and catalyst residues. The remaining polymer

was dissolved into chloroform and stirred with aqueous sodium diethyldithiocarbamate at 50 °C for 3 hours to remove palladium residues.[15] After work-up, the final polymers were precipitated from the minimum amount of hot chlorobenzene into methanol. All four polymers were isolated as dark red fibres in good yields (Table 14).

Table 14. Polymer yields and molecular weight data. Molecular weights were determined by GPC against polystyrene standards

Polymer	Yield (%)	M_n (kDa)	M_w (kDa)	PDI	DP[1]
IP-dTBT	68	40	81	2.1	39
IP-dTBT-F	59	37	66	1.8	35
IP-dTBT-OC_8H_{17}	63	78	105	1.3	61
IP-dTBT-$SC_{12}H_{25}$	61	77	120	1.6	54

[1]Degree of polymerisation is based on the number average molecular weight.

The molecular weights of all polymers were measured by gel permeation chromatography in chlorobenzene at 80 °C against polystyrene standards. The four polymerisations all produced reasonably high molecular weights with comparable polydispersity. The Mn was lower for both **IP-dTBT** and **IP-dTBT-F** in comparison to **IP-dTBT-OC_8H_{17}** and **IP-dTBT-$SC_{12}H_{25}$**. The fluorinated polymer has a slightly lower degree of polymerisation, which we attribute to the lower solubility of this polymer in comparison to the other three. This could limit the molecular weight by precipitation of the growing polymer chain from solution during the polymerisation process. Nevertheless in all cases the degree of polymerisation appears sufficiently high to allow for a reasonable comparison of the properties of each polymer.

Optical data and Energy Levels

The UV-Vis absorption spectra of the series of four polymers were recorded in order to obtain an understanding of the optical band gap and their optical behaviour in the solid state. The optical band gap is a key parameter on the operation of a solar cell,[16] and was measured here by at the point that the absorption and emission spectra overlap in the solid state. Chlorobenzene solutions and spin cast thin films were investigated to observe if there was

any change in the absorption spectrum on going from solution to film. The results can be seen in Figure 34 and summarised in Table 15.

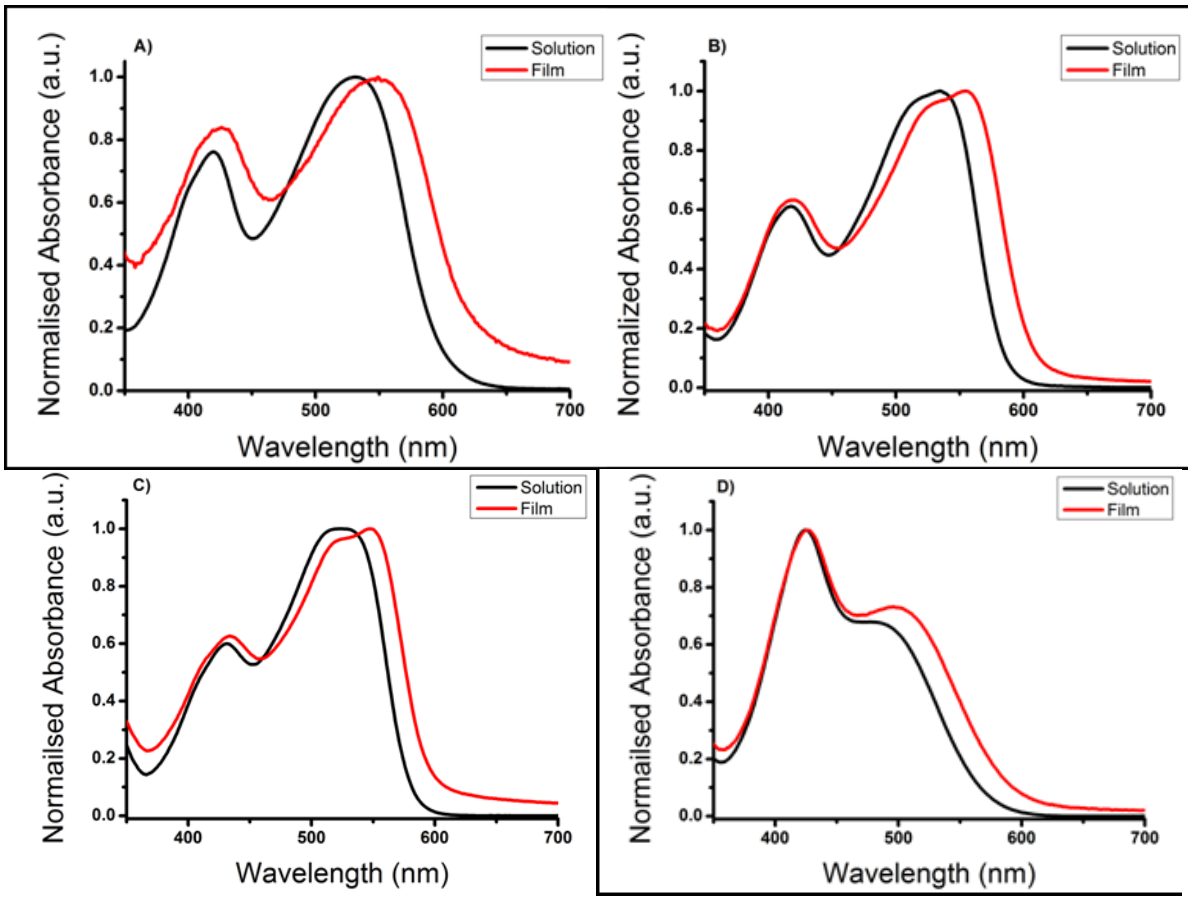

Figure 34. Absorption spectra of polymer IP-dTBT (A), IP-dTBT-F(B), IP-dTBT-OR (C) and IP-dTBT-SR (D)

The UV-Vis absorption spectra show that varying the substituents on the benzothiadiazole acceptor unit had a pronounced effect on the absorption maximum in both thin film and solution. The solution samples were dissolved in chlorobenzene and the thin films were spun from a solutin of 5mg/mL in chlorobenzene on to glass at a spin rate of 1000 rpm for 1 minute. When no substituent was present on the benzothiadiazole unit, **IP-dTBT**, the absorption spectrum in solution has two major feature peaks. The higher energy absorption at the shorter wavelength of 420 nm can be attributed to the $\pi - \pi^*$ transition, compared to the longer wavelength absorption at 531 nm which is often attributed to a charge transfer transition from the π orbital of the delocalised HOMO to the localised LUMO of the benzothiadiazole.[14] When the absorption of **IP-dTBT** was recorded in the solid state, a

bathochromic shift of both peaks was observed with the new maxima at 426 nm and 549 nm respectively. The red-shift in absorption can be attributed to an increase in polymer planarity and molecular ordering in the solid state resulting. The increase in backbone planarity results in better π – π overlap along the backbone, and therefore a smaller band gap.

Comparing **IP-dTBT** with **F-dTBT (F)**[17] and **IF-dTBT (G)**[17], all three show separate peaks relating to the π-π* transition and ICT transition. The λ_{max} in the solid state of **F-dTBT** was red-shifted 15 nm with respect to **IP-dTBT**, whilst **IF-dTBT** had a similar absorption that was blue-shifted by 4 nm. It was also interesting to note that whilst **IP-dTBT** and **F-dTBT** had absorptions where the ICT was more intense than the π-π* transition, **IF-dTBT** was the opposite with a more intense π-π* transition.

Table 15. Optical and energetic properties. The HOMO was measured via PESA.

Polymer	λ_{max} (nm) solution		λ_{max} (nm) film		λ_{onset} (nm)			
	π- π*	CT	π- π*	CT	Film	HOMO (eV) ±0.05	LUMO[1] (eV)	E_g^{opt} [2] (eV)
IP-dTBT	420	531	426	549	629	- 5.64	- 3.53	2.11
IP-dTBT-F	417	535	420	554	608	- 5.68	- 3.58	2.10
IP-dTBT-OR	431	523	434	547	594	- 5.62	- 3.55	2.07
IP-dTBT-SR	425	484	426	496	592	- 5.79	- 3.77	2.02

[1] LUMO was calculated taking the HOMO plus the E_g^{opt}

[2] E_g^{opt} was taken as the intersect of absorption and emission in the solid state.

With the introduction of the electron withdrawing fluorine onto the polymer backbone it was observed that the HOMO and LUMO energy levels of **IP-dTBT-F** deepened slightly with respect to that of **IP-dTBT**. The change was minor and within the error of the PESA measurements, but appears reasonable that the fluorine would withdraw electron density from the polymer backbone stabilising both energy levels. The major absorption peaks of **IP-dTBT-F** in solution were 417 and 535 nm, and 420 nm and 554 nm in the thin film i.e. very little change with respect to the non-fluorinated analogue. There was also the emergence of a

small shoulder in UV spectra at 525 nm**.** This shoulder is suggestive of aggregation arising from strong polymer chain packing in the solid state. The shift upon film formation in the π – π* transition peak is 3 nm, and 19 nm for the charge transfer transition peak. There is also a change in the relative intensities of the two absorption peaks compared to **IP-dTBT,** with the charge transfer transition becoming more prominent. The presence of the fluorine and its associated increase in electronegativity will likely cause the LUMO to be lower in energy and more localised on the acceptor unit leading to the minor red shift in the charge transfer band. The relative increase in absorption could be ascribed to an increase in the overlap of the wavefunctions of the initial and final states and is discussed in more detail in the density functional theory calculations.

Introducing the alkoxy side chain resulted in a slight increase of the ionisation potential of **IP-dTBT-OC$_8$H$_{17}$** with respect to the parent polymer. Although oxygen is electronegative the overall effect is an increase in the ionisation potential , due to the mesomeric donation of the oxygen lone pairs of electrons. The peaks assigned to the π – π* transition in both solution and thin film were bathochromically shifted at 431 nm and 434 nm with respect to **IP-dTBT** and **IP-dTBT-F**. The peaks associated with the ICT absorption are hypsochromically shifted to 523 nm and 547 nm with respect to **IP-dTBT** and **IP-dTBT-F**.

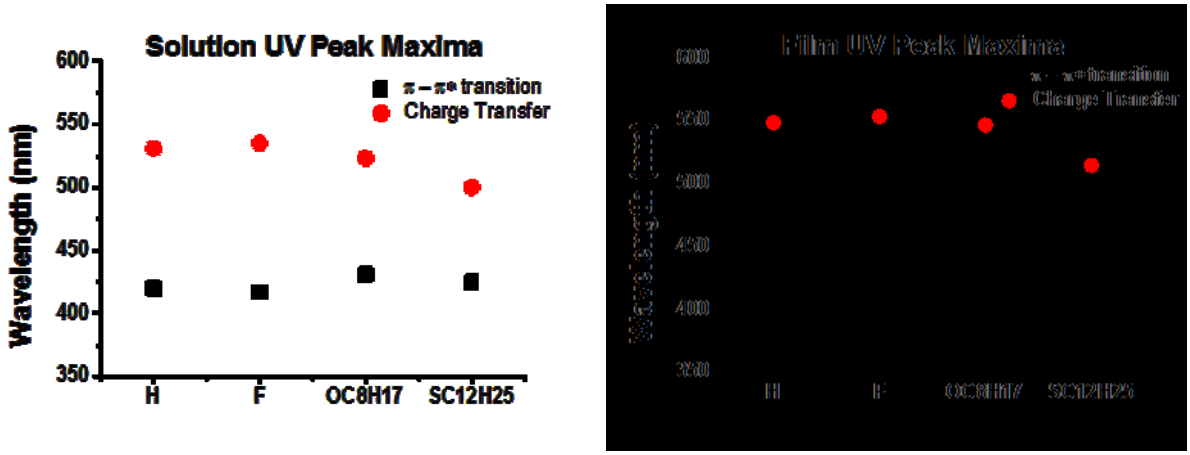

Figure 35. The peak maxima for both solution (left) and film (right) of the π – π* transition and the ICT absorption

In the case of the thioalkyl substituted polymer, the π – π* transition peak was observed at 425 nm in solution, very similar to that of the **IP-dTBT**. However the ICT absorption peak is greatly blue shifted to 500 nm. A similar situation arises with the absorption when the polymer is in the solid state, a similar π – π* absorption and a blue-shifted charge transfer is observed. The ratio of the strength of absorptions for **IP-dTBT-SC$_{12}$H$_{25}$** is the opposite of the three **IP-dTBT** polymers. The intensity of the ICT absorption is greatly reduced compared to the absorption of the π-π* transition. The weak ICT absorption could be attributed to the presence of the large sulphur atom on the BT unit, which causes a greater amount of twisting along the backbone between the BT and thiophene units. This twisting leads towards poor wavefunction overlap between the initial and final states resulting in a weak absorption being observed.

The ionisation potential of **IP-dTBT** was recorded to be -5.64 eV. From ionisation potentials estimated via PESA there is a small lowering of the HOMO level to -5.68 eV for **IP-dTBT-F**, but this difference is within the error of the technique (±0.05 eV), so it is difficult to make any conclusive interpretation of the effect of the electron withdrawing fluorine. **IP-dTBT-SC$_{12}$H$_{25}$** had the largest ionisation potential at -5.79 eV, whilst **IP-dTBT-OC$_8$H$_{17}$** had an ionisation potential close to that of **IP-dTBT** and **IP-dTBT-F** at -5.62 eV. In agreement with the literature the S-R containing polymer had the highest ionisation potential with a difference of ≈ 0.2 eV.[14]

Density Functional Theory

In order to probe the effect of the substituents on the backbone polymer conformation, computational models of trimers (i.e. three repeat units of the polymer chain) of the four polymers were calculated. In order to minimise the computational requirements, the actual sidechains were replaced with simple methyl groups. Calculations were run using DFT

methods, with Guassian 09 and a B3LYP/6-31G(*) basis set. All calculations were allowed to relax to an energy minimum from a variety of molecular conformations (i.e. thiophenes either cis or trans to the BT unit) and the lowest energy confomers are shown. A theoretical value for the HOMO was able to be predicted from calculation.

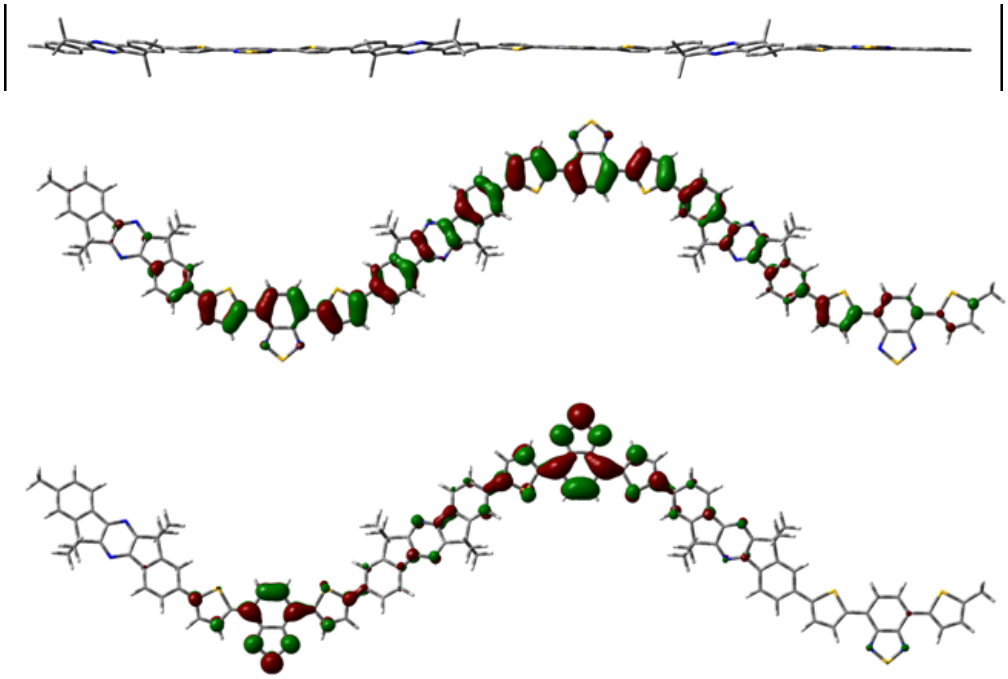

Figure 36. DFT calculation of IP-dTBT (top), HOMO orbitals (middle) and LUMO orbitals (bottom)

The results of the **IP-dTBT** calculation demonstrated that a partially twisted backbone was predicted (Figure 36). Along the backbone twisting occurs in two places. Using Figure 36 as a reference and measurements based around the central trimer, the first torsion angle twist is between the **IP - T** (plane of atoms 2 – 5) and has a value of 23°. The second torsion angle is between **T – BT** (plane of atoms 5 – 8) and in this case is smaller than the first angle with a value of 7.9°. Although we observed some twisting, it does not seem to strongly affect the delocalisation of the HOMO molecular orbital, which is distributed evenly along the full length of the conjugated backbone. In contrast the LUMO is more localised, however, being concentrated around the dTBT unit with only a slight presence across the indenopyrazine unit.

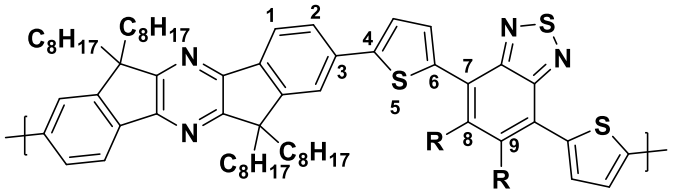

Figure 37. Chemical structure of the IP-dTBT frame work highlighting the atoms and subsequent torsion angles that are relevant.

Figure 38 shows the calculated structure of **IP-dTBT-F** and its associated HOMO and LUMO molecular orbital distributions. The introduction of the fluorine onto the BT unit appears to planarise the backbone with respect to the unsubstituted **IP-dTBT**. There is a reduction in the **IP-T** (atoms 2-5) torsion angle to 21.4' and a similar reduction to 3.7° of the **T-BT** (atoms 5-8) torsion angle. We believe this is due to an electronic interaction between fluorine and sulphur which promotes planarisation.[18] The change in conformation correlates with the difference seen in the relative intensity of the charge transfer absorption and the wavefunction overlap of the initial and final states. The distribution of the HOMO is relatively unchanged on the addition of F, but there is a slight concentration of the LUMO towards the BT unit. This slight concentration can be attributed to the greater electronegativity of the fluorine atom.

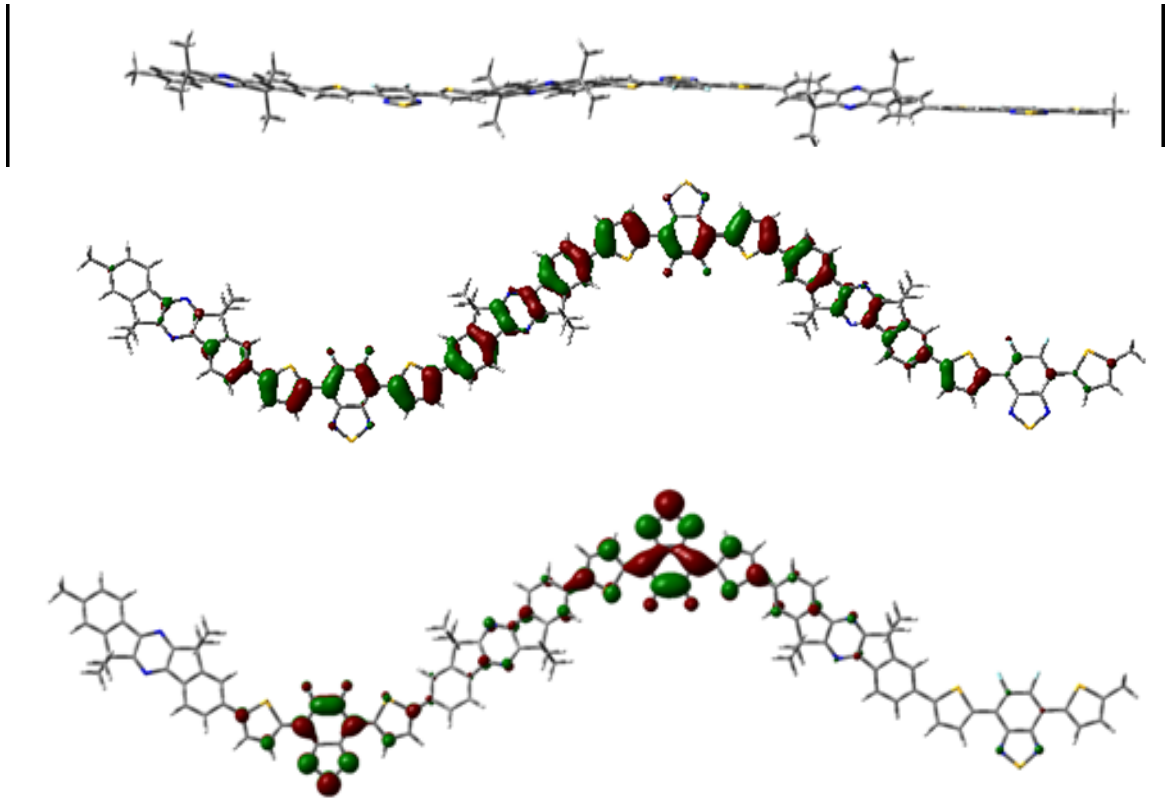

Figure 38. DFT calculation of IP-dTBT-F (top), HOMO orbitals (middle) and LUMO orbitals (bottom)

Table 16. Theoretical energy levels and predicted torsion angles of the four IP-DTBT polymers.

Polymer	HOMO (eV)	LUMO(eV)	Band gap (eV)	Torsion IP-T	Torsion T-BT
IP-dTBT	- 4.96	- 2.77	2.19	23.0°	7.0°
IP-dTBT-F	- 5.05	- 2.85	2.20	21.4°	3.7°
IP-dTBT-OC_8H_{17}	- 4.88	- 2.63	2.25	23.2°	9.9°
IP-dTBT-$SC_{12}H_{25}$	- 5.12	- 2.77	2.35	25.1°	54.9°

Figure 39 shows the DFT calculation of IP-DTBT-OC_8H_{17} . The calculation shows the twisting between the **IP-T** was almost the same as **IP-dTBT** at 23.0°, but there was an increase in the torsion angle between **T-BT**. This increase can be attributed to the relative size of the oxygen atom and its steric interaction with the thiophene substituent. Once again the HOMO molecular orbital was distributed evenly along the polymer backbone. The central LUMO was less localised on the BT unit compared to the parent polymer, and was

distributed over the adjacent aromatic units, likely due to the inductively withdrawing effects of the oxygen.

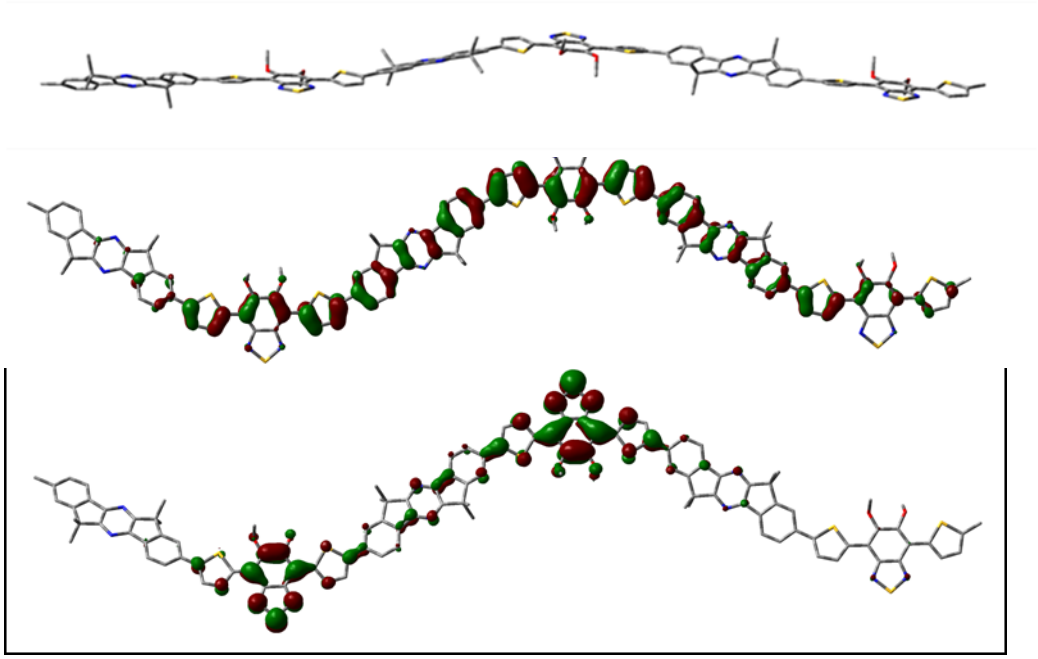

Figure 39. DFT Calculation of IP-DTBT- OC_8H_{17} (top), HOMO orbitals (middle) and LUMO orbitals (bottom).

The calculated minimum energy geometry of **IP-dTBT-$SC_{12}H_{25}$** is shown in Figure 40. Here we observe substantial differences to the alkoxy polymer with respect to the twisting of the dTBT unit. Thus whilst the **IP-T** backbone twist remained relatively comparable to the three other polymers, the torsion angle between **T-BT** was very large at 54.9°.

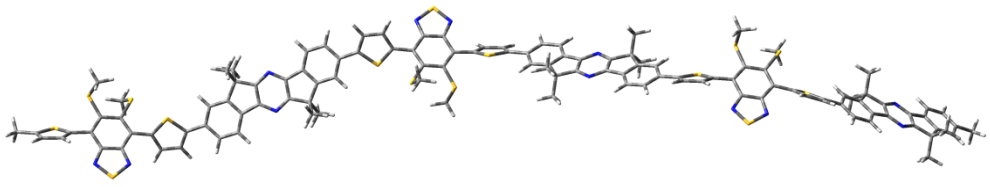

Figure 40. DFT Calculated minimum geometry of of IP-dTBT- $SC_{12}H_{25}$.

The large twisting was in agreement with the data recorded from UV-Vis spectroscopy. The spectra were dramatically different to the other three polymers. The charge transfer peak was

considerably lower than the $\pi - \pi^*$ transition. This suggests that there was poor wavefunction overlap between the initial and excited states of **IP-dTBT-SC$_{12}$H$_{25}$.** The thioalkyl substituent clearly caused a large deviation from backbone planarity around the electron accepting BT unit, reducing conjugation between the BT and the adjacent thiophene units and likely localising the LUMO on the BT.[19] The calculated value of the ionisation potential is in agreement with the trend observed from the PESA measurements being ≈ 0.15 eV higher.

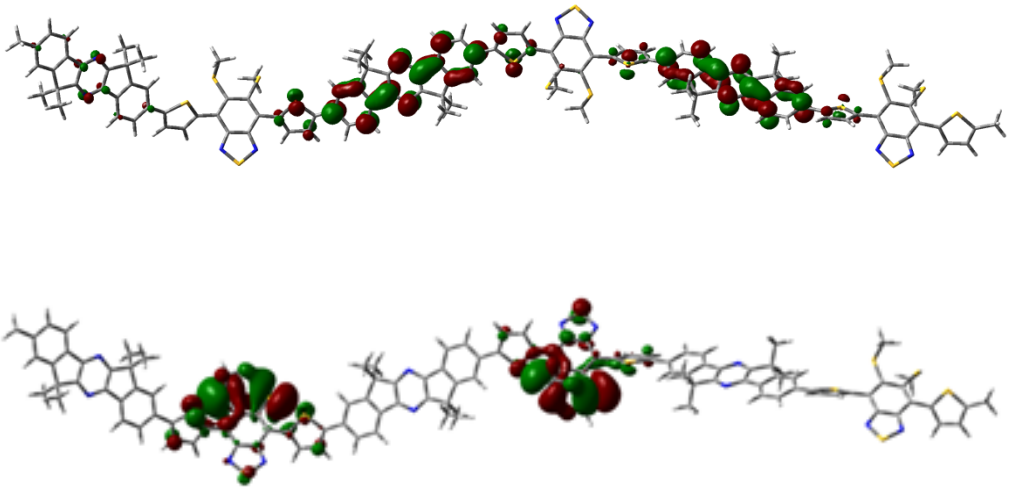

Figure 41 IP-DTBT- SC$_{12}$H$_{25}$ (top), HOMO orbitals (middle) and LUMO orbitals (bottom).

Due to the large twisting along the backbone the distribution of the HOMO orbital is greatly disrupted compared to the other three polymers in the series. The HOMO resides almost solely on the indenopyrazine unit whilst the calculated LUMO is confined to the BT unit. This is in agreement with the UV-Vis absorption spectra where we predict poor wavefunction overlap between the inital and final state of the HOMO and LUMO.

Photoluminescence Spectroscopy

The photoluminescence emissions were recorded for the four polymers in order to study the effects of varying the BT substituents on the emission wavelength. The crossover of the absorption and emission spectra was used to calculated the optical band gap. Films on glass were prepared by spin-coating from 5 mg / mL solutions in chlorobenzene. The UV and PL were recorded at room temperature.

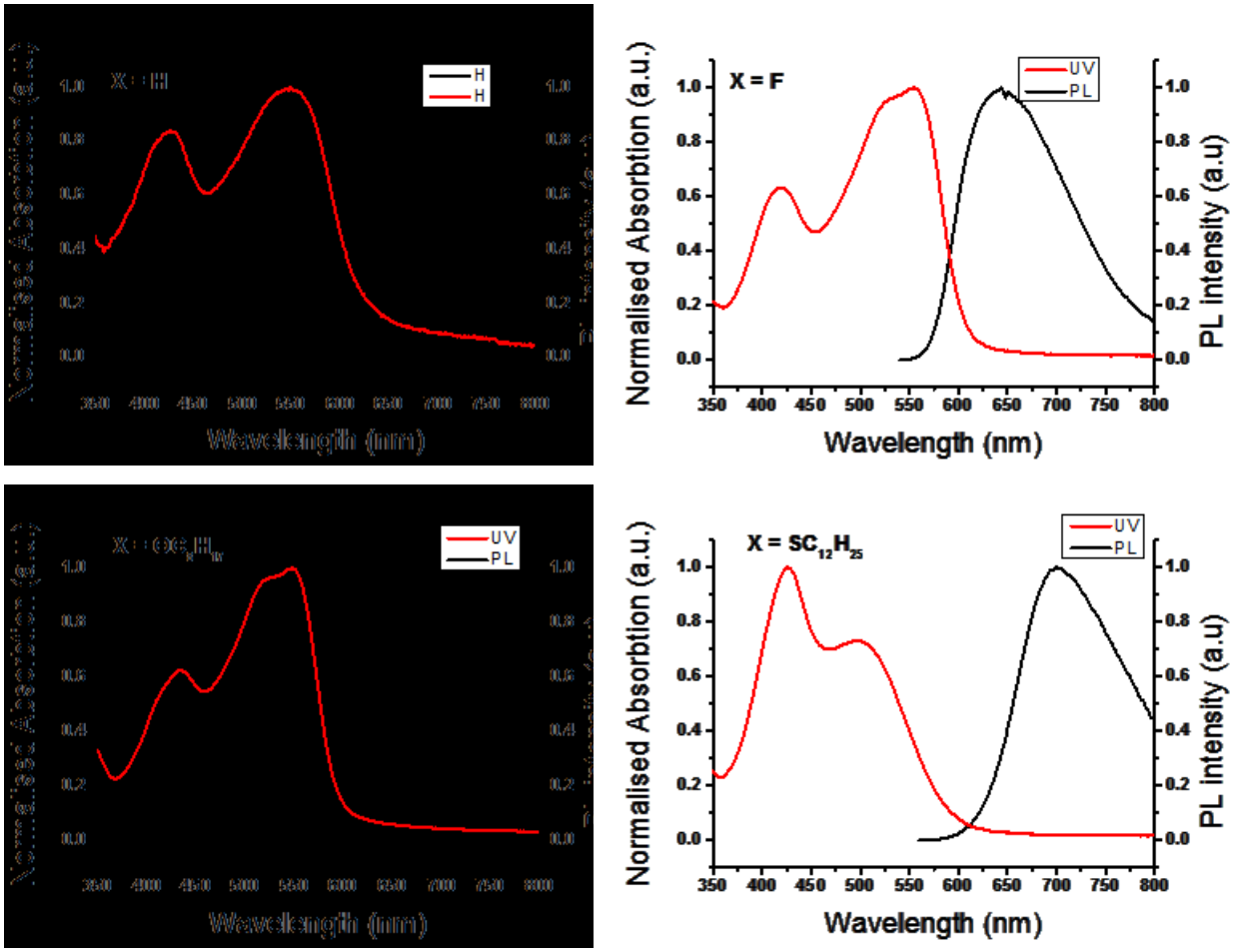

Figure 11. UV-Vis and PL spectra of the four IP-dTBT polymers.

Table 17. Optical absorption and emissiotn for thin films of .

Polymer	Absorption λ_{max}(nm)	Emission λ_{max}(nm)	$\Delta\lambda$ (nm)
IP-dTBT	426 / 549	632	101
IP-dTBT-F	420 / 554	644	109
IP-dTBT-OC_8H_{17}	434 / 547	678	155
IP-dTBT-$SC_{12}H_{25}$	426 / 496	700	204

The polymers did not exhibit a clear vibronic structure of emission as was seen in the indenopyrazine – fluorene series from chapter 2. This suggests that there was a wide range of emission wavelengths and not one dominant electronic transition. However all four polymers exhibit a large difference in the absorption and emission maximum. For **IP-dTBT** the emission maximum was 632 nm, corresponding to a Stokes shift of 101 nm. This large Stokes shift can be attributed to the difference in structure of the ground state and excited state structure of the polymer. **IF-dTBT** had an emission maximum bathochromically shifted with a λ_{max} of 613 nm with a smaller band gap of 1.97 eV.[17] This is in agreement with the proposed lowering on the LUMO of indenopyrazine polymers compared to indenofluorene because the first absorption peak at 420 nm (**IP-dTBT**) is smaller in energy that the associated absorption of the indenofluorene unit of 402 nm.

The emission wavelength was progressively red-shifted for the alkoxy and thioalkyl substituted polymers, and therefore the Stokes shift was progressively increased up to 204 nm for **IP-dTBT-SC$_{12}$H$_{25}$**. The large Stokes shift in the case of the of the thioalkyl substituted polymer can be ascribed to the large difference in geometry between the twisted ground state, and the more planar excited state, in analogy with that observed with carbazole polymers.[14]

Differential Scanning Calorimetry

Differential scanning calorimetry measurements were performed on all polymers. No melt or crystallisation peaks were observed on any of the 3 cycles. This suggests that all the polymers are amorphous between the temperature range of 50°C and 300°C.

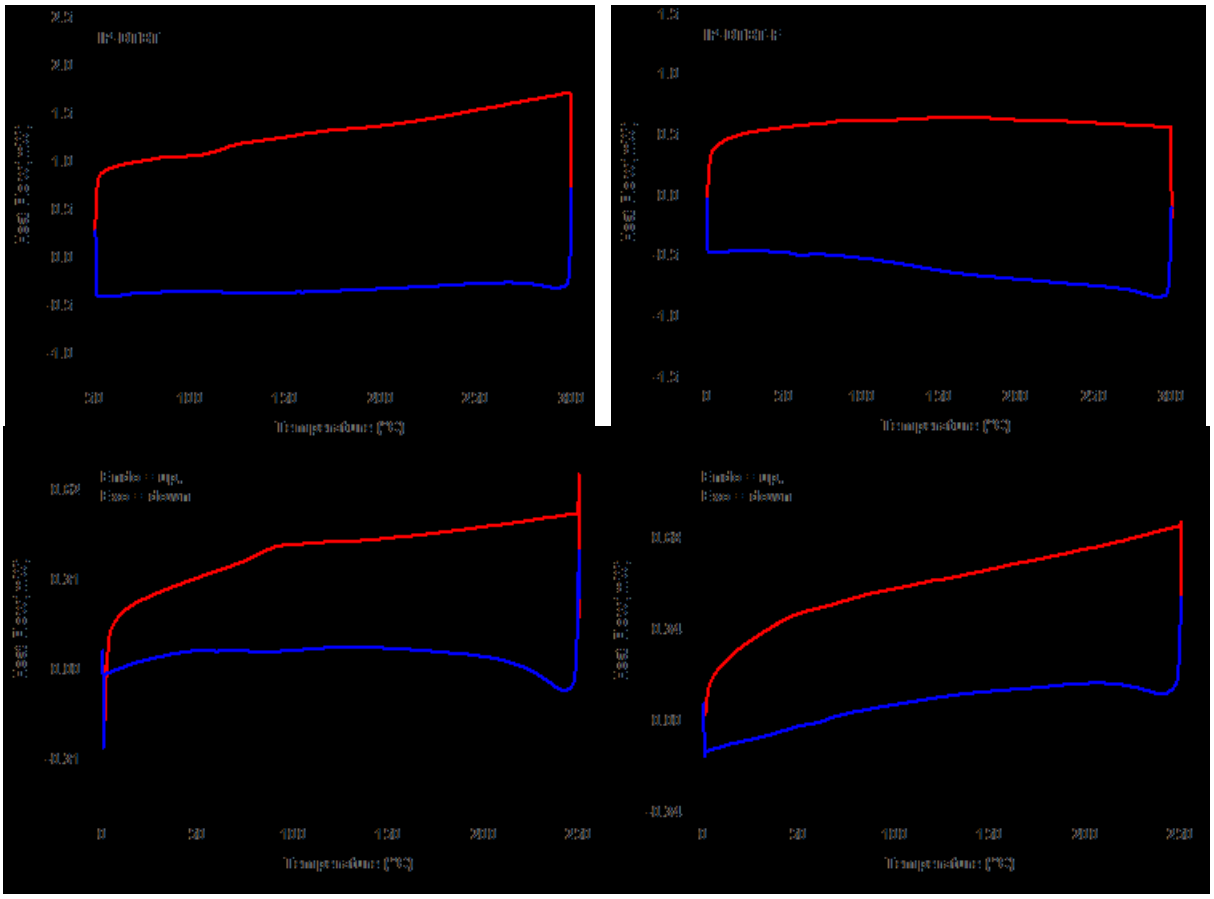

Figure 42. Differential scanning calorogrmas of of IP-dTBT (top left), IP-dTBT-F (top right), IP-dTBT-OR (bottom left) and IP-dTBT-SR (bottom left). All four are of the first cycle in the temperature range of 0-250 °C with a heating rate of 10°C/min

We note that attempts to fabricate field effect transistors from all polymers were unsuccessful. We ascribe this to the large injection barrier for injecting charge from the gold electrodes, due to the large ionisation potential of the polymers.

Photovoltaic devices

The photovoltaic properties of the four **IP-dTBT** polymers were investigated in blends with $PC_{70}BM$ (1:4) and the polymer concentration was 10 mg/mL. Devices were fabricated by

spin coating blends of the polymer from chlorobenzene, with an architecture of glass/ITO/PEDOT/active layer/Ca/Al.

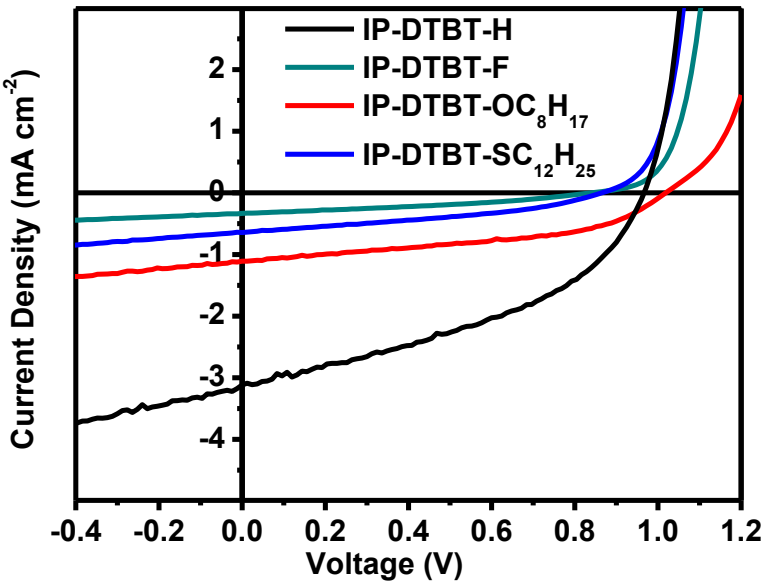

Figure 43. J-V curve of the four polymers in the IP-dTBT series with a device architecture of ITO/PEDOT:PSS/IPdTBT active layer/$PC_{71}BM$

From Figure 43 it can be seen that all four polymers have a similar V_{oc} close to 1 V with **IP-dTBT-OC_8H_{17}** having the highest. The cell voltages measured do not track well with the measured ionisation potentials. This probably relates to the fact that the cells were not well optimised with little effort being put into optimisation. Thus different blend ratios or solvent additives were not investigated. Unfortunately the measurements were performed by a collaborator and further optimisation would likely improve performance. Nevertheless we can clearly observe that high voltage is obtained in all cases, which may be useful for some applications. It is difficult to make many conclusions about the structure-property relationships due to the fact that all cells perform rather badly.

Table 18. Photovoltaic device parameters for blends with $PC_{71}BM$. Polymer:$PC_{71}BM$ ratio is 1:4 in all cases.

Polymer	J_{sc} (mA/cm^2)	V_{oc} (V)	Fill Factor	PCE (%)
IP-dTBT	3.12	0.97	0.42	1.27
IP-dTBT-F	0.33	0.84	0.34	0.09
IP-dTBT-OC_8H_{17}	1.11	1.02	0.46	0.52
IP-dTBT-$SC_{12}H_{25}$	0.64	0.86	0.36	0.2

Conclusion

Four novel indenopyrazine polymers were synthesised in order to investigate the effects of both indenopyrazine incorporation, and also the nature of the substituent of on the benzothiadiazole co-monomer. We found that that the incorporation of indenopyrazine instead of indenofluorene resulted in a slight blue shift in optical band gap. Tuning of the the benzothiadiazole substituents had a large influence on the optoelectronic properties, as a result of both electronic and geometrical effects. It was found that the introduction of large bulky substituents close to the polymer backbone greatly increased the degree of backbone twisting. Smaller substituents such as fluorine did not perturb backbone planarity, but resulted in a lowering of both the HOMO and LUMO. The fluorine also had a negative effect on the degree of polymerisation with its inclusion causing a reduction in chain length. Inclusion of thioalkyl sidechains resulted in polymers with a very large degree of backbone twisting. This degree of twisting had a negative effect on the overall OPV performance but it did produce a polymer that had a large Stoke shift of over 200 nm which could potentially be interesting in for use in applications where self-absorption should be minimised.

References

1. Independent statistics and analysis, *U.S. Energy Information Administration.* www.eia.gov/aer www.eia.gov/aer.

2. Forrest, S. R. The Path to unbiquitous and low-cost organic electronic appliances on plastic. *Nature Review Article* 911–918 (2004).

3. Li, G., Zhu, R. & Yang, Y. Polymer solar cells. *Nature Photonics* **6**, 153–161 (2012).

4. Thompson, B. C. & Fréchet, J. M. J. Polymer-fullerene composite solar cells. *Angewandte Chemie (International ed. in English)* **47**, 58–77 (2008).

5. Ameri, T., Khoram, P., Min, J. & Brabec, C. J. Organic Ternary Solar Cells: A Review. *Advanced Materials* 1–22 (2013)

6. McCulloch, I. Organic Electronics. *Advanced Materials* **25**, 1811–1812 (2013).

7. Sonar, P., Williams, E. L., Singh, S. P. & Dodabalapur, A. Thiophene–benzothiadiazole–thiophene (D–A–D) based polymers: effect of donor/acceptor moieties adjacent to D–A–D segment on photophysical and photovoltaic properties. *Journal of Materials Chemistry* **21**, 10532 (2011).

8. Li, W. *et al.* Tailoring side chains of low band gap polymers for high efficiency polymer solar cells. *Polymer* **51**, 3031–3038 (2010).

9. Kirkpatrick, J. *et al.* A Systematic Approach to the Design Optimization of Light-Absorbing Indenofluorene Polymers for Organic Photovoltaics. *Advanced Energy Materials* **2**, 260–265 (2012).

10. Li, J. *et al.* Synthesis and Photovoltaic Properties of Alternating Conjugated Polymers Derived from Thiophene-Benzothiadiazole Block and Fluorene/Indenofluorene Units. *Bulletin of the Korean Chemical Society* **35**, 505–512 (2014).

11. Hou, J. *et al.* Band gap and Molecular Energy Level Control of Conjugated Polymer Photovoltaic Materials Based on Benzo[1,2- b :4,5- b ′]dithiophene. *Macromolecules* **41**, 6012–6018 (2008).

12. Bouffard, J. & Swager, T. M. Jean Bouffard and Timothy M. Swager* Fluorescent Conjugated Polymers That Incorporate Substituted 2,1,3-Benzooxadiazole and 2,1,3-Benzothiadiazole Units.*Macromolecules* **41** 5559–5562 (2008).

13. Cho, N., Song, K., Lee, J. K. & Ko, J. Facile synthesis of fluorine-substituted benzothiadiazole-based organic semiconductors and their use in solution-processed small-molecule organic solar cells. *Chemistry (Weinheim an der Bergstrasse, Germany)* **18**, 11433–9 (2012).

14. Casey, A., Ashraf, R. S., Fei, Z. & Heeney, M. Thioalkyl-Substituted Benzothiadiazole Acceptors: Copolymerization with Carbazole Affords Polymers with Large Stokes Shifts and High Solar Cell Voltages. *Macromolecules* **47**, 2279–2288 (2014).

15. Schroeder, R. *et al.* Electrode specific electropolymerization of ethylenedioxythiophene: Injection enhancement in organic transistors. *Applied Physics Letters* **87**, 113501 (2005).

16. Günes, S., Neugebauer, H. & Sariciftci, N. S. Conjugated polymer-based organic solar cells. *Chemical reviews* **107**, 1324–38 (2007).

17. Zheng, Q., Jung, B. J., Sun, J. & Katz, H. E. Ladder-type oligo-p-phenylene-containing copolymers with high open-circuit voltages and ambient photovoltaic activity. *Journal of the American Chemical Society* **132**, 5394–404 (2010).

18. Babudri, F., Farinola, G. M., Naso, F. & Ragni, R. Fluorinated organic materials for electronic and optoelectronic applications: the role of the fluorine atom. *Chemical communications* **10**, 1003–1022 (2007).

19. Casey, A., Ashraf, R. S., Fei, Z. & Heeney, M. Thioalkyl-Substituted Benzothiadiazole Acceptors: Copolymerization with Carbazole Affords Polymers with Large Stokes Shifts and High Solar Cell Voltages. *Macromolecules* **47**, 2279–2288 (2014).

Chapter 4 - Synthesis, physical and doping characteristics of indenopyrazine - thiophene polymers for use in transistors

Introduction

Organic field effect transistors (OFETs) have become one of the leading technological applications of organic semiconductors.[1] It is the combination of their ability to be solution processed with good ambient stability and the constant improvements in charge carrier mobility that has led them to rival their inorganic counterparts.[2]

There are many different transistor designs for inorganic semiconductors but only the field effect transistors are popular within the field of organic electronic devices and the four general architectures are displayed in Figure 44. All are composed of an active organic semiconductor layer that links the source and drain electrodes. The gate electrode is separated from the active layer by a dielectric layer, commonly silicon dioxide. The most frequently used architecture is the bottom gate – bottom contact as these devices can come prefabricated with only the active layer requiring deposition for testing.

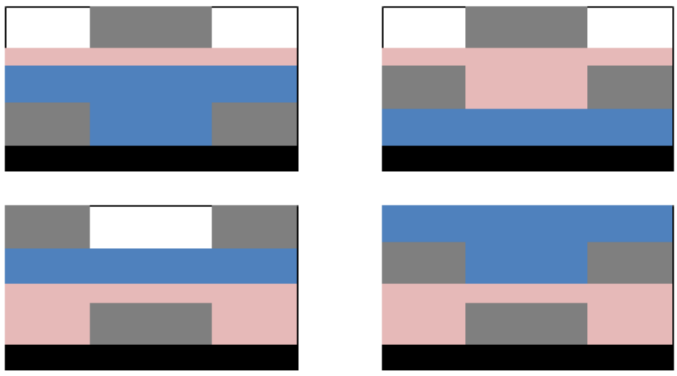

Figure 44. Structures of transistors (semiconductor = blue, dielectric = red, grey = electrodes) clockwise from top right. Top gate – top contact; bottom gate – bottom contact; bottom gate – top contact and top gate – bottom contact.

When a voltage is applied to the gate electrode it creates an electric field across the dielectric and in doing so attracts the charger carriers to the semiconductor – dielectric interface allowing current to flow from source to drain (Figure 45, b). Charge transport occurs when either an electron is in the LUMO or a hole is in the HOMO of the organic semiconductor. There are two ways of achieving this: one is through chemical doping but the more common

alternative is through the gate electrode. Applying a potential in the gate changes the energy level of the carriers with respect to the HOMO and LUMO.

Through the use of the applied voltages transistors are effectively on/off switches for electric circuits. A potential difference is used between the source and the drain to control the amount of current that can flow when the gate electrode is on. When no voltage is applied to the gate, ideally no current should flow from the source to drain (I_{off}). As the voltage is slowly increased at the gate a greater number of charges accumulate until a current is able to flow from source to drain. This is termed the turn on voltage and it is desirable to have a high ratio of I_{on}/I_{off}. Increasing the potential difference between the source and the drain (V_{SD}) increases the amount of current that flows from the source to the drain. Initially the increase in V_{SD} is proportional to the increase in I_{SD} and this is termed the linear region when analysing transistor performance (Figure 45a). Eventually an increase in V_{SD} no longer gives a proportional increase in I_{SD} and the device is starting to reach the saturation point.

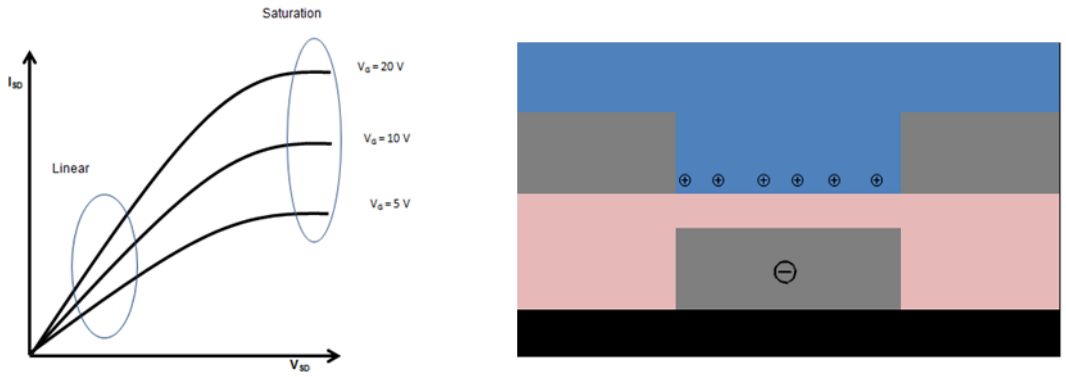

Figure 45. (a) typical current – voltage curve (b) the accumulation of positive charges at the semiconductor – dielectric

Doping

Doping was first shown to have an influence over carrier concentration in the halogen doped system of polyacetylene.[3] Doping is currently used in the thermally evaporated realm of OLEDs and they benefit from lower operating voltages, enhancement of lifetime and

reduction of the device's sensitivity to the electroded work function.[4] The challenges in moving from the thermally evaporated OLEDs to the solution processed organic transistors are the associated complications of solubility of the dopant, adduct and organic semiconductor as well as controlling the spatial distribution of the dopant throughout the film. Commonly used dopant molecules for p-type semiconductors are molecules with a high electron affinity. There is a formal charge transfer from the p-type organic semiconductor to the dopant.[5] Work by Leo *et al* demonstrated that tetrafluoro-tetracyano-quinodimethane (F_4TCNQ) was a good *p*-doping material in diodes. Devices were fabricated by co-sublimation with a phthalocyanine derivative.[6,7] F_4TCNQ was used because it could act as a strong electron acceptor with an electron affinity of -5.2 eV. The electron affinity (LUMO) of -5.2 eV matches very well with the ionisation potential of a wide range of organic semiconductors.[7] The F_4TCNQ works as a dopant by forming a charge-transfer complex with the undoped semiconductor where there is a formal charge transfer from the HOMO of the organic semiconductor to the LUMO of the dopant (Figure 46). There are two approaches to forming the charge transfer complex. The first is to match the LUMO of the dopant to the ionisation potential of the polymer, *p*-doping, or to match the ionisation potential of the dopant with the electron affinity of the polymer, *n*-doping. When solution processing dopants however, problems can arise with the co-solubility of the dopant, the semiconductor and the charge transfer complex. To further the work of charge transfer complexes, additional study is required to further lower the electron affinity of the dopant (to below -5.7 eV for IP-T based polymers) in order to enable electrons to transfer from the HOMO of the semiconductor to the electron accepting dopant.

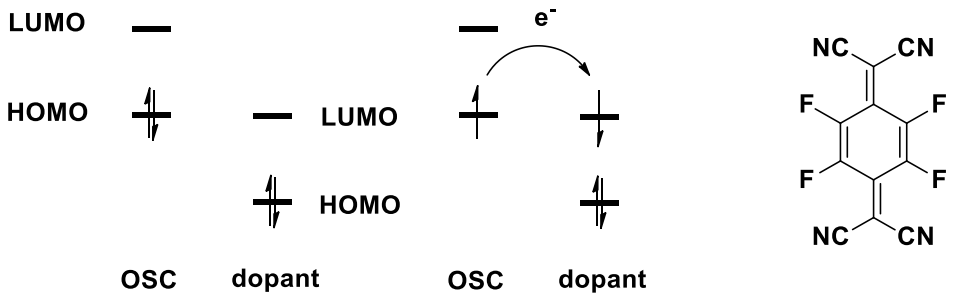

Figure 46. Formal transfer of integer charge and structure of p-dopant F_4TNCQ

Work by Salzmann *el al* has suggested that instead of the need to form an integer charge transfer complex, the formation of an intermolecular complex can also *p*-dope organic semiconductors (Figure 47).[8] Salzmann used a verity of dopants to demonstrate the overlap of the frontier molecular orbitals between the dopant and the organic semiconductor and the formation of an intermolecular complex (Figure 48).

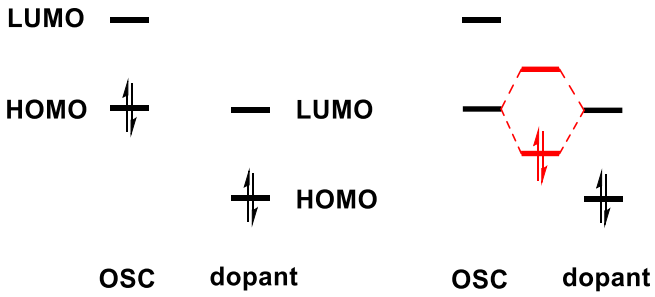

Figure 47. Mixing of HOMO of semiconductor with LUMO of dopant to form new hybrid orbitals (red).

Welch *et al* was able to demonstrate with small molecules, the interaction of lone pairs of electrons in the π–conjugated systems with Lewis acids.[9] Welch significantly adjusted the optoelectronic properties of the organic semiconductor by the formation of the Lewis acid-base complex. The electron accepting Lewis acid was used to withdraw π electron density away from the backbone and form a new set of hybrid orbitals, in doing so reducing the band gap.

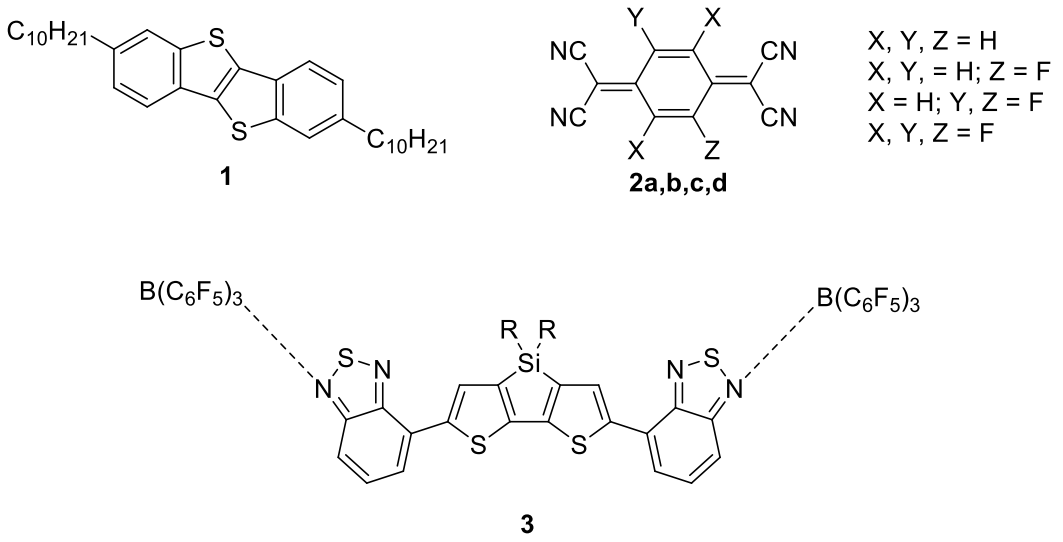

Figure 48. Structures of 1[8], 2a-d[8] and 3[9].

Aims

The aim of this work is to synthesis a range of organic semiconductors with the specific intention for use as hole transporting materials and to study the affect of doping that the Lewis acid tris(pentafluorophenyl)borane (**BCF**) has on device performance.

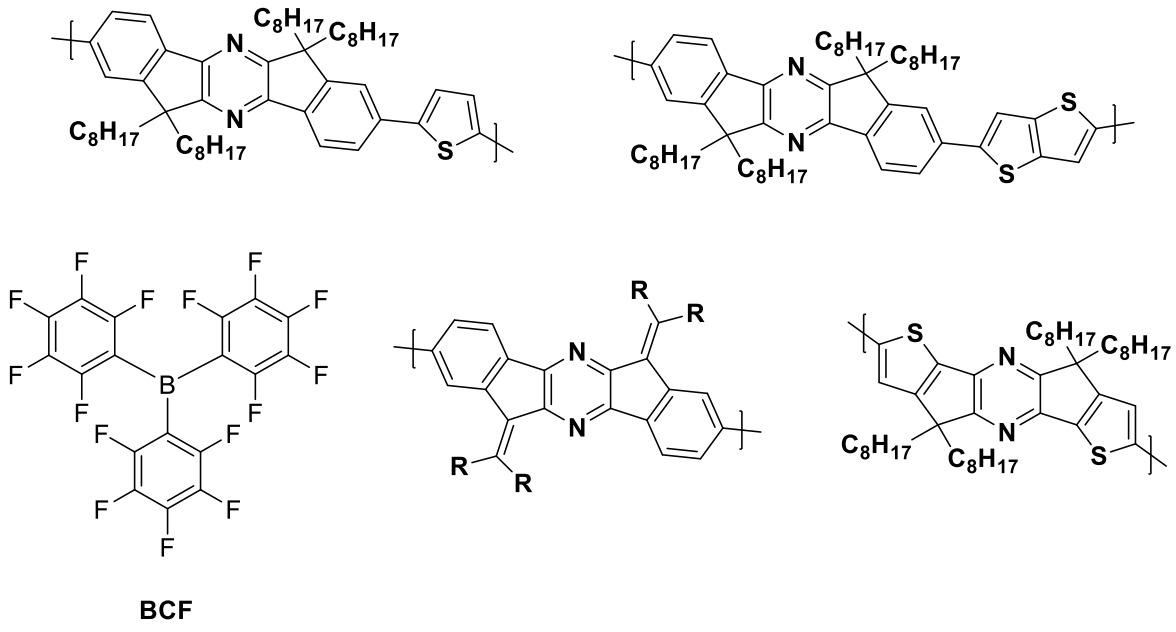

Figure 49. Target structures and BCF dopant

Indenofluorene has been heavily investigated as an OFET material due to its ambient air stability and easy of processability.[10–12] Previous work by *Friend et al.* produced a series of copolymers of indenofluorene with bithiophene and terthiophene (Figure 50).[13] They produced polymers of good molecular weights (20 kg/mol) with a modest hole mobility of 1.1 x 10^{-4} cm^2 V^{-1} s^{-1}. Their analysis of the HOMO – LUMO levels was performed via cyclic voltammetry and a HOMO value was established of 5.55 ± 0.05 eV. The reduction potential was not observable via cyclic voltammetry leading the authors to suggest that the two polymers would be more suited to hole rather than electron transport because of the high barriers to charge injection. They also showed that the number of the interspacing thiophene units influenced the chain packing, with the terthiophene copolymer displaying a higher degree of interchain order and a well-defined fibrillar morphology. A co-polymer of indenofluorene with thieno[3,2-b]thiophene has been reported with high molecular weights of 45 kg/mol, but a rather poor solubility (Figure 50).[14] This polymer afforded transistors with an order of magnitude higher mobility at 0.006 cm^2 V^{-1} s^{-1}.

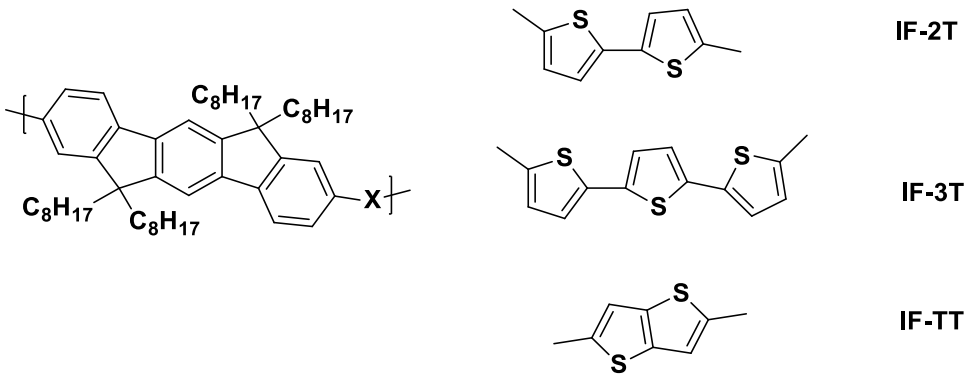

Figure 50. Structures of indenofluorene copolymerised with 2T, 3T and TT.

Building on this work the two polymers **IP-T** and **IP-TT** were designed and synthesised, with the co-monomers chosen because of their simplicity and to allow for comparison with previously made polymers. **BCF** was chosen as a dopant because of its strong Lewis acidity,

its resistance to air and moisture and the stability towards the boron – carbon bond. Due to its empty p_z orbital it can readily accept a lone pair of electrons.[15]

Synthesis of IP –T and IP – TT

The synthesis and purification of 2,8-dibromo-6,6,12,12-tetraoctyldiindeno[1,2-b:1,2-e]pyrazine was explained in Chapter 2. Both polymers were synthesised via palladium catalysed Stille coupling (Scheme 9). The monomers were heated in chlorobenzene in the presence of the $Pd(dba)_2$ and tri(o-tolyl)phosphine. The polymerisation proceeded rapidly via microwave assisted heating and were purified by soxhlet extraction with methanol, acetone and hexane to remove low molecular oligomers and catalyst residues. The remaining polymer was dissolved into chloroform and stirred with aqueous sodium diethyldithiocarbamate at 50 °C for 3 h to remove palladium residues.[16] After work-up, the final polymers were precipitated from the minimum amount of hot chlorobenzene into methanol. Both polymers were isolated as dark yellow fibres in good yields as tabulated in Table 19.

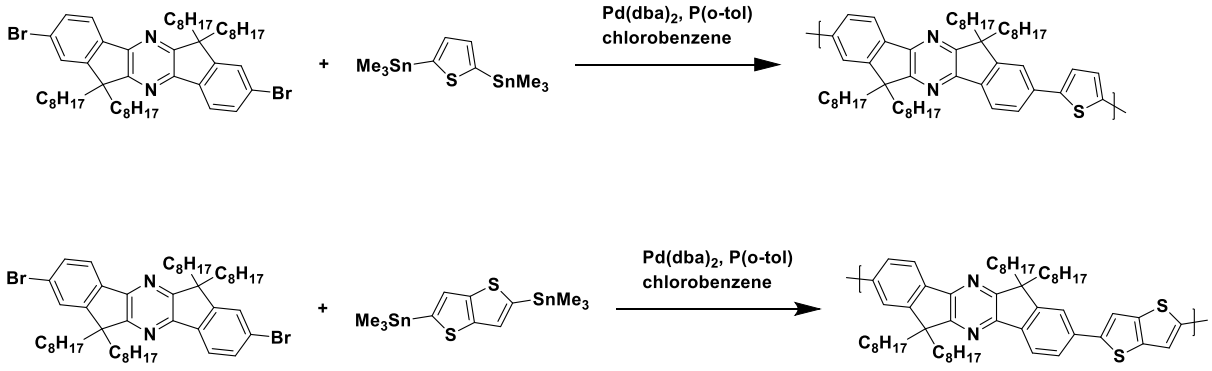

Scheme 9. Synthetic route to polymerisation of IP-T and IP-TT

Table 19. Polymer and molecular weight data

Polymer	Yield mg (%)	M_n (kg/mol)	M_w (kg/mol)	PDI	DP[1]
IP-T	125 (69 %)	23	53	2.3	28
IP-TT	94 (48%)	20	42	2.1	23

[1]Degree of polymerisation is based on Mn.

The molecular weights of the polymers were measured by gel permeation chromatography in chlorobenzene at 80 °C against polystyrene standards. The polymerisations both produced reasonably high molecular weights with comparable polydispersity. The Mn was lower for **IP-TT** compared to **IP-T** which we relate to the lower solubility the thieno[3,2-b]thiophene repeat unit compared to thiophene. This could limit the molecular weight by precipitation of the growing polymer chain from solution during the polymerisation process. Nevertheless in all cases the degree of polymerisation appears sufficiently high to allow for a reasonable comparison of the properties of each polymer. Similar work on the **IF-2T** and **IF-3T** series, which were also synthesised by Stille coupling produced polymers of similar molecular weight (20 kg/mol).[13] We note that differential scanning calorimetry of the two polymers gave no evidence of crystallinity between the temperature range 50 – 300 °C.

Optical data and Energy Levels

The UV-Vis absorption spectra of the two polymers were recorded in order to obtain an understanding of the optical band gap and observe the difference in optical behaviour in the solid state. The results can be seen in Figure 51 and summarised in Table 20.

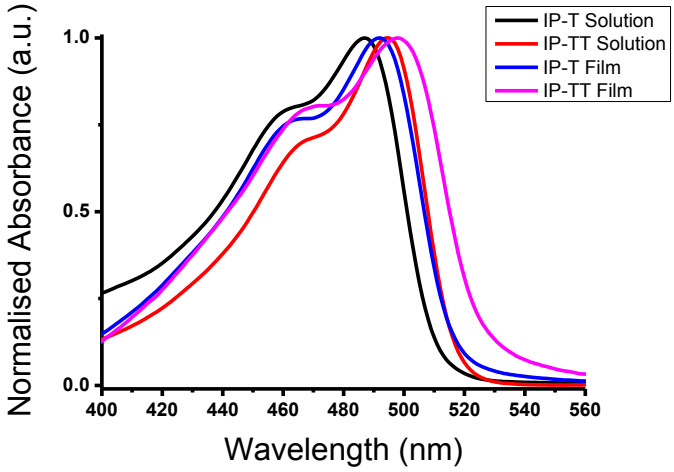

Figure 51. The UV-Vis spectra of IP-T and IP-TT in both solution (chlorobenzene) and as thin films .

Table 20. Optical and energetic properties of IP-T and IP-TT.

Polymer	λ_{max}(nm) Solution	Film	λ_{onset}(nm) Film	I.P. (eV)[1]	LUMO (eV)[2]	E_g^{opt} (eV)
IP-T	487	492	515	5.78	-3.38	2.40
IP-TT	495	498	525	5.82	-3.46	2.36

[1]Ionisation potential was measured by PESa

[2] LUMO was estimated from the onset of absorption

The solution samples were dissolved in chlorobenzene and the thin films were spun from a solution of 5mg/mL in chlorobenzene on to glass at a spin rate of 1000rpm for 1 minute. The absorption of **IP-TT** was slightly bathochromically shifted by 8 nm in both film and solution compared to **IP-T** and the optical band gap, estimated from the onset of absorption was slightly smaller. This can be attributed to the presence of the more electron rich thieno[3,2-b]thiophene unit compared to thiophene. The measured ionisation potentials via PESA are similar, within the error limits of the measurement (±0.05 eV). Comparing the absorption spectra of **IP-T** and **IP-TT** with the reported for **IF-2T** and **IF-3T**, the absorption spectra of the pyrazine containing polymers are red-shifted by approximately 30 nm. **IF-2T** has a similar band gap of 2.38 eV whilst **IF-3T** has a reduced band gap of 2.10 eV. It is difficult to compare the ionisation potentials, since the **IP** based polymers were measured by cyclic voltammetry versus photon electron spectroscopy in the current case. However according to the reported values, the ionisation potential of the **IP** based polymers were increased by 0.2 eV in comparison to the **IF** polymer, which would be in agreement with the presence of the electron withdrawing pyrazine.

Transistor and doping

IP-T and **IP-TT** were tested as p-type materials for use in OFETs. As well as being tested as pristine charge carrying semiconductors they were also doped using the strong Lewis acid **BCF** in order to observe if there was an improvement in charge carrier mobility. Devices

were fabricated in a bottom contact/top gate architecture on glass substrates using an Au source-drain electrodes and CYTOP™ as a dielectric. The Au electrodes were treated with pentafluorobenzene thiol (PFBT) SAM to increase the work function. The polymers were dissolved in chlorobenzene (5 mg/ml) and spin cast at 2000 rpm from a hot solution for 60 s before being annealed at 160 °C for 30 min and cooled slowly to room temperature.

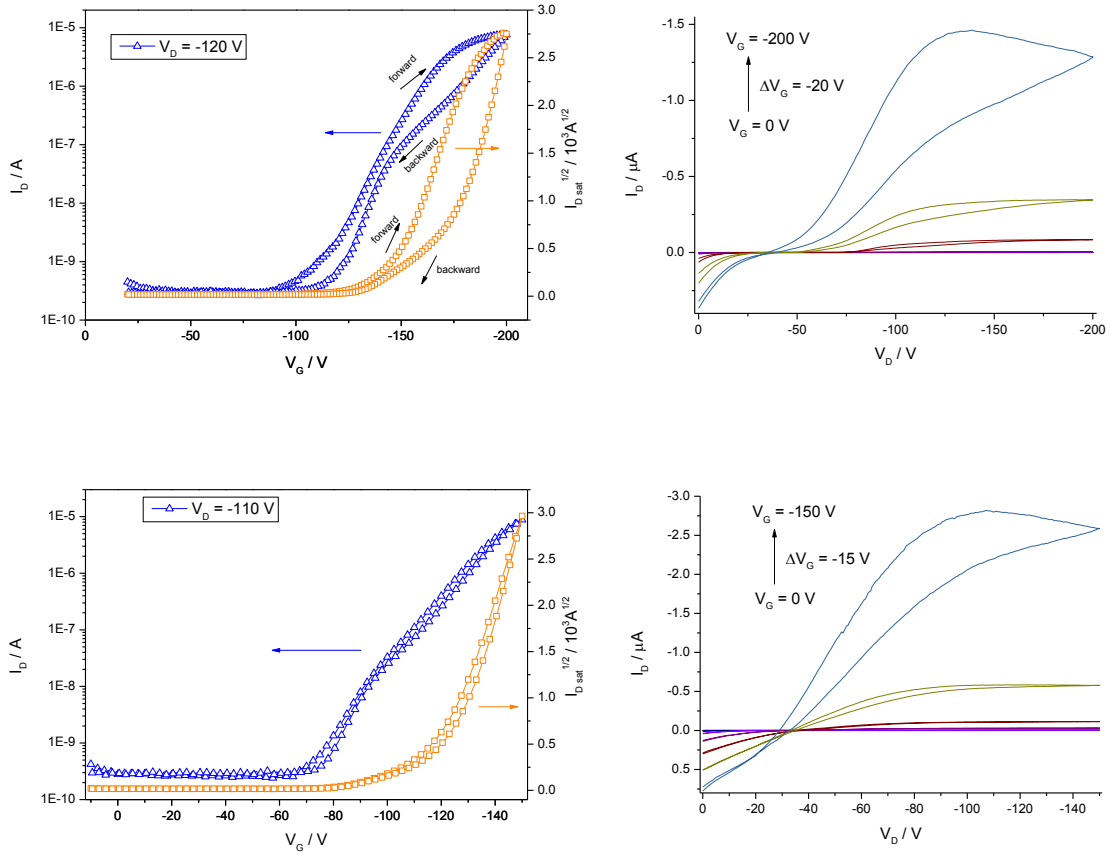

Figure 52. Transfer (left) and output characteristics (right) of IP-T. Device dimensions W = 1000 µm L = 40 µm

The initial performance of both **IP-T** and **IP-TT** was very poor, and the devices displayed substantial deviations from the expected behaviour (Figure 52). Devices could only be operated under very high gate voltages, and under these conditions substantial leakage currents are expected through the dielectric, contributing to an overestimation of the charge carrier mobility. We believe the reason transistors of **IP-T** and **IP-TT** require such high operating voltages is because they both possess very high ionisation potentials and so the

contact resistance between the electrode and semiconductor is very high leading to injection problems. Therefore no meaningful charge carrier mobilities were extracted.

In order to reduce the injection barrier we incorporated the dopant **BCF** into the film. Based on the previous work by Bazan et al.[17] The polymer was dissolved in chlorobenzene (10 mM) and mixed with different amounts of **BCF** solution (10 mM in chlorobenzene). Extra solvent was added to each solution to keep the concentration of the polymer constant, which was 6.67 mM. Bottom contact/top gate devices were then fabricated on glass substrates using Au source-drain electrodes and CYTOP dielectric. Au electrodes were treated with pentafluorobenzene thiol (PFBT) SAM to increase the work function. The solution was spin cast at 2000 rpm for 60 s. The channel width and length of the transistors are 1000 µm and 30 µm, respectively. Mobility was extracted from the slope of $I_D^{1/2}$ vs. V_G.

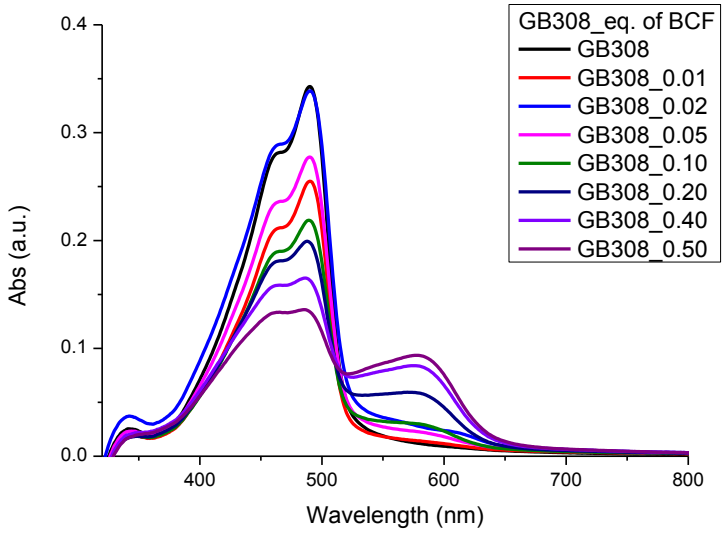

Figure 53. Absorption spectra of IP-T varying concentration of BCF.

The UV-Vis spectra of **IP-T** with varying concentration of **BCF** spun on glass are shown in Figure 53. The un-doped film has a λ_{max} at 495 nm with a strong shoulder around 450 nm and λ_{onset} of 515 nm. **BCF** is known to show no absorption in the wavelength range of 400 – 800 nm and this was confirmed experimentally. For the blend films, as the concentration of **BCF** increases there is a noticeable reduction in the intensity of λ_{max} and the emergence of a new

peak at longer wavelength. This new peak absorbs at 590 nm with a λ_{onset} of 640 nm. The emergence of this new peak is consistent with the formation of a complex between the pyrazine lone pair and the **BCF**. Such a complex would be expected to withdraw electron density from the pyrazine, resulting in the formation of zwitterionic type complex with **BCF** and therefore a lower energy charge transfer type band. We also note the isosbestic point at 520 nm, which suggests two separate species exist in the film, the uncomplexed and the complexed polymer chains.

Transistors of **IP-T/BCF** were fabricated under identical conditions and the performance is summarised in Table 21 and Figure 54. The addition of **BCF** has a significant impact on device performance. Most importantly the turn-on voltage shifts to more positive values with even small amounts present. Since the formation of the polymer.**BCF** complex would be expected to make the polymer harder to oxidise i.e. more difficult to inject holes in a transistor devices, we suspect that the reduction in the apparent injection barrier may be due to interfacial dipole effects or perhaps due to trap filling. More investigation is needed in this area. Gratifyingly the charge carrier mobility increases at low loadings of **BCF**, peaking at 0.039 $cm^2\ V^{-1}\ s^{-1}$ with 0.05 equivalents before dropping at higher loading. The on/off ratio remains reasonable at these loadings.

Table 21. Mobility and operating voltages of different concentrations of BCF in IP-T

eq. of BCF	μ ($cm^2V^{-1}s^{-1}$)	V_{on} (V)	V_{Th} (V)	on/off ratio
0	0.0063	-54	-68	53
0.01	0.016	-35	-47	2.3×10^2
0.04	0.028	-23	-45	6.4×10^2
0.05	0.039	-20	-37	2.0×10^3
0.10	0.016	-31	-47	4.4×10^2
0.20	0.012	-16	-34	8.3×10^2
0.40	0.0039	-16	-28	6.2×10^2
0.50	5.6×10^{-4}	-14	-24	72

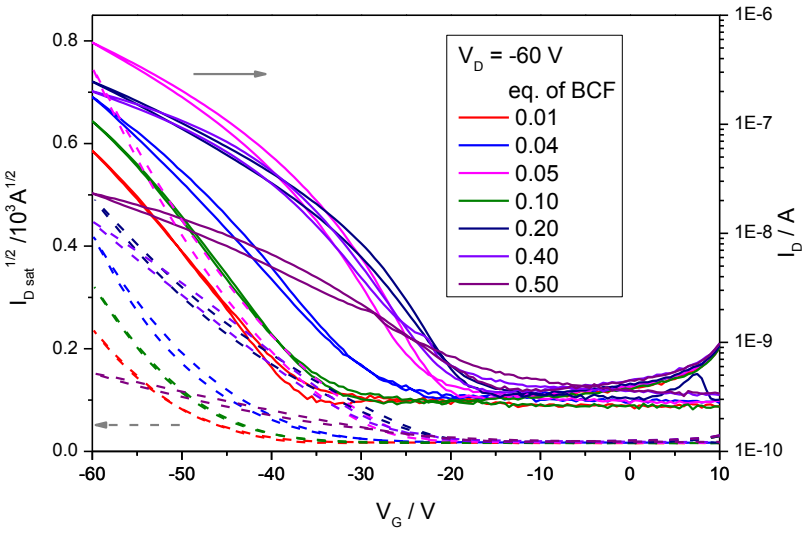

Figure 54. The transfer characteristics of IP-T

Plotting the λ_{max} absorption intensity, the absorption intensity at 590 nm and the hole mobility against the concentration of **BCF** dopant added, shows the increase in mobility reaches a maximum prior to the emergence of the strong absorption at 590 and before the intensity of the initial peak falls (Figure 55). At higher concentration of BCF we believe the formation of BCF clusters hinders the charge transport as the polymer chain become saturated.

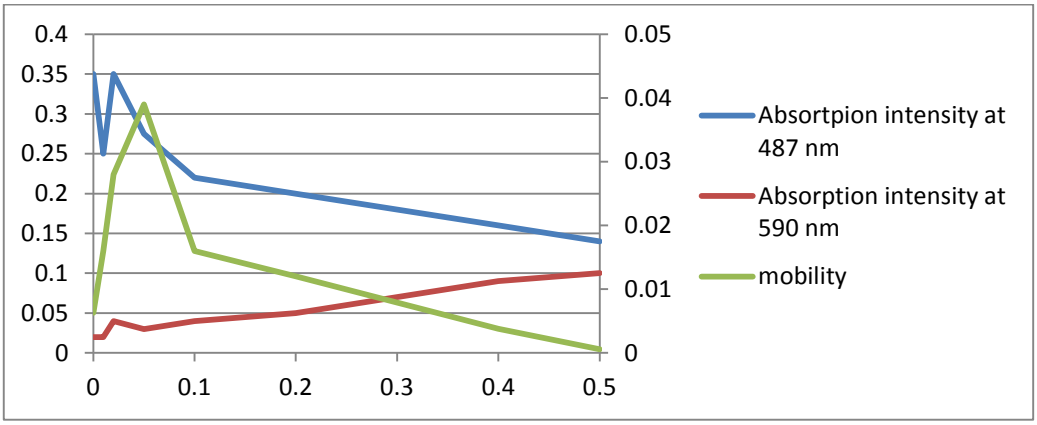

Figure 55. λ_{max} Absorption intensity, the absorption intensity at 590 nm and the hole mobility against concentration of BCF **dopant added**

IP-TT was also doped with the same concentration range of **BCF** and the hole mobility recorded. The UV-vis absorption profile is shown in Figure 56. Very much like changes seen in the absorption profile of **IP-T**, there is a reduction in the absorption at λ_{max} as the

concentration of **BCF** increases. Likewise, there is the emergence of a new absorption peak with a λ_{onset} of 675 nm.

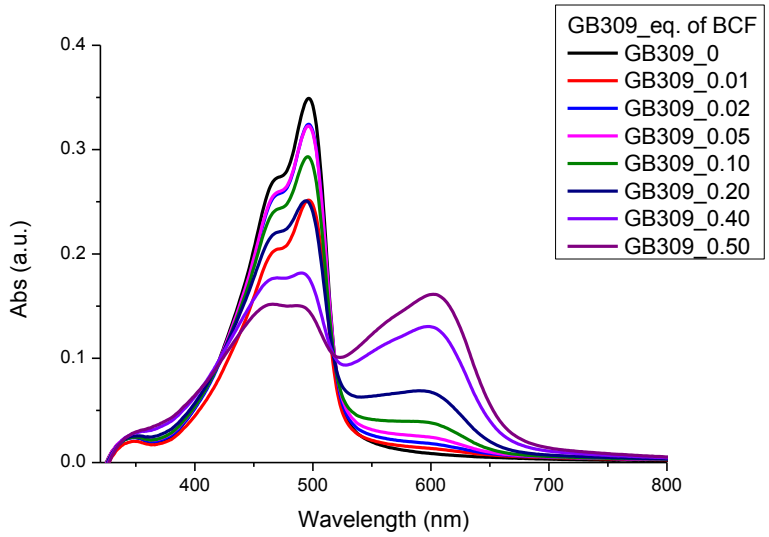

Figure 56. Absorption spectra of IP-TT varying concentration of BCF.

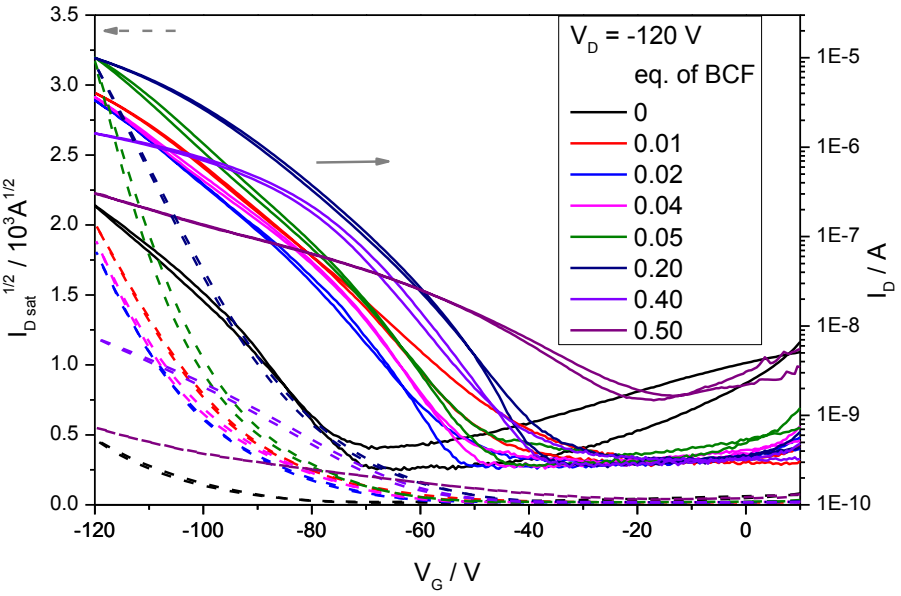

Figure 57. The transfer characteristics of IP-TT

The transistor results show a similar trend as for **IP-T**. As the initial concentration of **BCF** increases there is a substantial shift in the onset towards positive voltages, and a large increase in the hole mobility. Again the mobility peaks at 0.05 equivalents of **BCF**, before

dropping at high loadings. The maximum hole mobility is an order of magnitude greater for **IP-TT** than **IP-T** at 0.43 $cm^2/V.s$.

Table 22. Mobility and operating voltages of different concentrations of BCF in IP-TT.

eq. of BCF	μ ($cm^2V^{-1}s^{-1}$)	V_{on} (V)	V_{Th} (V)	on/off ratio
0	0.019	-70	-97	9.1×10^2
0.01	0.24	-41	-90	1.5×10^4
0.02	0.19	-52	-95	1.3×10^4
0.04	0.25	-48	-93	1.4×10^4
0.05	0.43	-43	-94	3.7×10^4
0.20	0.16	-38	-79	3.8×10^4
0.40	0.019	-38	-57	5.4×10^3
0.50	0.0071	-22	-57	2.1×10^2

In both cases there appears to be a sharp fall in the peak intensity of the λ_{max} at **BCF** concentration 0.01 eq.

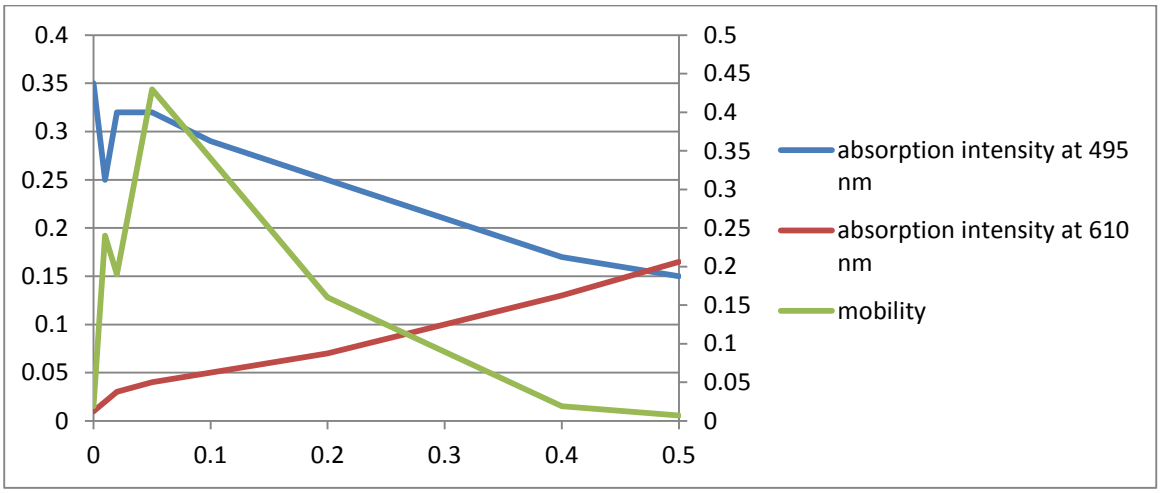

Figure 58. λ_{max} Absorption intensity, the absorption intensity at 610 nm and the hole mobility against concentration of BCF **dopant added**

Comparing these results to the previous work by Bazan et al, who studied the polymer series poly[(4,4-di2-ethylhexyldithieno[3,2-b:2′,3′-d]silole)-2,6-diyl-alt-(1,4-pyridyl)] (**DTS-Py**) (Figure 59) and doping with **BCF** they observed similar tendencies for an increase in mobility up to dopant concentration of 0.02 eqv.[17]

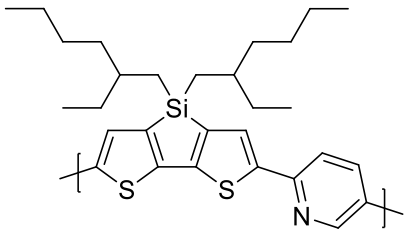

Figure 59. Structure of DTS-Py.

At the optimum doping levels of 0.02 eq they observed an increase of two orders of magnitude in bulk charge carrier mobility from 3.2 x 10^{-5} cm^2 V^{-1} s^{-1} to 2.5 x 10^{-3} cm^2 V^{-1} s^{-1}. For both **IP-T** and **IP-TT** we observed optimum doping levels that were double that of **DTS-Py** at 0.05 eqv and resulted in an increases of an order of magnitude in hole mobility. They also invested the temperature dependence in hole only diode devices, which enabled them to calculate the activation energy for each system. It was found that the 0.02 eqv doping levels resulted in a 90 meV decrease in activation energy.

Conclusion

Indenopyrazine – thiophene and indenopyrazine - thienothiophene polymers were investigated for use as active layers in organic transistors. Hole injection was achieved under high voltages to obtain mobilities of 0.0063 $cm^2V^{-1}s^{-1}$ and 0.019 $cm^2V^{-1}s^{-1}$ respectively. Use of BCF dopant increased the charge carrier mobility whilst also reducing the operating voltages with the optimum doping level determined to be 0.05 eq of **BCF**. Addition of the dopant saw improved mobilities of 0.039 cm^2 V^{-1} $s^{-1}$and 0.43 cm^2 V^{-1} s^{-1} respectively. We believe this is the first demonstration of BCF doping in a transistor device. Additional work could involve testing a verity of different dopants and investigating if the number of doping sites per repeat unit affects the quantity of dopant required to achieve maximum gains in mobility.

Alkylidene Indenopyrazine

Alkylidene based indenofluorene at the time of writing have not yet been published, but the analogous work done by *Heeney et al* [18] on the fluorene system has shown that changing the sp^3 carbon at the 9 position of fluorene to an sp^2 C – C double bone planarizes the backbone, which causes a red shift in the absorption spectra. The field effect mobilities were also measured and in the order of 10^{-4} cm^2 V^{-1} s^{-1}.[18] (Figure 60)

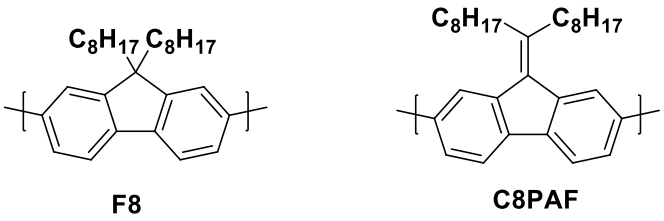

Figure 60. Structures of polyfluorene and poly-alkylidene-fluorene

Computational studies of both polymers by Salaneck *et al* suggested that both polymers should have identical ionisation potentials. However the experimentally observed value was 0.4 eV lower for C8PAF (as measured by UPS). The authors rationalised these differences to solid state packing effects, which were more pronounced for C8PAF.[19] The aim of this work is to synthesise alkylidene-indenopyrazine to produce a polymer that has a higher HOMO energy level and function as a hole transporting material.

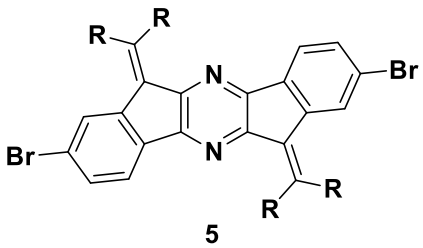

Figure 61. Target alkylidene indenopyrazine

Synthesis of alkylidene indenopyrazine

The synthesis of the target polymer is shown in Scheme 10 and is based upon the route developed to C8PAF. Here the key step was the formation of a ketene dithioacetal and subsequent nucleophilic displacement of the thiol groups with a Grignard reagent in the presence of a copper catalyst.

The dihydrodiindenopyrazine building block **3** was prepared as reported in previous chapters. The dihydrodiindenopyrazine anion was formed via reaction with the non-nucleophilic strong base sodium *tert*-butoxide in DMSO. The formation of a ketene dithioacetal by condensation of the dihydrodiindenopyrazine anion with carbon disulfide was followed by the in situ alkylation of the resulting diketene dithiolate anion with methyl iodide to give the dimethylated thioacetal as a red solid in a good yield of 80 %. The reaction of the dimethylated thioacetal with 4.4 eqv of Grignard reagent at -5°C in THF in the presence of a catalytic amount of Kuchi's salt gave the product as a yellow oil. Purification via filtration through celite and subsequent column chromatography over silica (eluent hexane) with an aluminium oxide plug yielded a yellow solid in a moderate yield of 30 %.

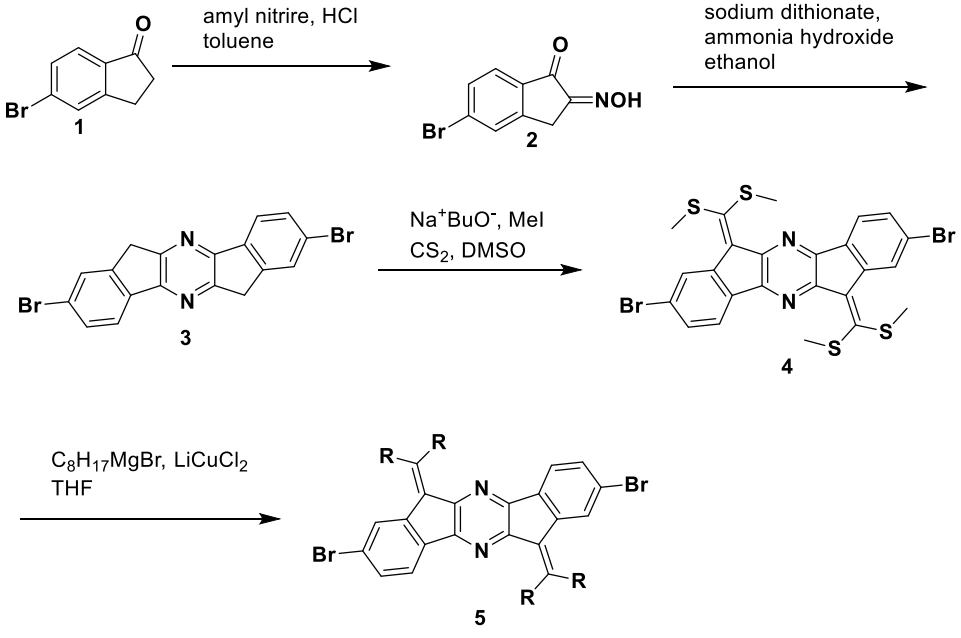

Scheme 10. Synthesis of alkylidene indenopyrazine

The homopolymerisation was carried out under Yamamoto polymerisation conditions in sealed microwave vial and the results are recorded in Table 23. After an initial 1 hour of heating, a colour change from dark green to a much lighter luminescent green/blue was observed. The polymerisation was carried out for 72 h to ensure a high molecular weight was achieved because of the step growth method of polymerisation. The resulting polymer was precipitated into methanol and low molecular weight impurities and catalyst residues removed by extraction (Soxhlet) with methanol and acetone. The polymer was then extracted into hexane, concentrated, re-dissolved in chlorobenzene and precipitated into cold methanol to yield the resulting polymer as yellow fibres.

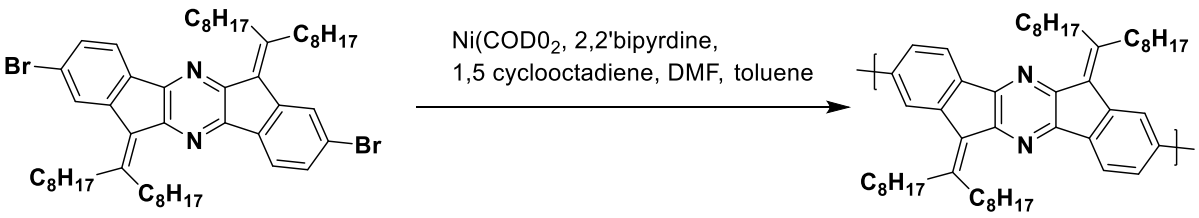

Scheme 11. Synthesis of poly alkylidene indenopyrazine

Table 23. Physical properties of AIP

Polymer	Yield (%)	M_n/kg/mol	M_w/kg/mol	PDI	Degree Polymerisation[1]
AIP-C8	34	22	48	2.2	30

[1] Degree of polymerisation is based on Mn divided by molecular weight of repeat unit

A large portion of the polymer was removed in the acetone washing of the soxhlet due to its low molecular weight. Like **IP-C8** the polymer was very soluble in hexane and had a high degree of polymerisation.

Optical properties and Energy levels

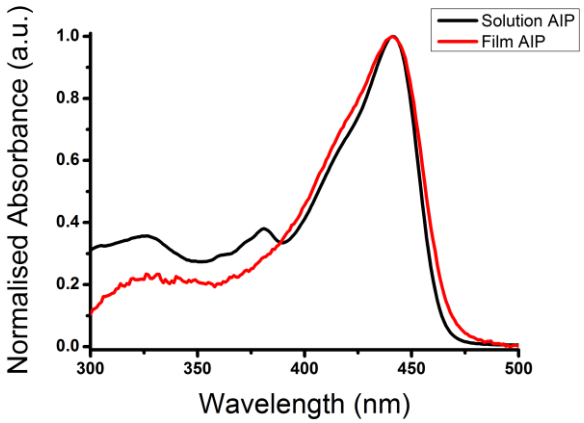

Figure 62. Absorption spectroscopy of AIP

Table 24. Optical and energetic properties of AIP.

Polymer	λ_{max}(nm) (M^{-1} cm^{-1}) Solution	Film	λ_{onset}(nm) Film	I.P. (eV)	LUMO (eV)	E_g^{opt} (eV)
AIP-C8	441	441	468	5.75	3.11	2.64

The ionisation potential energy of **AIP-C8** was measured by PESA as 5.75 eV. In comparison to **IP-C8**, the introduction of the alkylidene decreases the ionisation potential by 0.25 eV. The optical band gaps are very similar, and if the LUMO energy is estimated by subtracting the optical gap from the ionisation potential, then AIP-C8 has higher lying LUMO of 3.11 eV compared to 3.37 eV of **IP-C8**.

The main premise of the introduction of the alkylidene side chain was in order to induce more planarity in the backbone and therefore raise the HOMO energy level. This was achieved with raising the HOMO by 0.25 eV, however when the materials were tested as hole transporting materials no charge injection was observed.

Conclusion

The synthesis of novel alkylidene indenofluorene homopolymer was demonstrated and the desired increase in HOMO energy was achieved, increasing from the deep – 6.00 eV of **IP-C8** to – 5.75 eV. Despite the raising of the HOMO however, charge injection was still not

achievable. Future co-polymerisation with thiophene and thienothiophene should raise the HOMO further and with increased planarization of the backbone high mobilities should be achieved.

Towards the synthesis of IPDT

Indacenodithiophene (IDT) has been heavily studied but it was *Zhang et al.* who first copolymerised it with thienothiophene producing excellent hole mobilities in the order of 0.15 cm^2 V^{-1} s^{-1}. Comparing **IDT-TT** with **IF-TT** the degree of polymerisation was slightly higher (64 kg/mol). The polymer was amorphous in the solid state with a HOMO energy level of -5.4 eV. The introduction of the terminal thiophene make the monomer more electron rich and therefore raises the HOMO closer to the vacuum level.[20]

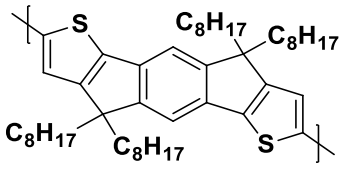

Figure 63. Structure of poly(indacenodithiophene)

The aim of this work was to synthesise the pyrazine analogue of IDT. Having already observed the benefits of indenopyrazine compared to indenofluorene we predicted that **IDPz** would observe a similar reduction in the LUMO energy level whilst simultaneously raising the HOMO energy level to produce conditions favourable to both hole and electron charge injection whilst still maintaining the excellent optical properties previously observed for indenopyrazine.

Synthesis

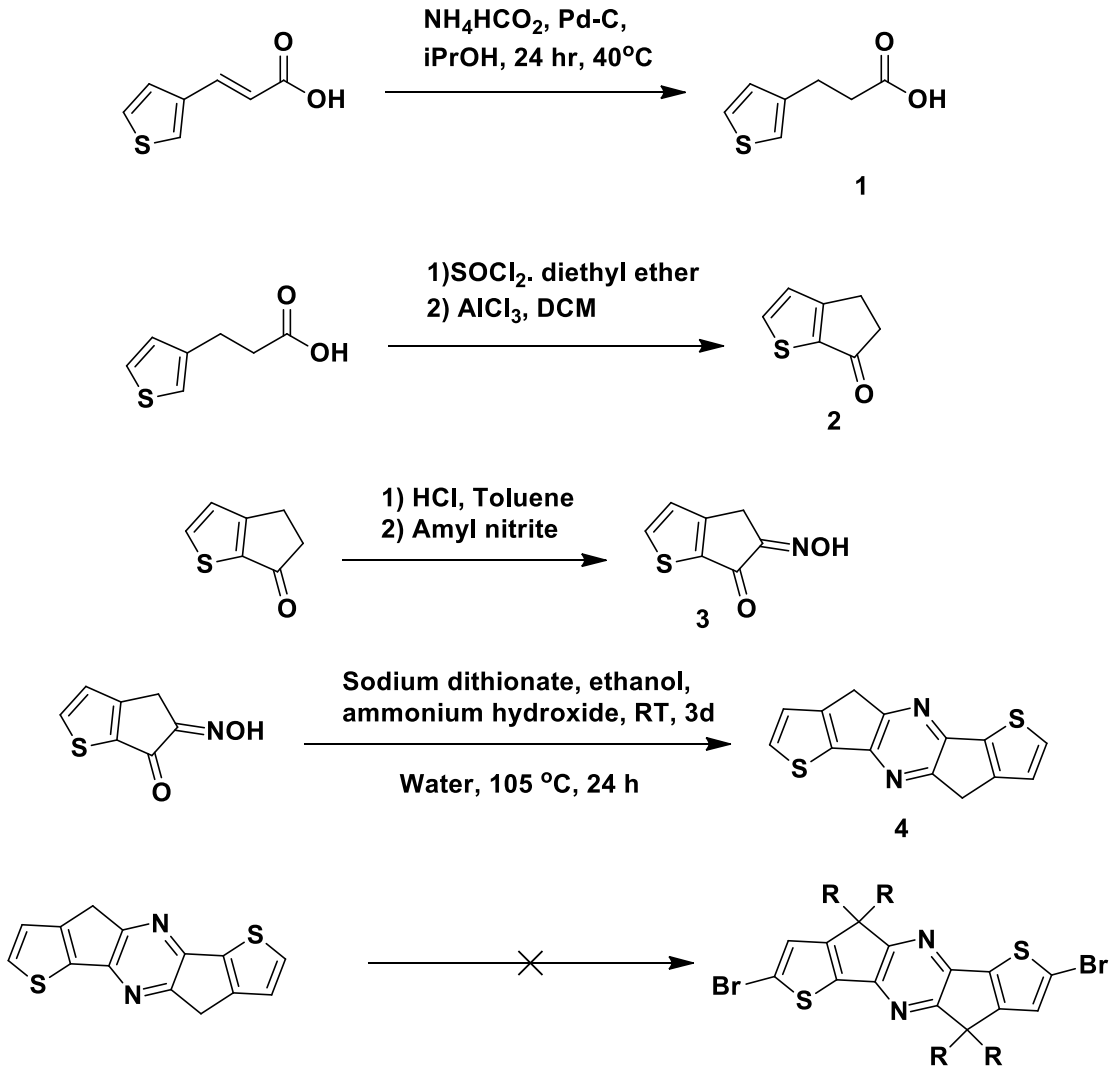

Scheme 12. Synthesis of target monomer IPDT

The synthesis of the target materials is shown in Scheme 12. The synthesis of **1** was performed via a literature procedure.[21] Under an argon atmosphere, 3-(3-thienyl)-2-propenoic acid was dissolved in isopropanol. Ammonium formate and Pd-C were then added in one portion and the reaction stirred at 40°C for 24 h. Small scale reactions proceeded in good yield. On scaling up of the reaction care had to be taken on the addition of Pd-C to prevent excessive heat and the subsequent evolution of hydrogen gas. The reaction gave a good yield of 83.6% and experimental data was in accordance with literature.[21]

The next step was the intramolecular Friedal-Crafts acylation to form the cyclic ketone. Various conditions were investigated including direct ring closure of the carboxylic acid in the presence of dehydrating acids like conc. H_2SO_4 or poyl(phosphonic) acid without success. However the reaction of the acid chloride was found to be most promising. Therefore 3-(thien-3-yl)propanoic acid was dissolved in dry diethyl ether and thionyl chloride added. The reaction was heated to 50 °C for 3.5 h and on cooling the solvent was removed under reduced pressure. The acid chloride was used immediately. Dissolving in dichloromethane it was transferred to a solution of $AlCl_3$ in dry dichloromethane. The reaction was stirred at room temperature for 5 h before being quenched with HCl/ice water obtaining a final yield of 41%.

The subsequent formation of the oxime was performed via the formation of the enolate and addition of amyl nitrite. In previous work on the benzo analogue the formation of the enolate was evident because of the formation of a partially soluble white precipitate. With the thiophene analogue 4,5-dihydro-6H-cyclopenta[b]thiophen-6-one there was no evidence of precipitate formation on the addition of the acid. A low rate of enolate formation was proposed as a factor to the low reaction yield, currently below 10 %. Optimum conditions were found to be cold addition of concentrated acid followed by warming to room temperature overnight.

Formation of 4,9-dihydro-s-indenopyrazine[1,2-b:5,6-b']-dithiophene by the reduction of 4,-dihydro-6H-cyclopenta[b]thiophene-2-one-3-oxime in the presence of ammonia proceeded over 3 days to give a poor yield of product. Purification was hampered by poor solubility and the crude product was therefore used in the next alkylation step. However no product could be isolated.

Overall despite over 24 months work towards the target material, the low yields and difficulties with purification meant the synthesis was unsuccessful. Although a promising

route to the cyclic ketone has been found, the rest of the synthesis route remains problematic. Future work should concentrate upon alternative routes.

Conclusion

Based on the success of **IDT** and the high mobilities it has achieved and combining that with the order of magnitude improvement in mobility observed in the doping of **IP-TT** the potential for a doped **IDPT-TT** system would take the device performance well above that of commercially available silicon. The difficulty arises in finding a convenient synthetic route to obtain the monomers. Due to the incurred solubility issues observed one such approach would be to attempt to alkylate the initial 3-(thien-3-yl)propanoic acid in order to make the products more soluble in common organic solvents. There were two other routes that were proposed but initial steps in synthesis were problematic.

References

1. Forrest, S. R. The Path to unbiquitous and low-cost organic electronic appliances on plastic. *Nature Review Article* 911–918 (2004).

2. Holliday, S., Donaghey, J. E. & Mcculloch, I. Advances in Charge Carrier Mobilities of Semiconducting Polymers Used in Organic Transistors. *Chemistry of Materials* **26**, 647-683 (2014).

3. Shirakawa, H. & Macdiarmid, A. G. Electrical Conductivity in Doped Polyacetylen. *Physical Review Letters* **39**, 1098–1101 (1977).

4. Pfeiffer, M. *et al.* Doped organic semiconductors: Physics and application in light emitting diodes. *Organic Electronics* **4**, 89–103 (2003).

5. Lüssem, B., Riede, M. & Leo, K. Doping of organic semiconductors. *Physical Status Solid (a)* **210**, 9–43 (2013).

6. Blochwitz, J., Pfeiffer, M., Fritz, T. & Leo, K. Low voltage organic light emitting diodes featuring doped phthalocyanine as hole transport material. *Applied Physics Letters* **73**, 729 (1998).

7. Yim, K.-H. *et al.* Controlling Electrical Properties of Conjugated Polymers via a Solution-Based p-Type Doping. *Advanced Materials* **20**, 3319–3324 (2008).

8. Méndez, H. *et al.* Doping of Organic Semiconductors: Impact of Dopant Strength and Electronic Coupling. *Angewandte Chemie* **125**, 7905–7909 (2013).

9. Welch, G. C., Coffin, R., Peet, J. & Bazan, G. C. Band gap control in conjugated oligomers via Lewis acids. *Journal of the American Chemical Society* **131**, 10802–3 (2009).

10. Setayesh, S., Marsitzky, D. & Mu, K. Bridging the Gap between Polyfluorene and Ladder-Poly-p-phenylene : Synthesis and Characterization of Poly-2 , 8-indenofluorene. *Macromolecules* 33, 2016–2020 (2000).

11. Li, J. *et al.* Synthesis and Photovoltaic Properties of Alternating Conjugated Polymers Derived from Thiophene-Benzothiadiazole Block and Fluorene/Indenofluorene Units. *Bulletin of the Korean Chemical Society* **35**, 505–512 (2014).

12. Kirkpatrick, J. *et al.* A Systematic Approach to the Design Optimization of Light-Absorbing Indenofluorene Polymers for Organic Photovoltaics. *Advanced Energy Materials* **2**, 260–265 (2012).

13. Sonar, P. *et al.* Synthesis, characterization and comparative OFET behaviour of indenofluorene–bithiophene and terthiophene alternating copolymers. *Synthetic Metals* **160**, 468–474 (2010).

14. Pan, J., Meyer, F., Ludemann, A. & Buesing, A. Copolymers of indenofluorene and thiophene. *US Patent,* WO2008009343 A1, (2006).

15. Piers, W. E., Chivers, T. & Piers, W. Pentafluorophenylboranes: from obscurity to applications. *Chemical Society Review* **26**, 345-354 (1998).

16. Schroeder, R. *et al.* Electrode specific electropolymerization of ethylenedioxythiophene: Injection enhancement in organic transistors. *Applied Physics Letters* **87**, 113501 (2005).

17. Zalar, P. *et al.* Increased mobility induced by addition of a Lewis acid to a Lewis basic conjugated polymer. *Advanced materials* **26**, 724–7 (2014).

18. Heeney, M. *et al.* Alkylidene Fluorene Liquid Crystalline Semiconducting Polymers for Organic Field Effect Transistor Devices. *Macromolecules* **37**, 5250–5256 (2004).

19. Osikowicz, W. *et al.* Electronic structure of a novel alkylidene fluorene polymer in the pristine state. *Chemical Physics Letters* **385**, 184–188 (2004).

20. Zhang, W. *et al.* Indacenodithiophene semiconducting polymers for high-performance, air-stable transistors. *Journal of the American Chemical Society* **132**, 11437–9 (2010).

21. Hauze, D. B. & Joulli, M. M. Novel Synthesis Of Thianinhydrin. *Tetrahedron* **53**, 4239–4246 (1997).

Chapter 5 - Experimental

General Experimental

Unless otherwise stated, all reactions were conducted under argon, using an argon filled dual manifold and standard Schlenk line techniques. All solvents and reagents were obtained from commercial sources (Aldrich, Acros, Thermo Fisher, VWR and Fluorochem) and used as received. Flash column chromatography was performed on Merck Kieselgel 60 (230-400 mesh) silica. Analytical thin layer chromatography (TLC) was performed on pre-coated 0.25 mm thick Merck 5715 Kieselgel 60 F_{254} silica gel plates and observed under 254 nm or 366 nm ultraviolet light. ^{1}H NMR spectra were measured on a Bruker Av-400 (400 MHz) instrument and $^{13}C\{^{1}H\}$ NMR were measured on a Bruker Av-400 (101 MHz). Chemical shifts are reported in ppm, relative to the residual protons in the deuterated solvents. All spectra were analysed using MestreNova v5.3 software, from *MestreLab*. UV-Vis spectra were recorded at 298 K on a UV-1601 Shimadzu UV-Vis spectrometer. Solution UV-Vis spectra were carried out in chloroform solutions at concentrations of ~10^{-6} M. Thin films of polymers were spin coated from chlorobenzene solutions with a concentration of 5 mg/mL, on a Laurell spin coater at 1000 rpm for 1 min. Photoelectron spectroscopy in air (PESA) measurements were made using a Riken Keiki AC-II at CSIRO Materials Science and Engineering, Australia. Electrospray (ESI) mass spectrometry was performed with a Thermo Electron Corporation DSQII mass spectrometer. Electron Ionization (EI) mass spectrometry was performed on a Micromass Autospec Premier instrument. Elemental Analyses were determined by Mr. Stephen Boyer at London Metropolitan University, North Campus, Holloway Road, London, N7. GPC data was collected using an Agilent Technologies 1200 series instrument, with two mixed B columns, in series, at 80 °C and using chlorobenzene as the eluent, at a flow rate of 1 mL/min. The instrument was calibrated using narrow polydispersity polystyrene standards. Devices were fabricated on ITO-coated glass substrates were cleaned with acetone and isopropyl alcohol, followed by drying and oxygen plasma

treatment. A 30 nm layer of PEDOT:PSS (AI4083) was spin-coated onto the plasma-treated ITO substrate and annealed at 150 °C for 30 min. An active layer consisting of 1:3 blend of polymer (10 mg/mL) and $PC_{71}BM$ (30 mg/mL, Solenne) dissolved in *o*-dichlorobenzene (*o*-DCB) was spin-coated on the PEDOT:PSS layer and then Ca (30 nm)/Al (100 nm) cathode was finally deposited by thermal evaporation under high vacuum (10^{-6} mbar) through a shadow mask. The pixel size, defined by the spatial overlap of the ITO anode and Ca/Al cathode, was 0.045 cm^2. The device characteristics were obtained using a xenon lamp at AM1.5 solar illumination (Oriel Instruments).

Synthesis of 5-bromo-2,3-dihydro-2-(hydroxyimino)inden-1-one

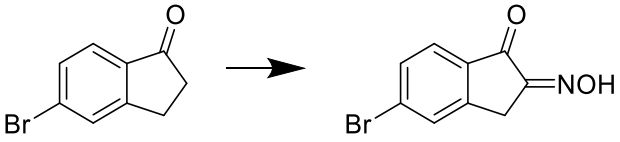

To a solution of 5-bromo-indanone (17.48 g, 82.80 mmol) in toluene (250 mL) was added 2 M HCl (30 mL). The solution was stirred at room temperature for 30 min before isoamyl nitrate (13.35 mL, 99.40 mmol) was added drop wise over 45 min. The reaction was warmed to 40°C and stirred overnight at that temperature. The reaction was cooled to room temperature, filtered and the solid washed with MeOH (100 mL). The product was collected and slurried in diethyl ether, and then filtered to obtain the product as an off-white solid. Yield = 16.08 g, 81%. Mpt. 202°C (Lit = 204°C[1]). MS (GCMS, EI^+): 160.0, 162.0 (M^+). ^1H NMR (400 MHz, $CDCl_3$) δ (ppm): 12.72 (s, 1H), 7.92 (s, 1H), 7.70 (s, 2H), 3.80 (s, 2H).

Synthesis of 2,8-dibromo-6,12-dihydrodiindeno[1,2-b:1,2-e]pyrazine

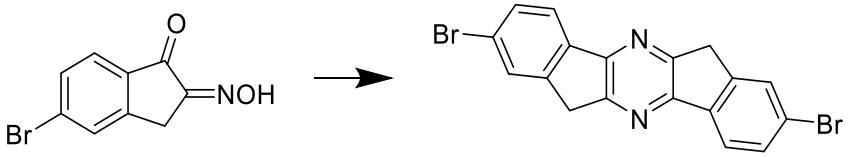

5-Bromo-2,3-dihydro-2-(hydroxyimino)inden-1-one (16.08 g, 67.00 mmol) and sodium dithionate (14.00 g, 80.40 mmol) were dissolved in ethanol (125 mL) and degassed. Ammonia solution (125 mL, 28%) was added under argon and the solution stirred for 72 hr in the absence of light. Water (100 mL) was then added and the mixture heated to reflux in air for 24 hr. The resulting solution was cooled to room temperature, filtered, rinsed with methanol and diethyl ether and dried to obtain the product as an orange solid. Yield = 8.32 g, 61 %. MS (GCMS, EI^+):= 414.0 (M^+). ^1H NMR (400 MHz, $CDCl_3$) δ (ppm): 8.01 (d, J = 8.4 Hz, 2H), 7.82 (d, J = 1.4 Hz, 2H), 7.67 (dd, J = 8.4, 1.4 Hz, 2H), 4.06 (s, 4H).

Synthesis of 2,8-dibromo-6,6,12,12-tetraoctyldiindeno[1,2-b:1,2-e]pyrazine

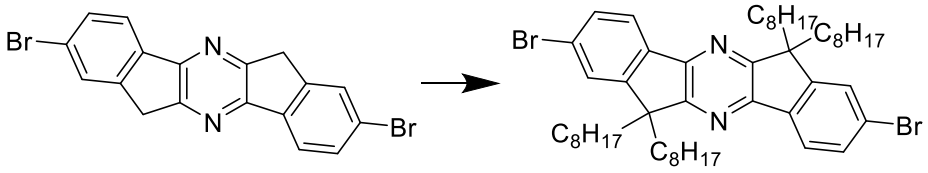

2,8-Dibromo-6,12-dihydrodiindeno[1,2-b:1,2-e]pyrazine (2.00 g, 4.85 mmol), tetrabutylammonium bromide (0.08 g, 0.24 mmol) and 1-bromooctane (4.12 g, 21.30 mmol) were dissolved in toluene (50 mL) and thoroughly degassed. A solution of thoroughly degassed sodium hydroxide (1.94 g, 48.50 mmol) in water (50 mL) was added and the reaction mixture refluxed for 48 h in the absence of light. The solution was allowed to cool to room temperature and most of the toluene was removed under reduced pressure. The remaining aqueous emulsion was extracted with chloroform. The chloroform extracts were combined, dried ($MgSO_4$), filtered and concentrated under reduced pressure to afford the

crude product. Purification via column chromatography over silica (eluent: hexane) afforded the product as a white solid. Yield = 2.59 g, 72%. Mpt 100 – 101 °C. MS (GCMS, EI^+): 862.3 (M^+). ^1H NMR (400 MHz, $CDCl_3$) δ (ppm): 7.97 (d, *J* = 6.9 Hz, 2H), 7.59 (s, 2H), 7.57 (d, 6.9 Hz, 2H), 2.26 (t, *J* = 12.7, 4H), 1.98 (t, *J* = 12.7, 4H), 1.06-1.24 (m, 48H), 0.81 (t, *J* = 7.3Hz, 12H).

Synthesis of 2,8-dibromo-6,6,12,12-tetra-2-methylbutyldiindeno[1,2-b:1,2-e]pyrazine

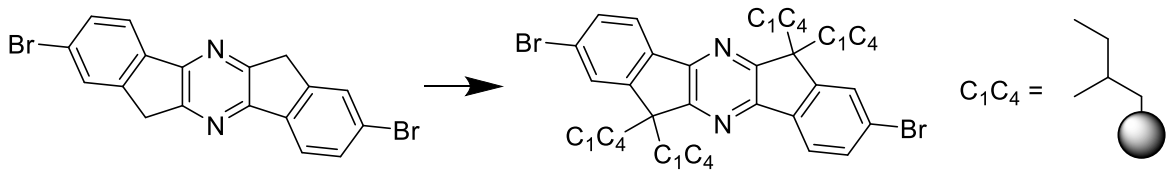

2,8-Dibromo-6,12-dihydrodiindeno[1,2-b:1,2-e]pyrazine (4.00 g, 9.60 mmol), tetrabutylammonium bromide (0.16 g, 0.96 mmol) and 1-bromo-2-methylbutane (6.63 g, 42.24 mmol) were dissolved in toluene (100 mL) and thoroughly degassed. A solution of thoroughly degassed sodium hydroxide (3.84 g, 96.00 mmol) in water (100 mL) was added and the reaction mixture refluxed for 48 hr in the absence of light. The solution was allowed to cool to room temperature and most of the toluene was removed under reduced pressure. The remaining aqueous emulsion was extracted with chloroform. The chloroform extracts were combined, dried ($MgSO_4$), filtered and concentrated under reduced pressure to afford the crude product. Purification via column chromatography over silica (eluent hexane) afforded the product as a white solid. Yield = 1.82 g, 32 %. Mpt. 196 – 197 °C. MS (GCMS, EI^+): = 694.4 (M^+). Anal. Calcd. for ($C_{38}H_{50}Br_2N_2$): C, 65.71; H, 7.26; N, 4.03. Found: C, 65.80; H, 7.36; N, 4.14. ^1H NMR (400 MHz, $CDCl_3$) δ (ppm): 7.99 (d, *J* = 8.0 Hz, 2H), 7.62 (m, 4H), 2.45 (dd, *J* = 13.8, 5.0 Hz, 2H), 2.24 (dd, *J* = 13.8, 8.2 Hz, 2H), 2.07 (dd, *J* =

13.9, 3.5, 2H), 1.86 (dd, *J* = 13.8, 5.8 Hz, 2H), 0.99-0.40 (m, 30H), 0.20-0.15 (m, 6H). ^{13}C NMR (101 MHz, $CDCl_3$) δ: 163.38, 152.42, 130.73, 127.19, 123.13, 122.54, 52.87, 46.34, 46.10, 31.04, 30.86, 30.60, 30.10, 21.04, 20.44, 11.04, 10.41.

Synthesis of 2,8-dibromo-6,6,12,12-tetraethylhexyldiindeno[1,2-b:1,2-e]pyrazine

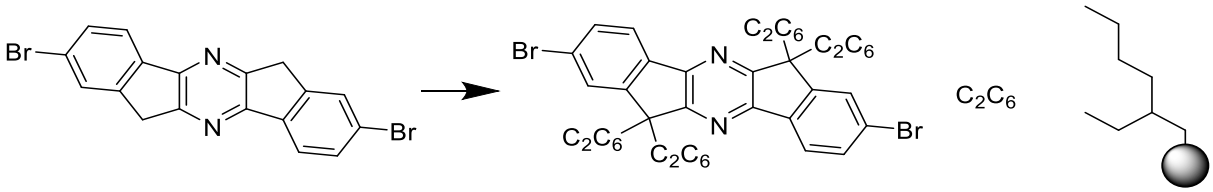

2,8-Dibromo-6,12-dihydrodiindeno[1,2-b:1,2-e]pyrazine (4.00 g, 9.60 mmol), tetrabutylammonium bromide (0.16 g, 0.96 mmol) and 1-bromo-2-ethyl-hexane (9.38 g, 48.30 mmol) were dissolved in toluene (100 mL) and thoroughly degassed. A solution of thoroughly degassed sodium hydroxide (3.84 g, 96.00 mmol) in water (100 mL) was added and the reaction mixture refluxed for 48 hr in the absence of light. The solution was allowed to cool to room temperature and most of the toluene was removed under reduced pressure. The remaining aqueous emulsion was extracted with chloroform. The chloroform extracts were combined, dried ($MgSO_4$), filtered and concentrated under reduced pressure to afford the crude product. Purification via column chromatography over silica (eluent hexane) afforded the product as a colourless oil. Yield = 2.20 g, 52%. Mpt = 20 - 21°C; MS (GCMS, EI^+): 862.0 (M^+); Anal. calcd. for ($C_{50}H_{74}Br_2N_2$): C, 69.59; H, 8.64; N, 3.25. Found: C, 69.51; H, 8.66; N, 3.15. ^{1}H NMR (400 MHz, $CDCl_3$) δ (ppm): 7.92 (d, *J* = 8.1, 2H), 7.62 (s, 2H), 7.56 (d, *J* = 8.1, 2H), 2.32 (m, 4H), 1.91 (m, 4H), 1.27 (m, 4H) 0.95 – 0.42 (m, 62H). ^{13}C NMR (101 MHz, $CDCl_3$) δ: 162.95, 152.50, 151.68, 137,62, 130.57, 125.99, 123.40, 122.50, 53.23, 38.61, 32.72, 28.70, 30.02, 29.57, 23.79, 22.67, 13.89.

General procedure for salt wash purification

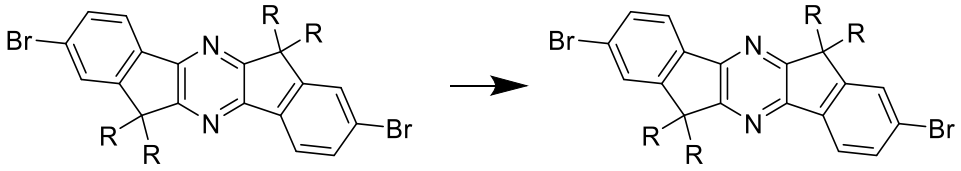

R = C_8H_{17},
$C_2C_6H_{17}$,
$C_1C_4H_9$

The monomer (200 mg) was dissolved in dry THF (50 mL). 1 M Potassium tert-butoxide (4.5 mL in THF) was added dropwise and the reaction stirred for 15 min. THF was removed under reduced pressure and the remaining precipitate was dissolved in dry hexane (25 mL). Filtration through alumina and subsequent removal of the hexane under reduced pressure yielded the purified product. This was repeated twice for each monomer.

Synthesis of poly(6,6,12,12-tetraoctyldiindeno[1,2-b:1,2-e]pyrazine)

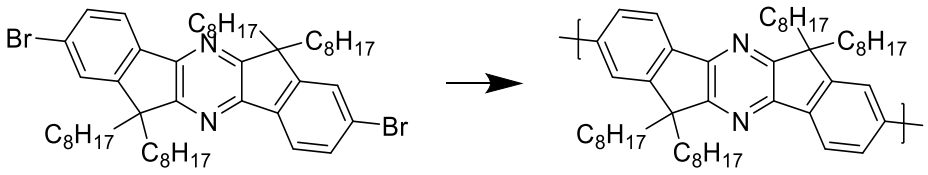

A thoroughly degassed solution of 2,8-dibromo-6,6,12,12-tetraoctyldiindeno[1,2-b:1,2-e]pyrazine (0.20 g, 0.24 mmol) in toluene (0.5 mL) and DMF (0.5 mL) was added to a degassed solution of $Ni(COD)_2$ (0.15g, 5.30 mmol), 2,2'-bipyridine (0.08 g, 0.53 mmol) and 1,5-cyclooctadiene (0.06 mL, 0.53 mmol) in toluene (2 mL) and DMF (2 mL) under an inert atmosphere in a sealed microwave vial. The combined solution was heated to 85 ^oC for 72 h. The resulting solution was poured into cold methanol, filtered and the polymer extracted (soxhlet) with methanol, acetone, hexane and chloroform. The chloroform fraction was concentrated under reduced pressure and dissolved in chloroform/water solution (100 mL/100

mL). Sodium diethyldithiocarbamate trihydrate (0.50 g) was added and the solution was stirred vigorously at 50 °C for 3 h. The chloroform solution was washed with water, dried ($MgSO_4$), concentrated and precipitated from chlorobenzene into cold methanol to yield the polymer as bright yellow fibres. Yield = 86 mg, 42 %. GPC: Mn = 37 000 Da, PDI = 2.2

^{1}H NMR (400 MHz, $CDCl_3$) δ (ppm): 8.26 (s, 2H), 7.85-7.79 (m, 4H), 2.38 (b, 4H), 2.16 (b, 4H), 1.60-1.49 (b, 40H), 1.13 (b, 8H), 0.82 (m, 12H).

Synthesis of poly(6,6,12,12-tetramethylbutyldiindeno[1,2-b:1,2-e]pyrazine)

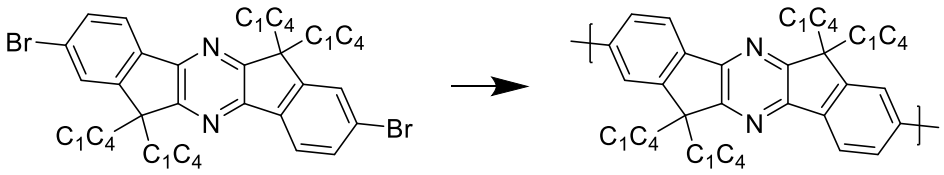

A thoroughly degassed solution of 2,8-dibromo-6,6,12,12-tetramethylbutyldiindeno[1,2-b:1,2-e]pyrazine (0.20 g, 0.28 mmol) in toluene (1.3 mL) and DMF (1.3 mL) was added to a degassed solution of $Ni(COD)_2$ (0.18 g, 0.63 mmol), 2,2'-bipyridine (0.01 g, 0.63 mmol) and 1,5-cyclooctadiene (0.07 mL, 0.63 mmol) in toluene (2 mL) and DMF (2 mL) under an inert atmosphere in a sealed microwave vial. The combined solution was heated to 85 °C for 72 h. The resulting solution was poured into cold methanol, filtered and the polymer extracted (soxhlet) with methanol, acetone, hexane and chloroform. The chloroform fraction was concentrated under reduced pressure and dissolved in chloroform/water solution (100 mL/100 mL). Sodium diethyldithiocarbamate trihydrate (0.5 g) was added and the solution was stirred vigorously at 50 °C for 3 h. The chloroform solution was washed with water, dried over $MgSO_4$, concentrated and precipitated from chlorobenzene into cold methanol to yield the polymer as bright yellow fibres. Yield = 19 mg, 12 %. GPC: Mn = 8 000 Da, PDI = 1.8

^{1}H NMR (400 MHz, $CDCl_3$) δ (ppm): 8.32 (s, 2H), 7.75 (m, 4H), 2.50 (b, 4H), 2.04 (b, 4H), 1.50 (b, 12H), 1.00 (m, 12H), 0.72 (t, 12H),

Synthesis of poly(6,6,12,12-tetra-2-ethylhexylldiindeno[1,2-b:1,2-e]pyrazine)

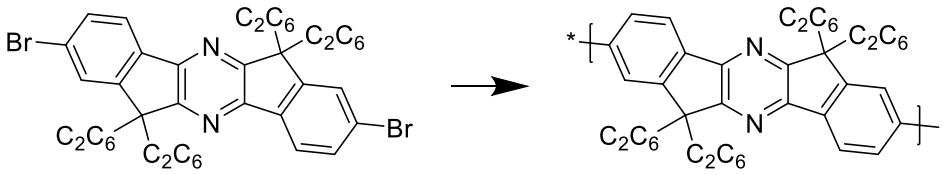

A thoroughly degassed solution of 2,8-dibromo-6,6,12,12-tetraethylhexyldiindeno[1,2-b:1,2-e]pyrazine (0.20 g, 0.23 mmol) in toluene (0.5 mL) and DMF (0.5 mL) was added to a degassed solution of Ni(COD) (0.14 g, 5.10 mmol), 2,2'bipyridine (0.08 g, 0.51 mmol) and 1,5- cyclooctadiene (0.06 mL, 0.51 mmol) in toluene (2 mL) and DMF (2 mL) under an inert atmosphere in a sealed microwave vial. The combined solution was heated to 85 ^oC for 72 h. The resulting solution was poured into cold methanol, filtered and the polymer extracted (soxhlet) with methanol, acetone, hexane and chloroform. The chloroform fraction was concentrated under reduced pressure and dissolved in chloroform/water solution (100 mL/100 mL). Sodium diethyldithiocarbamate trihydrate (0.50 g) was added and the solution was stirred vigorously at 50°C for 3 hr. The chloroform solution was washed with water, dried over $MgSO_4$, concentrated and precipitated from chlorobenzene into cold methanol to yield polymer as bright yellow fibres. Yield = 82 mg, 40%. GPC: Mn = 16 000 Da, PDI = 1.5.

^{1}H NMR (400 MHz, $CDCl_3$) δ (ppm): 8.36 (s, 2H), 7.79 (m, 4H), 2.56 (b, 4H), 2.11 (b, 4H), 1.50 (b, 36H), 1.00 (b, 12H), 0.72 (m, 12H).

Synthesis of poly(6,6,12,12-tetraoctyldiindeno[1,2-b:1,2-e]pyrazine-co-9-9-dipropylfluorene)

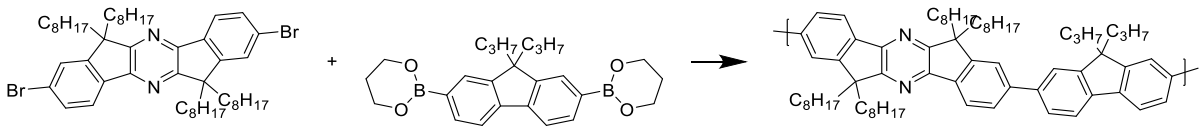

2,8-Dibromo-6,6,12,12-tetraoctyldiindeno[1,2-b:1,2-e]pyrazine (0.20 g, 0.23 mmol), 9,9-di-n-propyl-2,7-bis-(1,3,2-dioxaborolan-2-yl)fluorene (0.13 g, 0.23 mmol), dry toluene (4 mL) and aliquot 336 (2 drops) were placed in a microwave vial and thoroughly degassed. $Pd(PPh_3)_4$ (4 mg, 1.3 eq) was added quickly and finally degassed 1 M K_2CO_3 (aq) (1 mL) was added in one portion. The reaction mixture was further degassed for 15 min before being heated in an oil bath to 110 °C for 48 h. The resulting solution was poured into cold methanol, filtered into a soxhlet thimble and then extracted (soxhlet) using methanol, acetone, hexane and chloroform. The chloroform fraction was concentrated under reduced pressure and subsequently dissolved in chloroform/water solution (100 mL/100 mL) and sodium diethyldithiocarbamate trihydrate (0.50 g) was added. The solution was stirred vigorously at 50 °C for 3 h. After allowing to cool to room temperature the chloroform solution was washed with water, dried ($MgSO_4$), concentrated and precipitated from chlorobenzene into cold methanol to yield the polymer as bright yellow fibres. Yield = 87 mg, 44 %. GPC: Mn = 12 000 Da, PDI = 1.8. ^{1}H NMR (400 MHz, $CDCl_3$) δ (ppm): 8.25 (d, *J* = 8.1 Hz, 2H), 7.90 (d, *J* = 8.1 Hz, 2H), 7.82 (d, *J* = 8.1 Hz, 2H), 7.78 - 7.74 (b, 6H), 2.49 - 2.31 (b, 4H), 2.25 - 2.03 (b, 8H), 1.12 (m, 38H), 0.99 – 0.88 (b, 8H), 0.82 (m, 24H).

Synthesis of poly(6,6,12,12-tetraoctyldiindeno[1,2-b:1,2-e]pyrazine-co- 9-9-dioctylfluorene)

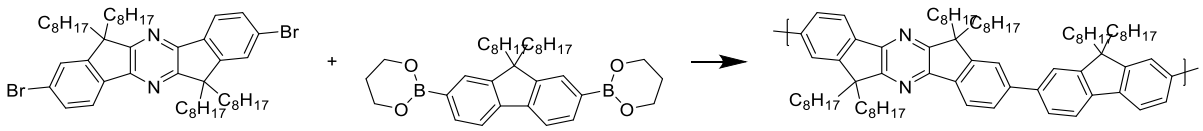

2,8-Dibromo-6,6,12,12-tetraoctyldiindeno[1,2-b:1,2-e]pyrazine (0.20 g, 0.23 mmol), 9,9-di-n-octyl-2,7-bis-(1,3,2-dioxaborolan-2-yl)fluorene (0.16g, 0.23 mmol) dry toluene (4 mL) and aliquot 336 (2 drops) were placed in a microwave vial and thoroughly degassed. $Pd(PPh_3)_4$ (4 mg, 1.3 eq.) was added quickly and finally degassed 1 M K_2CO_3 (aq) (1 mL) was added in one portion. The reaction mixture was further degassed for 15 min before being heated to 110 °C for 48 h. The resulting solution was poured into cold methanol, filtered into a soxhlet thimble and then extracted (soxhlet) using methanol, acetone, hexane and chloroform. The chloroform fraction was concentrated under reduced pressure and subsequently dissolved in chloroform/water solution (100 mL/100 mL) and sodium diethyldithiocarbamate trihydrate (0.50 g) was added. The solution was stirred vigorously at 50 °C for 3 h. After allowing to cool to room temperature the chloroform solution was washed with water, dried ($MgSO_4$), concentrated and precipitated from chlorobenzene into cold methanol to yield the polymer as bright yellow/green fibres. Yield = 125mg, 56 %. GPC: Mn = 22 000 Da, PDI = 2.2. ^{1}H NMR (400 MHz, $CDCl_3$) δ (ppm): 8.22 (d, J = 8.1 Hz, 2H), 7.89 (d, J = 8.1 Hz, 2H), 7.82 – 7.67 (m, 8H), 2.45 - 2.32 (b, 4H), 2.23 - 2.02 (b, 8H), 1.17 - 1.12 (m, 70H), 0.84 (m, 24H).

Synthesis of poly(6,6,12,12-tetramethylbutyldiindeno[1,2-b:1,2-e]pyrazine-co-9-9 dipropylylfluorene)

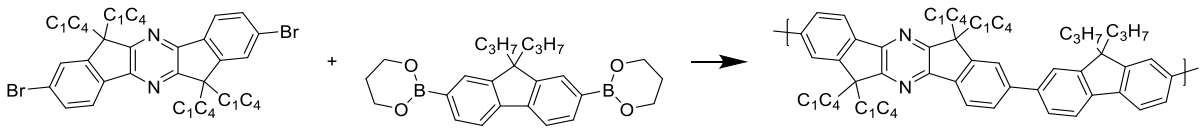

2,8-Dibromo-6,6,12,12-tetramethylbutyldiindeno[1,2-b:1,2-e]pyrazine (0.20 g, 0.29 mmol), 9,9-di-n-propyl-2,7-bis-(1,3,2-dioxaborolan-2-yl)fluorene (0.12 g, 0.29 mmol) dry toluene (4 mL) and aliquot 336 (2 drops) were placed in a microwave vial and thoroughly degassed. $Pd(PPh_3)_4$ (4 mg, 1.3 eq.) was added quickly and finally degassed 1 M K_2CO_3 (aq) (1 mL) was added in one portion. The reaction mixture was further degassed for 15 min before being heated to 110 °C for 48 h. The resulting solution was poured into cold methanol, filtered into a soxhlet thimble and then extracted (soxhlet) using methanol, acetone, hexane and chloroform. The chloroform fraction was concentrated under reduced pressure and subsequently dissolved in chloroform/water solution (100 mL/100 mL) and sodium diethyldithiocarbamate trihydrate (0.50 g) was added. The solution stirred vigorously at 50 °C for 3 h. After cooling to room temperature the chloroform solution was washed with water, dried ($MgSO_4$), concentrated and precipitated from chlorobenzene into cold methanol to yield the polymer as bright yellow/green fibres. Yield = 69 mg, 43 %. GPC : Mn = 12 000 Da, PDI = 1.6. ^{1}H NMR (400 MHz, $CDCl_3$) δ (ppm): 8.27 (b, 4H), 7.88 (b, 2H), 7.79 (b, 4H), 7.70 (b, 2H), 2.20-2.02 (b, 12H) 1.50 (b, 14H), 0.90 (b, 8H), 0.70 (m, 12H), 0.57 - 0.49 (m, 12H).

Synthesis of poly(6,6,12,12-tetramethylbutyldiindeno[1,2-b:1,2-e]pyrazine-co-9-9 dioctylfluorene)

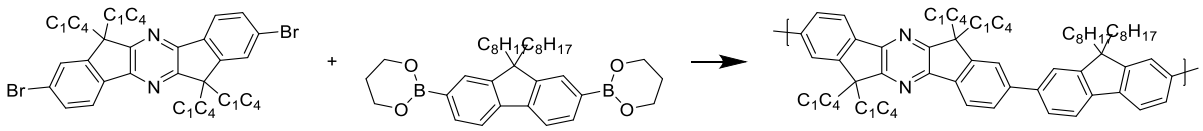

2,8-Dibromo-6,6,12,12-tetramethylbutyldiindeno[1,2-b:1,2-e]pyrazine (0.20 g, 0.29 mmol), 9,9-di-n-octyl-2,7-bis-(1,3,2-dioxaborolan-2-yl)fluorene (0.16 g, 0.29 mmol) dry toluene (4 mL) and aliquot 336 (2 drops) were placed in a microwave vial and thoroughly degassed. $Pd(PPh_3)_4$ (4 mg, 1.3 eq.) was added quickly and finally degassed 1 M K_2CO_3 (aq) (1 mL) was added in one portion. The reaction mixture was further degassed for 15 min before being heated to 110 °C for 48 h. The resulting solution was poured into cold methanol, filtered into a soxhlet thimble and then extracted using methanol, acetone, hexane and chloroform. The chloroform fraction was concentrated under reduced pressure and subsequently dissolved in chloroform/water solution (100 mL/100 mL) and sodium diethyldithiocarbamate trihydrate (0.5 g) was added. The solution was stirred vigorously at 50 °C for 3 h. After allowing to cool to room temperature the chloroform solution was washed with water, dried ($MgSO_4$), concentrated and precipitated from chlorobenzene into cold methanol to yield the polymer as bright yellow/green fibres. Yield = 92 mg, 50 %. GPC : Mn = 37 000 Da, PDI = 2.0. ^{1}H NMR (400 MHz, $CDCl_3$) δ (ppm): 8.25 (b, 2H), 7.91 (b, 2H), 7.80 (b, 4H), 7.71 (b, 4H), 2.59 - 2.16 (b, 12H) 1.16 (b, 24H), 0.84 (b, 12H), 0.73 (m, 12H), 0.49 (m, 12H).

Synthesis of (4-4,4,5,5-tetramethyl)-4-(4,4,5,5-tetramethyl-1,3,2-dioxaborolan-2-yl)-N-(2,4-dimethyl-phenyl)benzenamine

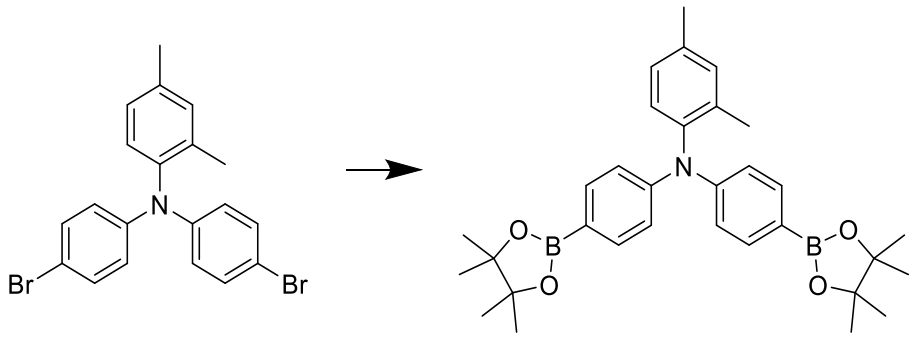

To a solution of (4-4,4,5,5-tetramethyl)-4-(4,4,5,5-tetramethyl-1,3,2-dioxaborolan-2-yl)-N-(2,4-dimethyl-phenyl)benzenamine (2.00g, 4.63 mmol) in dry THF (50 mL) at -78^{o}C was added n-butyllithium (4.00 mL of a 2.5 M solution in hexane, 10.00 mmol) dropwise over 20 min. The solution stirred at -78 °C for 30 min before 2-isopropoxy-4,4,5,5-tetramethyl-1,3,2-dioxaborolane (2.50 g, 14.00 mmol) was added in one portion. The reaction warmed to room temperature overnight and was quenched with water followed by extraction with CH_2Cl_2. The organic layers were combined, dried ($MgSO_4$), filtered and concentrated under reduced pressure. The crude product was purified via column chromatography over silica (eluent: hexane:DCM 1:1) and recrystallised from methanol. Yield = 1.65 g, 68 %. Mpt. = 221 - 222°C. MS (GCMS, EI) 525.0 (M^+). ^{1}H NMR (400 MHz, $CDCl_3$) δ (ppm): 7.66 (d, J = 8.5 Hz, 4H), 7.08 (s, 1H), 7.02 (m, 2H), 6.98 (d, J = 8.5 Hz, 4H), 2.37 (s, 3H), 1.98 (s, 3H), 1.35 (s, 24H). ^{13}C NMR (101 MHz, $CDCl_3$) δ: 149.56, 148.61, 138.02, 136.39, 135.81, 132.41, 129.59, 128.19, 122.92, 120.41, 117.24, 109.32, 83.51, 28.52, 24.84, 21.03, 18.30.

Synthesis of poly-6,6,12,12-tetraoctyldiindeno[1,2-b:1,2-e]pyrazine-co-4-phenyl-N-(2,4-dimethyl-phenyl)benzenamine

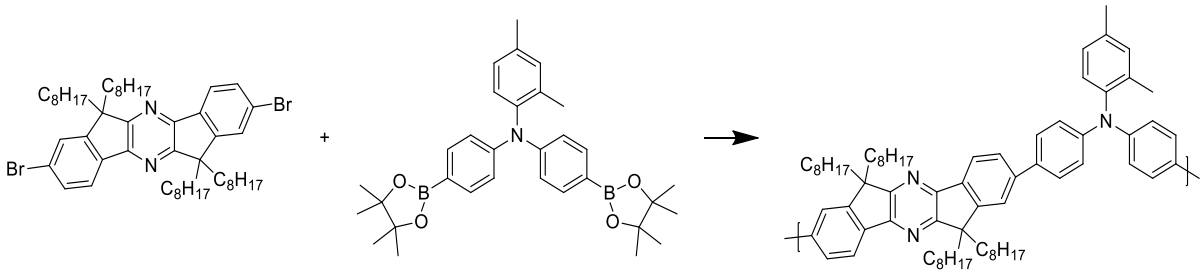

2,8-Dibromo-6,6,12,12-tetraoctyldiindeno[1,2-b:1,2-e]pyrazine (0.20 g, 0.23 mmol), (4-4,4,5,5-tetramethyl)-4-(4,4,5,5-tetramethyl-1,3,2-dioxaborolan-2-yl)-N-(2,4-dimethyl-phenyl)benzenamine (0.12 g, 0.23 mmol), dry toluene (4 mL) and aliquot 336 (2 drops) were placed in a microwave vial and thoroughly degassed. $Pd(PPh_3)_4$ (4 mg, 1.3 eq.) was added quickly and finally degassed 1 M K_2CO_3 (aq) (1 mL) was added in one portion. The reaction mixture was further degassed for 15 min and then heated to reflux in an oil bath for 48 h. The reaction was cooled, poured into cold methanol, filtered into a soxhlet thimble and extracted with methanol, acetone, hexane and chloroform. The chloroform fraction was concentrated under reduced pressure and subsequently dissolved in chloroform/water solution (100 mL/100 mL) and sodium diethyldithiocarbamate trihydrate (0.50 g) was added. The solution was stirred vigorously at 50 °C for 3 h. After allowing to cool to room temperature the chloroform solution was washed with water, dried ($MgSO_4$), concentrated and precipitated from chlorobenzene into cold methanol to yield the polymer as bright yellow/green fibres. Yield = 96 mg, 48 %. GPC : Mn = 20 000 Da, PDI = 1.5. ^{1}H NMR (400 MHz, $CDCl_3$) δ (ppm): 8.17 (b, 2H), 7.75 – 7.47 (b, 9H), 7.18 – 7.07 (b, 6H), 2.42 (s, 3H), 2.34 (b, 4H), 2.15 (s, 3H), 2.09 (b, 4H), 1.34 (m, 8H), 1.24-1.02 (b, 44H), 0.80 (t, 12H).

Synthesis of poly-6,6,12,12-tetramethylbutyldiindeno[1,2-b:1,2-e]pyrazine-co-4-phenyl-N-(2,4-dimethyl-phenyl)benzenamine

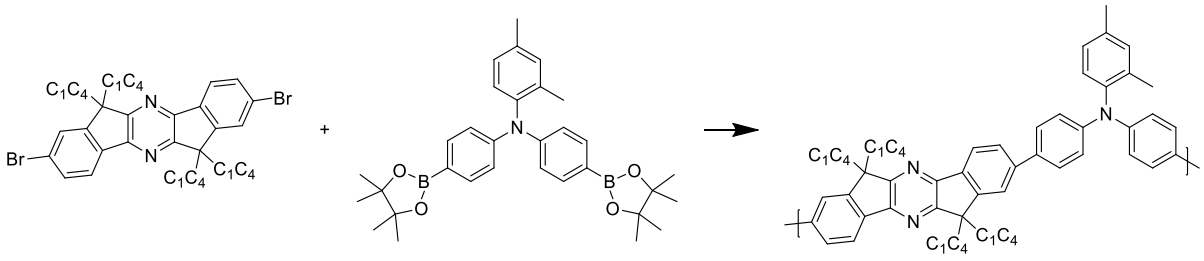

2,8-Dibromo-6,6,12,12-tetramethylbutyldiindeno[1,2-b:1,2-e]pyrazine (0.20 g, 0.28 mmol), (4-4,4,5,5-tetramethyl)-4-(4,4,5,5-tetramethyl-1,3,2-dioxaborolan-2-yl)-N-(2,4-dimethyl-phenyl)benzenamine (0.15 g, 0.28 mmol), dry toluene (4 mL) and aliquot 336 (2 drops) were placed in a microwave vial and thoroughly degassed. $Pd(PPh_3)_4$ (4 mg, 1.3 eq.) was added quickly and finally degassed 1 M K_2CO_3 (aq) (1 mL) was added in one portion. The reaction mixture was further degassed for 15 min and then heated to reflux in an oil bath for 48 h. The reaction was cooled, poured into cold methanol, filtered into a soxhlet thimble and extracted (soxhlet) with methanol, acetone, hexane and chloroform. The chloroform fraction was concentrated under reduced pressure and subsequently dissolved in chloroform/water solution (100 mL/100 mL) and sodium diethyldithiocarbamate trihydrate (0.50 g) was added. The solution was stirred vigorously at 50 °C for 3 h. After allowing to cool to room temperature the chloroform solution was washed with water, dried ($MgSO_4$), concentrated and precipitated from chlorobenzene into cold methanol to yield the polymer as bright yellow/green fibres. Yield = 63 mg, 38 %. GPC ; Mn = 8 000 Da, PDI = 1.8. ^{1}H NMR (400 MHz, $CDCl_3$) δ (ppm): 8.16 (d, *J* = 8.2 Hz, 2H), 7.75 (m, 2H), 7.68 (b, 4H), 7.59 (d, *J* = 8.2 Hz, 2H), 7.19 (m, 6H), 7.12 (b, 1H), 2.50 (b, 2H), 2.42 (s, 3H), 2.29 (b, 2H), 2.16 (s, 3H), 2.09 (m, 2H), 1.95 (m, 2H), 1.71 (m, 4H), 1.44 - 1.35 (b, 8H), 0.95 (m, 12H), 0.66 (m, 12H),

Synthesis of 2,8-bis-(4,4,5,5-tetramethyl-1,3,2-dioxaborolan-2-yl)-6,6,12,12-tetraoctyl-6,12-dihydrodiindeno[1,2-b:1',2'-e]pyrazine

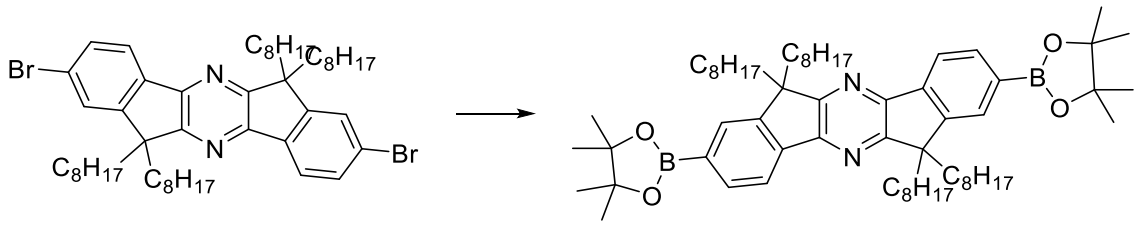

To a solution of 2,8-dibromo-6,6,12,12-tetraoctyldiindeno[1,2-b:1,2-e]pyrazine (1.56 g, 1.81 mmol) in dry THF (40 mL) at -78°C was added n-butyllithium (4.53 mL, 1.6M in hexane, 7.24 mmol) dropwise over 20 min and the solution stirred for 2 h at -78 °C. 2-Isopropoxy-4,4,5,5-tetramethyl-1,3,2-dioxaborolane (1.85 mL, 9.05 mmol) was added in one portion and the solution warmed to room temperature overnight. The reaction was quenched with water and extracted with chloroform. The organic layers were combined, dried ($MgSO_4$), filtered and the solvent removed under reduced pressure. The crude product was recrystallised from hot hexane to afford a white solid. Yield = 0.59 g, 34 %. Mpt. 144 - 145°C. ^{1}H NMR (400 MHz, $CDCl_3$) δ (ppm): 8.11(d, *J*= 7.6 Hz, 2H), 7.91 (d, *J*= 7.6Hz, 2H), 7.86 (s, 2H), 2.34-2.23 (m, 4H), 2.10-2.00 (m, 4H), 1.43 (s, 24H), 1.20-1.10 (m, 48H), 0.80 (t, 12H). ^{13}C NMR (101 MHz, $CDCl_3$) δ (ppm): 164.62, 152.33, 148.54, 142.29, 135.90, 130.10, 120.34, 84.83, 54.10, 38.99, 32.82, 30.81, 30.01, 29.76, 25.60, 24.92, 23.18, 14.59.

Synthesis of IP-DTBT-H

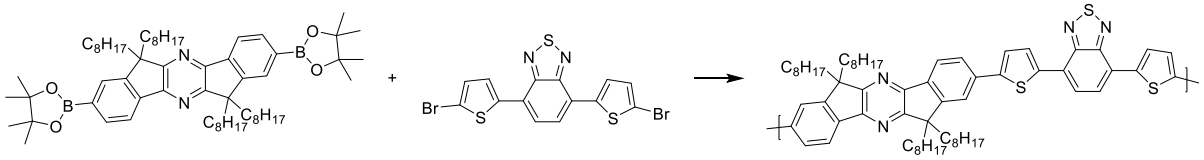

To a thoroughly degassed solution of toluene (4 mL) and aliquot 336 (2 drops) was added 2,8-dibromo-6,6,12,12-tetraoctyldiindeno[1,2-b:1,2-e]pyrazine (0.15 g, 0.16 mmol), 4,7-bis(5-bromothiophen-2-yl)benzo[c]-[1,2,5]thiadiazole (0.07 g, 0.16 mmol) and $Pd(PPh_3)_4$ (2.7 mg, 1.25 eq.). 1 M K_2CO_3 (aq) (1 mL) were added in one portion and the reaction was heated in an oil bath to 105 °C for 72 h, after which the reaction was poured into cold methanol, filtered through a soxhlet thimble and extracted (soxhlet) with methanol, acetone and hexane. The polymer was then dried under vacuum and dissolved in chloroform/water (100 mL/100 mL). Sodium diethyldithiocarbamate trihydrate (0.50 g) was added and the solution was stirred vigorously at 50 °C for 3 h. The chloroform solution was washed with water, dried ($MgSO_4$), concentrated and precipitated from chlorobenzene into cold methanol to yield the polymer as a dark red fibre. Yield = 112 mg, 68 %. GPC : Mn 40 000 Da, PDI = 2.1. ^{1}H NMR (400 MHz, $CDCl_3$) δ (ppm): 8.23 (s, 2H), 8.16 (d, *J* = 7.5 Hz, 2H), 8.02 (s, 2H), 7.87 (d, *J* = 7.5 Hz, 2H), 7.82 (s, 2H), 7.62 (s, 2H), 2.44 - 230 (b, 4H), 2.17 – 2.06 (b, 4H), 1.20 – 1.01 (b, 48H), 0.81 (t, *J* = 6.7 Hz, 12H).

Synthesis of IP-DTBT-F

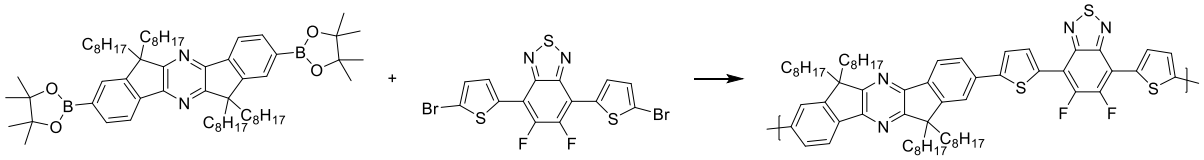

To a thoroughly degassed solution of toluene (4 mL) and aliquot 336 (2 drops) was added 2,8-dibromo-6,6,12,12-tetraoctyldiindeno[1,2-b:1,2-e]pyrazine (0.15 g, 0.16 mmol), 4,7-bis(5-bromothiophen-2-yl)benzo[c]-[1,2,5]5,6-difluorothiadiazole (0.08 g, 0.16 mmol) and $Pd(PPh_3)_4$ (2.7 mg, 1.25 eqv). 1 M K_2CO_3 (aq) (1 mL) was added in one portion and the reaction was heated in an oil bath to 105 °C for 72 hr, after which the reaction was poured

into cold methanol, filtered through a soxhlet thimble and extracted (soxhlet) with methanol, acetone and hexane. The polymer was then dried under vacuum and dissolved in chloroform/water (100 mL/100 mL). Sodium diethyldithiocarbamate trihydrate (0.50 g) was added and the solution was stirred vigorously at 50°C for 3 hr. The chloroform solution was washed with water, dried ($MgSO_4$), concentrated and precipitated from chlorobenzene into cold methanol to yield the polymer as a dark red fibre. Yield = 100 mg, 59 %. GPC : Mn = 37 000 Da, PDI = 1.8. ^{1}H NMR (400 MHz, $CDCl_3$) δ (ppm): 8.37 (b, 2H), 8.15 (b, 2H), 7.98 (b, 2H), 7.87 (b, 2H) 7.70 (b, 2H), 7.63 (b, 2H), 2.52 (b, 2H), 2.35 (b, 4H), 2.13 (m, 4H), 1.99 (m, 2H), 1.83 (m, 2H), 1.76 (m, 2H), 1.48-1.27 (b, 40H), 0.87 (t, 12 H)

Synthesis of IP-DTBT-OC_8H_{17}

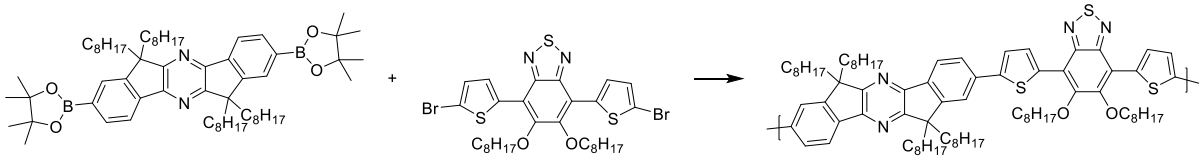

To a thoroughly degassed solution of toluene (4 mL) and aliquot 336 (2 drops) was added 2,8-dibromo-6,6,12,12-tetraoctyldiindeno[1,2-b:1,2-e]pyrazine (0.15 g, 0.16 mmol), 4,7-bis(5-bromothiophen-2-yl)benzo[c]-[1,2,5]5,6-2-octyloxythiadiazole (0.11 g, 0.16 mmol) and $Pd(PPh_3)_4$ (2.7 mg, 1.25 eq.). 1M K_2CO_3 (aq) (1 mL) was added in one portion and the reaction was heated to 105 °C for 72 h, after which the reaction was poured into cold methanol, filtered through a soxhlet thimble and extracted (soxhlet) with methanol, acetone and hexane. The polymer was then dried under vacuum and dissolved in chloroform/water (100 mL/100 mL). Sodium diethyldithiocarbamate trihydrate (0.50 g) was added and the solution was stirred vigorously at 50 °C for 3 h. The chloroform solution was washed with water, dried ($MgSO_4$), concentrated and precipitated from chlorobenzene into cold methanol

to yield the polymer as a red fibre. Yield = 130 mg, 63 %. GPC : Mn = 78 000 Da, PDI = 1.3. ^{1}H NMR (400 MHz, $CDCl_3$) δ (ppm): 8.57 (b, 2H), 8.14 (m, 2H), 7.80 (b, 2H), 7.70 (b, 4H), 4.23 (b, 4H), 2.49 (b, 4H), 2.35 (m, 4H), 2.10-2.02 (m, 48H), 1.48 (b, 18H), 1.31 (t, 12H), 1.10 (t, 12H).

Synthesis of IP-DTBT-$SC_{12}H_{25}$

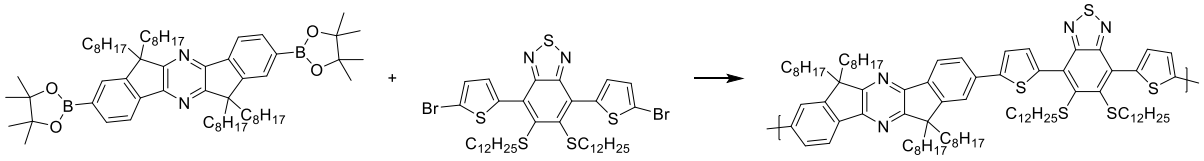

To a thoroughly degassed solution of toluene (4 mL) and aliquot 336 (2 drops) was added 2,8-dibromo-6,6,12,12-tetraoctyldiindeno[1,2-b:1,2-e]pyrazine (0.15 g, 0.16 mmol), 4,7-bis(5-bromothiophen-2-yl)benzo[c]-[1,2,5]5,6–dodecylthiothiadiazole (0.13 g, 0.16 mmol) and $Pd(PPh_3)_4$ (2.7 mg, 1.25 eq.). 1 M K_2CO_3 (aq) (1 mL) was added in one portion and the reaction heated to 105 °C for 72 h, after which the reaction was poured into cold methanol, filtered through a soxhlet thimble and extracted (soxhlet) with methanol, acetone and hexane. The polymer was then dried under vacuum and dissolved in chloroform/water (100 mL/100 mL). Sodium diethyldithiocarbamate trihydrate (0.50 g) was added and the solution was stirred vigorously at 50 °C for 3 h. The chloroform solution was washed with water, dried ($MgSO_4$), concentrated and precipitated from chlorobenzene into cold methanol to yield the polymer as a red fibre. Yield = 140 mg, 61 %. GPC : Mn = 77 000 Da, PDI = 1.6. ^{1}H NMR (400 MHz, $CDCl_3$) δ (ppm): 8.17 (b, 2H), 7.98 (b, 2H), 7.77 (b, 2H) 7.71-7.57 (b, 4H), 2.87 (m, 4H), 2.45 (b, 2H), 2.33 (m, 2H), 2.08 (m, 2H), 1.98 (s, 2H), 1.76 (m, 2H), 1.56 (m, 3H), 1.48 (b, 34H), 1.33-1.10 (b, 44H), 0.88-0.79 (m, 24H).

Synthesis of 2,8-dibromo-6,12-bis(methylsulfanyl) methylene diindeno [1,2-b:1,2-e]pyrazine

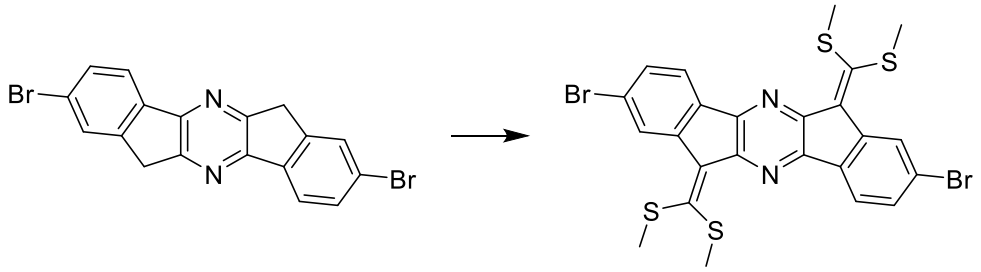

Sodium tert-butoxide (2.02 g, 21.26 mmol) was added in portions to a stirred solution of 2,8-dibromo-6,12-dihydrodiindeno[1,2-b:1,2-e]pyrazine (2.00 g, 4.84 mmol) in anhydrous DMSO (40 mL) at room temperature. CS_2 (0.80 g, 10.62 mmol) was added via a syringe and the reaction mixture stirred for 20 min. MeI (3.02 g, 21.26 mmol) was added drop wise over 5 min and stirring continued for 4 h. The reaction was quenched into a mixture of ice water (500 mL) and concentrated ammonia (25 mL). The resulting precipitate was filtered, rinsed with water and dried under vacuum to afford a dark crimson solid. Recrystallisation from hot hexane gave the product as red needles. Yield = 2.43g, 80 %; Mpt. = 165 - 166°C. MS (GCMS, EI): 620.8 $(M\text{-}H)^+$. ^1H NMR (400 MHz, $CDCl_3$) δ (ppm): 8.81 (d, *J* = 1.8 Hz, 2H), 8.01 (d, *J* = 7.9 Hz, 2H), 7.56 (dd, J = 7.9, 1.8 Hz, 2H), 2.78 (s, 12H). ^{13}C NMR (101 MHz, $CDCl_3$) δ 183.84, 173.36, 160.18, 148.71, 137.78, 127.85, 114.18, 113.80, 104.10, 103.98, 43.60.

Synthesis of 2,8-dibromo-6,12-(1'-octylnonylidene)diindeno[1,2-b:1,2-e]pyrazine

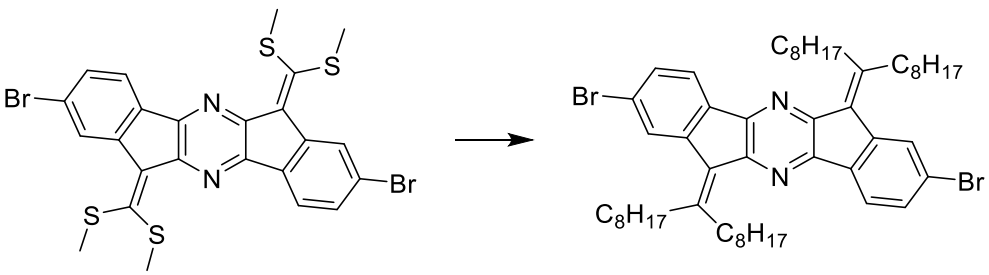

To a solution of 2,8-dibromo-6,12-bis(methylsulfanyl) methylene diindeno [1,2-b:1,2-e]pyrazine (0.40 g, 0.64 mmol) in anhydrous THF (100 mL) at -5 °C was added dilithium tetrachlorocuprate (7 mg, 0.03 mmol) and octylmagnesium bromide (1.40 mL of 2 M solution in diethyl ether, 2.81 mmol). The solution was stirred for 4 h at -5°C and quenched with 10% sodium hydroxide solution (100 mL). The precipitates were removed by filtration through celite and washed with ethyl acetate. The organic layer was washed with 10% sodium hydroxide (aq) (100 mL), brine (100 mL), dried ($MgSO_4$), filtered and concentrated under vacuum. The resulting oil was purified by passing through a column of silica with a basic alumina plug (eluent: petroleum spirit). Recrystallisation from hexane yielded yellow needles. Yield = 0.20 g, 36 %. Mpt. 102 – 103 °C. ^{1}H NMR (400 MHz, $CDCl_3$) δ (ppm): 7.98 (d, *J* = 1.4 Hz, 2H), 7.96 (d, *J* = 8.1 Hz, 2H), 7.56 (dd, *J* = 8.1, 1.4 Hz, 2H), 3.47 (t, *J* = 7.9 Hz, 4H), 2.82 (t, *J* = 7.9 Hz 4H), 1.77 (m, 4H), 1.70 (m, 4H) 1.60 (m, 8H) 1.49-1.28 (m, 32H) 0.94- 0.88 (m, 12H). ^{13}C NMR (101 MHz, $CDCl_3$) δ 170.84, 144.73, 136.43, 129.80, 127.57, 119.46, 116.06, 107.86, 86.65, 42.98, 31.93, 30.57, 29.70, 29.44, 29.43, 29.29, 22.67, 14.14.

Synthesis of 2,8-dibromo-6,12-(1'-(2''-ethylhexyl)-2'-ethylheptyl-idene)diindeno[1,2-b:1,2-e]pyrazine

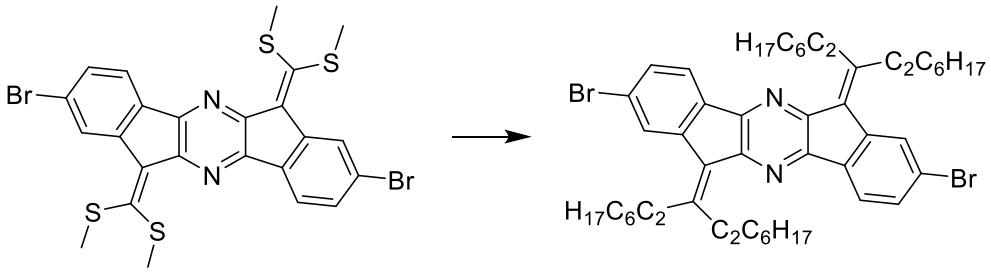

To a solution of 2,8-dibromo-6,12-bis(methylsulfanyl) methylene diindeno [1,2-b:1,2-e]pyrazine (0.40 g, 0.64 mmol) in dry THF (100 mL) at -5 °C was added lithium tetrachlorocuprate (7 mg, 0.03 mmol) and 1-ethyl-2-hexyl magnesium bromide (1.40 mL of

2 M solution in diethyl ether, 2.81 mmol). The solution was stirred for 4 h at -5°C and quenched with 10% sodium hydroxide solution (100 mL). The precipitates were removed by filtration through celite and washed with ethyl acetate. The organic layer was washed with 10% sodium hydroxide (aq) (100 mL), brine (100 mL), dried ($MgSO_4$), filtered and concentrated under vacuum. The residue was filtered through a silica plug (3 x 3 x 3 cm) consisting of a thin layer of basic alumina (1 x 3 x 3 cm) on top (eluent: petroleum spirit 40-60). After concentration the product was recrystallised from hexane yielding a yellow solid. Yield = 0.16 g, 30 %. Mpt. = 86 – 87 °C. ^{1}H NMR (400 MHz, $CDCl_3$) δ (ppm): 8.13 (d, *J* = 1. 2 Hz, 2H) 7.98 (d, *J* = 8.1 Hz, 2H) 7.57 (dd, *J* = 8.1, 1.2 Hz, 2H), 3.66 (m, 4H), 2.87 (m, 4H), 1.95 (m, 4H), 1.87 (m, 4H), 1.46 – 1.25 (m, 28H), 0.96 - 0.82 (m, 24H). ^{13}C NMR (101 MHz, $CDCl_3$) δ 171.68, 144.65, 139.87, 133.78, 127.56, 118.00, 118.41, 108.94, 85.60, 40.77, 31.72, 31.44, 31.30, 30.48, 30.47, 30.46, 21.22, 14.84.

Synthesis of Poly(6,12-(1'-octylnonylidene)diindeno[1,2-b:1,2-e]pyrazine - AIP

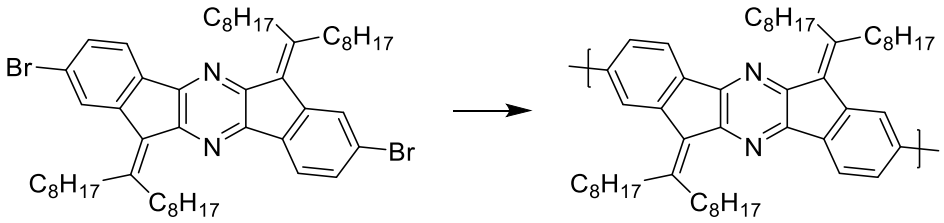

A thoroughly degassed solution of 2,8-dibromo-6,12-(1'-octylnonylidenediindeno[1,2-b:1,2-e]pyrazine (0.20 g, 0.24 mmol) in toluene (0.5 mL) and DMF (0.5 mL) was added to a degassed solution of $Ni(COD)_2$ (0.15 g, 0.53 mmol), 2,2'-bipyridine (0.08 g, 0.53 mmol) and 1,5-cyclooctadiene (0.06 mL, 0.53 mmol) in toluene (2 mL) and DMF (2 mL) in a sealed microwave vial. The combined solution was heated to 85 °C for 72 h. The resulting solution was poured into cold methanol and subsequent soxhlet extraction with methanol, acetone, hexane and chloroform. The chloroform fraction was concentrated under reduced pressure

and dissolved in chloroform/water solution (100 mL/100 mL). Sodium diethyldithiocarbamate trihydrate (0.50 g) was added and the solution was stirred vigorously at 50 °C for 3 h. The chloroform solution was washed with water, dried ($MgSO_4$), concentrated and precipitated from chlorobenzene into cold methanol to yield the polymer as bright yellow fibres. Yield = 56 mg, 34 %. GPC : Mn = 22 000 Da, PDI = 2.2. ^{1}H NMR (400 MHz, $CDCl_3$) δ (ppm): 8.26 (b, 4H), 7.77 (b, 2H), 3.04 (b, 4H), 2.11 (b, 4H), 1.95 (b, 4H), 1.43-1.23 (b, 44H), 0.87 (t, 12H).

Synthesis of poly(6,6,12,12-tetraoctylldiindeno[1,2-b:1,2-e]pyrazine-co-2,5-thiophene) - IP-T

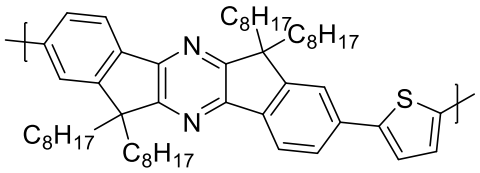

2,8-Dibromo-6,6,12,12-tetraoctyldiindeno[1,2-b:1,2-e]pyrazine (0.20 g, 0.23 mmol), 2,5-bis-(trimethylstannyl)thiophene (0.10 g, 0.23 mmol), $Pd(dba)_2$ (4.2 mg, 2 % eq.) and $P(o\text{-}tolyl)_3$ (5.6 mg, 0.02 mmol) were added to a microwave vial. Dry chlorobenzene (4 mL) was added and the mixture headed under microwave irradiation for 5 min at 100 °C, 5 min at 120 °C, 10 min at 160 °C and 20 min at 180 °C. After cooling to 50 °C the resulting solution was poured into cold acidic methanol (MeOH 100mL/ HCl 5 mL), filtered into a soxhlet thimble and extracted (soxhlet) using methanol, acetone and hexane. The remaining polymer was removed from the thimble, dried and dissolved in chloroform/water solution (100 mL/100 mL) and sodium diethyldithiocarbamate trihydrate (0.50 g) was added. The solution was stirred vigorously at 50 °C for 3 h. The chloroform solution was washed with water, dried ($MgSO_4$), concentrated and precipitated from chlorobenzene into cold methanol to yield the polymer as dark red fibres. Yield = 125 mg, 69 %. GPC: Mn = 23 000 Da, PDI = 2.3. ^{1}H

NMR (400 MHz, $CDCl_3$) δ (ppm): 8.15 (d, *J* = 7.6 Hz, 2H), 7.81 (d, *J* = 7.6 Hz, 2H), 7.76 (s, 2H), 7.53 (b, 2H), 2.43 - 2.27 (b, 4H), 2.19 - 2.01 (b, 4H), 1.20 - 1.10 (b, 48H) 0.81 (t, *J* = 6.6 Hz, 12H).

Synthesis of poly(6,6,12,12-tetramethylbutyldiindeno[1,2-b:1,2-e]pyrazine-co-2,5-thieno[3,2-b]thiophene) – IP-TT

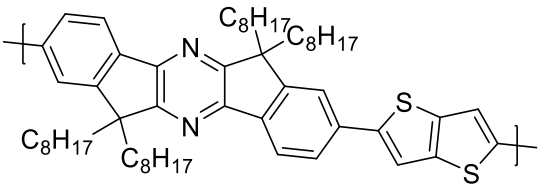

2,8-Dibromo-6,6,12,12-tetraoctyldiindeno[1,2-b:1,2-e]pyrazine (0.2 g, 0.23 mmol), 2,5-bis(trimethylstannyl)thieno[3,2-b]thiophene (0.11 g, 0.23 mmol), $Pd(dba)_2$ (4.2 mg, 0.005 mmol) and $P(o\text{-tolyl})_3$ (5.6 mg, 0.02 mmol) were added to a microwave vial. Dry chlorobenzene (4 mL) was added and the mixture heated under microwave irradiation for 5 min at 100 °C, 5 min at 120 °C, 10 min at 160 °C and 20 min at 180 °C. After cooling to 50 °C the resulting solution was poured into cold acidic methanol (MeOH 100mL/ HCl 5 mL), filtered into a soxhlet thimble and extracted (soxhlet) using methanol, acetone and hexane. The remaining polymer was removed from the thimble, dried under vacuum and dissolved in chloroform/water solution (100 mL/100 mL) and sodium diethyldithiocarbamate trihydrate (0.50 g) was added. The solution was stirred vigorously at 50 °C for 3 h. The chloroform solution was washed with water, dried ($MgSO_4$), concentrated and precipitated from chlorobenzene into cold methanol to yield the polymer as dark red fibres. Yield = 94 mg, 48 %. GPC: Mn = 20 000 Da, PDI = 2.1. ^{1}H NMR (400 MHz, $CDCl_3$) δ (ppm): 8.16 (b, 2H), 7.75 - 7.70 (b, 6H), 2.43 - 2.27 (b, 4H), 2.17 - 2.01 (b, 4H), 1.20 - 1.10 (b, 48H), 0.81 (t, *J* = 7.2 Hz, 12H).

Synthesis of 3-(thien-3-yl)propanoic acid

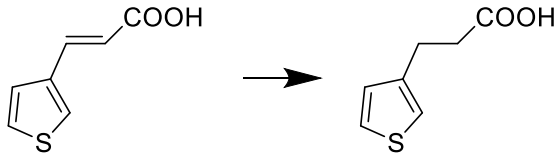

3-(3-Thienyl)acrylic acid (9.74 g, 63.2 mmol) and ammonium formate (11.95 g, 189.50 mmol) were dissolved in isopropanol (200 mL). Palladium on carbon (5.74 g, 10 % wt) was added portion-wise and the reaction heated to reflux overnight. The resulting solution was cooled to room temperature, filtered through celite and rinsed with isopropanol. The solvent was removed under vacuum to obtain a white solid. Yield = 8.25 g, 83.6 %. Mpt. 61 – 62 °C (lit = 62 – 63 °C[2]). ^{1}H NMR (400 MHz, $CDCl_3$) δ (ppm): 7.30 (dd, *J* = 4.4, 2.4 Hz, 1H), 7.02 (m, 1H), 6.97 (dd, *J* = 4.4, 2.4 Hz, 1H), 3.01 (t, *J* = 7.7 Hz, 2H), 2.72 (t, *J* = 7.7 Hz, 2H).

Synthesis of 4,5-dihydro-6H-cyclopenta[b]thiophen-6-one

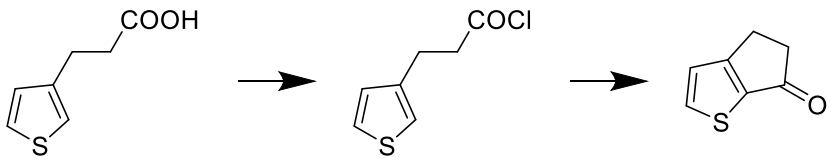

To a solution of 3-(thien-3-yl)propanoic acid (10.91 g, 69.80 mmol) in dry ether (100 mL) was added thionyl chloride (15.6 mL, 216 mmol) dropwise at room temperature. The reaction was heated to reflux for 3 h. After cooling, the ether was removed under reduced pressure. The resulting acid chloride was dissolved in dry CS_2 (50 mL) and transferred into a dropping funnel. The funnel was attached to a 3-neck flask that was previously charged with a suspension of $AlCl_3$ (9.30 g, 69.80 mmol) and dry CS_2 (100 mL). The acid chloride was added dropwise over 1 h at room temperature and the reaction stirred at room temperature overnight and then refluxed for 2 h. The resulting solution was poured into concentrated HCl/ice water (30 mL/ 200 mL) and extracted with DCM (3 x 50 mL), dried over $MgSO_4$,

filtered and concentrated under reduced pressure to afford the product as a brown solid, which was purified via column chromatography over silica (eluent: hexane/diethyl ether). Yield = 3.95 g, 41 %. Mpt. = 89 – 90 °C (lit mpt. 90 - 91°C)[3]. MS (GCMS, EI) 137.0 $(M-H)^+$. ^{1}H NMR (400 MHz, $CDCl_3$) δ (ppm): 7.91 (d, *J* = 4.9 Hz, 1H), 7.06 (d, *J* = 4.9 Hz, 1H), 3.09-2.99 (m, 4H). ^{13}C NMR (101 MHz, $CDCl_3$) δ: 197.17, 168.84, 142.99. 142.54, 124.87, 40.13, 22.87

Synthesis of 4,-dihydro-6H-cyclopenta[b]thiophene-2-one-3-oxime

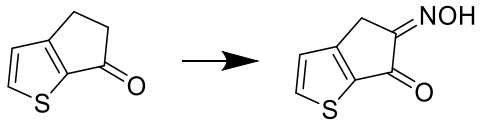

To a solution of 4,5-dihydro-6H-cyclopenta[b]thiophen-6-one (4.50 g, 32.6 mmol) in toluene (50 mL) at 0°C was added concentrated HCl (4 mL). The solution was stirred at 0°C for 30 min before isoamylnitrate (5.2 mL, 39 mmol) was added drop wise and the reaction warmed to room temperature overnight. The resulting suspension was filtered, washed with ether and dried to obtain a crude brown solid. The solid was triturated with hot diethyl ether to obtain the product as an off-white solid. Yield = 1.52 g, 28 %. Mpt. = 177 - 178°C.MS (GCMS, EI): 166.9 (M^+). ^{1}H NMR (400 MHz, $CDCl_3$) δ (ppm): 8.12 (d, *J* = 4.9 Hz, 1H), 7.31 (d, *J* = 4.9 Hz, 1H), 3.62 (s, 2H). ^{13}C NMR (101 MHz, $CDCl_3$) δ 198.63, 178.27, 160.79, 142.96, 142.43, 125.22, 36.00.

Synthesis of 4,9-dihydro-s-indenopyrazine[1,2-b:5,6-b']-dithiophene

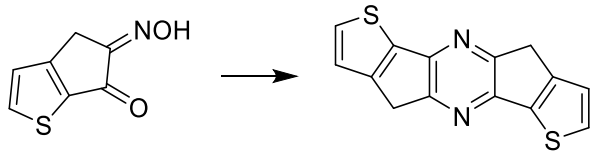

4,5-Dihydro-6H-cyclopenta[b]thiophene-2-one-3-oxime (1.95 g, 11.6 mmol) and sodium dithionate (5.90 g, 34.80 mmol) were dissolved in ethanol (30 mL) and degassed. Ammonia solution (30 mL, 28%) was added under argon and the solution stirred for 72 hr in the absence of light. Water (100 mL) was added and the reaction heated to reflux in air for 24 hr. The solution was cooled to room temperature, filtered, rinsing with methanol and diethyl ether to obtain the crude product. MS. (GCMS, EI): 268.0 (M^+). ^{1}H NMR (400 MHz, DMSO) δ (ppm): 7.63 (m, 2H), 6.90 (m, 2H), 4.31 (m, 4H).

References

1. J. Herbert Hall1, Joseph Yuming Chien1, Joel M. Kauffman2, Peter T. Litak, Jeffrey K. Adams, R. A. H. and R. A. H. Syntheses and photophysical properties of some 5(2)-aryl-2(5)-(4-pyridyl)oxazoles and related oxadiazoles and furans. *Journal of Heterocyclic Chemistry* **29**, 1245–1273 (1992).

2. Bonini, B. *et al.* Diastereoselective Synthesis of Thieno[3,2:4,5]cyclopenta[1,2-d][1,3]oxazolines. New Ligands for the Copper-Catalyzed Asymmetric Conjugate Addition of Diethylzinc to Enones. *European Journal of Organic Chemistry* **21**, 4442–4451 (2004).

3. Blanchard, P., Brisset, H., Illien, B., Riou, A. & Roncali, J. Bridged Dithienylethylenes as Precursors of Small Band gap Electrogenerated Conjugated Polymers. *The Journal of Organic Chemistry* **62**, 2401–2408 (1997).